Digital Twin Assisted Process Monitoring and Control

by

Parsa Bakhshandeh

B.Sc., Sharif University of Technology, 2020

A THESIS SUBMITTED IN PARTIAL FULFILLMENT OF

THE REQUIREMENTS FOR THE DEGREE OF

MASTER OF APPLIED SCIENCE

in

THE FACULTY OF GRADUATE AND POSTDOCTORAL STUDIES

(Mechanical Engineering)

THE UNIVERSITY OF BRITISH COLUMBIA

(Vancouver)

December 2022

The following individuals certify that they have read, and recommend to the Faculty of Graduate and Postdoctoral Studies for acceptance, the thesis entitled:

Digital Twin Assisted Process Monitoring and Control

submitted by Parsa Bakhshandeh in partial fulfillment of the requirements for

the degree of Master of Applied Science

in Mechanical Engineering

Examining Committee:

Dr. Yusuf Altintas, Mechanical Engineering, UBC
Supervisor

Dr. Xiaoliang Jin, Mechanical Engineering, UBC
Supervisory Committee Member

Dr. Kefei Wen, Mechanical Engineering, UBC
Supervisory Committee Member

Abstract

Monitoring and control systems for machine tools are essential for increasing productivity and maintaining the quality of machined parts. A robust monitoring system, coupled with the ability to use machining state signals predicted by the digital models is key to the implementation of such systems in production environment. This thesis presents the use of machining simulations as virtual feedback to CNC-inherent or accessible data collected from sound, vibration, and force sensors. Through the combination of simulations and on-line measurements, a digital twin is created to detect chatter, tool breakage, and tool wear.

First, the machining process states such as force, torque, power, and cumulative chip removal are simulated along the tool path. The actual and virtual positions of the tool along the tool path are synchronized during actual machining so that measured and simulated states can be compared.

A new tool wear monitoring algorithm is proposed. The cutter – workpiece engagement area and cumulative chip removed by the cutting edge are computed at discrete tool path positions using the Virtual Machining software (MACHPRO) developed in the laboratory. The spindle servo motor current is collected from the CNC and normalized by the engagement area to isolate cutting force coefficients that are sensitive to tool wear. The tool wear is correlated to cumulative chip thickness and an increase in the geometry-independent spindle motor current using a few (3-4) tool wear measurements during machining. It is shown that the tool wear progress can effectively be monitored by integrating digital simulation and motor current extracted from the CNC system during machining.

Similarly, chatter is also detected from sound spectrum measurement along the tool path by differentiating it from the air cut, transient vibrations and changes in the workpiece geometry with the aid of digital simulations. Chatter detection and avoidance algorithm is also enhanced by deactivating it at transient cutting zones.

In some applications such as adaptive force control, it is necessary to measure cutting forces during machining. A commercial tool holder equipped with accelerometers is used to predict cutting forces from vibration data. The transfer function between the vibrations measured by the instrumented tool holder and the applied force is modeled. The cutting forces are predicted from the vibration measurements with the aid of Kalman filter and compared against the digital estimations along the tool path.

The proposed methods are experimentally proven and integrated into an in-house developed monitoring system called IntelCut.

Lay Summary

A lack of information about geometric changes in the cutting operation makes the monitoring and control methods for machining processes insufficiently reliable to be implemented in the industry. Several of the few reliable methods are based on unfriendly sensors that are difficult to work with in an industrial setting. To create an intelligent software system capable of automatically controlling cutting operations, a digital twin system has been developed wherein the machining states are measured by available sensors and are aided by virtual feedback during the machining process.

This thesis proposes methods to monitor chatter, tool breakage and tool wear by using a digital twin system. Specifically, this study seeks to develop reliable methods that may be applied to on-line measurements, combined with simulations and verified for integration into process monitoring software.

Preface

Chapters 3 to 5 contain original contributions developed by the author under the supervision of Prof. Altintas. This thesis is based on previous research by former Ph.D. student Deniz Aslan. Throughout the thesis, the author carried out developing the algorithms, simulations, experimental tests (except sloped and pocket machining experiments in Chapter 3 which were conducted by former Ph.D. student Yen-Po Liu) and result analysis.

Table of Contents

List of Tables

List of Figures

List of Symbols

A	Area of cut
A_{force} , $A_{force\_\exp}$	Normalized equivalent and expanded system matrices of sensory tool holder
a_{c_0} , a_{c_1}	Y-intercept and slope used to estimate flank wear as a function of cumulative chip thickness
a_{I_0} , a_{I_1}	Y-intercept and slope used to estimate flank wear as a function of average normalized current
a_{I,c_0} , a_{I,c_1} , a_{I,c_2}	Coefficients used to estimate tool wear as a function of cumulative chip thickness and average normalized current
B_{force} , $B_{force\_\exp}$	Normalized equivalent and expanded input matrices of sensory tool holder
c	Cumulative chip thickness
C_{force} , $C_{force\_\exp}$	Normalized equivalent and expanded output matrices of sensory tool holder
D	Tool diameter

E	Young's Modulus
f	Feedrate of the machine
f_i	Feedrate in each iteration in MACHpro[1]
F	Cutting force at the tooltip
F_t	Tangential cutting force
F_r	Radial cutting force
F_x , F_y	Cutting force in X and Y directions
F_{DC} , F_{AC}	DC (static) and AC (harmonic) components of the actual cutting force at the tooltip
g	Gravitational constant
I	Area moment of inertial
I_a	Average spindle current per tooth period

ΔI_a	First differences of average spindle currents at every tooth period
$\Delta^N I_a$	Differences of average spindle current at every tooth period from one spindle period
$I_{in\text{-}cut}$	Distinguished spindle current for in-cut state
$I_{nom,spindle}$	Digital commanded spindle motor current from CNC
$I_{Normalized}$	Normalized spindle current.
$\overline{I}_{Normalized}$	Average normalized current
j	Index number in virtual feedback file
K_{ts}	Spindle's motor constant
K	Kalman Filter gain
k	Spring constant
$LIMIT_1$, $LIMIT_2$	Threshold factors in tool breakage detection

L	Noise coupling matrix
L_i	Distance that the tool travels in feed direction in each iteration in MACHpro[1]
m	Number of tooth period
N	Number of cutter's flute
n	Number of spindle samples collected at each tooth period
P	Estimation error covariance matrix of sensory tool holder
p_c	Assigned weight to cumulative chip thickness
p_I	Assigned weight to average normalized current
$p_{end\_entrance}$	End point index for the entrance state
p_{end_exit}	End point index for the exit state
$p_{start\_entrance}$	Start point index for the entrance state

p_{start_exit}	Start point index for the exit state
Q	System noise covariance matrix of sensory tool holder
R	Measurement noise covariance matrix of sensory tool holder
r	Tool radius
r_A	Time variant radial deflection of sensory tool holder
$t_{transient}$	Duration of transient state of tool
Sr	Number of spindles revolutions
t_d	Discrete Sampling Time
v_A	Total length of tool and tool holder
v_{force}	Measurement noise term
$w_{estimated_c}$	Estimated flank wear from cumulative chip thickness
$w_{estimated_I}$	Estimated flank wear from average normalized current

$w_{estimated_{c,I}}$	Estimated flank wear from average normalized current and cumulative chip thickness
w_{flank}	Tool's flank wear
w_{AC}	AC periodic disturbance noise
w_{DC}	DC periodic disturbance noise
w_{force}	Process noise term
x_0	Static eccentricity
X_i, Y_i, Z_i	Tool center positions in each iteration in MACHpro[1]
$x_{force}, x_{force\_\exp}$	Normalized equivalent and expanded state vector in sensory tool holder
$\tilde{x}_{force\_\exp}$	Estimation error between actual and estimated state in sensory tool holder
$\hat{x}_{force\_\exp}$	Estimated state vector in sensory tool holder
$y_{force}, y_{force\_\exp}$	Normalized equivalent and expanded output vector of sensory tool holder

Z_{wear}	Wear zone
α_1 , α_2	Predetermined threshold factors for tool breakage alarm
α_k , β_k	Residues of mode k in transfer function
ε_1 , ε_2	Residues of time series filters applied on average spindle current per tooth in the tool breakage detection algorithm
Φ_{sys}	FRF between force at the tool tip and vibration sensors (accelerometer in sensory tool holder)
$\Phi_{sys_{KL}}$	Kalman Filter FRF
$\hat{\phi}_1$, $\hat{\phi}_2$	First-order adaptive time series filters to remove varying DC trend and runout on the signal
θ_{DC} , θ_{AC}	DC (static) and AC (harmonic) noise ratio terms
τ_t	Spindle torque

ζ_k	Damping ratio of mode k
$\omega_{updated}$	Updated spindle frequency in chatter avoidance
$\omega_{chatter}$	Detected chatter frequency in chatter detection
$\omega_{initial}$	Initial spindle frequency of the cutting operation
ω_{sp}	Spindle speed
ω_{sp-rs}	Spindle speed in revolution per second
ω_{nk}	Natural frequencies of mode k

List of Abbreviations

FRF	Frequency Response Function
FFT	Fast Fourier Transform
CWE	Cutter-Workpiece Engagement
CSYS	Coordinate System
CNC	Computer Numerical Control
ML	Machine Learning
NEO	Teager-Kaiser Nonlinear Energy Operator
SK	Sanathanan-Koerner
AISI	American Iron and Steel Institute
FE	Finite Element
RLS	Standard Recursive Least Square
DC	Direct Current (Zero Frequency Component)
MEMS	Microelectromechanical Systems
HSK	Hollow Taper Shank
NaN	Not-a-Number-Value

Acknowledgements

Professor Yusuf Altintas has been a great support and source of guidance throughout my M.Sc. studies. It was his excellent supervision and insightful ideas in research that helped me to improve every day. With deep gratitude, I reflect on the experiences I gained during my time in this laboratory. I am grateful to him for the opportunity he provided and for the trust he placed in me.

I would like to express my gratitude to my friends and lab mates at MAL who always offered me assistance with my research. I would like to thank Behnam Karimi for providing me with many valuable ideas during my research. I want to thank Yaser Mohammadi for his many helpful comments on my thesis. I also want to express my gratitude to staff engineers especially Tayfun Ozdemir, Nima Dabiri and Pouya Abdolhosseinvand Fanid.

There are no words to express how grateful I am to my supportive family. It was my kind mother, my loving father, and my best friend brother who always stood by me in every difficult situation. I would not have been able to be who I am today without their love, support, and inspiration.

I could have not undertaken my time in Canada without Sahar as my companion. I will do my best to reflect her love and support back.

I am genuinely thankful to Pary Rousta and Salman Bazogh and their wonderful family who supported me from my very first day in Canada.

Lastly, I am indebted to all women and men fighting for freedom of my homeland, Iran. No roof is too high for their courage and determination, which are the greatest inspirations for anyone, including me. I will never forget the sacrifices they are making. To WOMAN, LIFE, FREEDOM.

This research has been sponsored by NSERC, Pratt & Whitney Canada and Sandvik Coromant under the Industrial Research Chair grant in virtual machining. The instrumented tool holder was donated by Prof. F. Bleicher of Technical University Vienna.

Chapter 1: Introduction

There has been a recent trend in the manufacturing industry to use an intelligent process monitoring and control system to improve the machining process. An on-line process monitoring and control system that can monitor machining states such as force, torque, and power and detect certain undesirable events and adjust the cutting conditions to avoid failures is needed in the manufacturing industry.

The objective of this thesis is to investigate how virtual process simulations can assist on-line process monitoring systems in machining. Machining processes such as turning, milling, and drilling involve removing material from the workpiece to give the final shape.

The machining operation may encounter unstable vibrations (so-called chatter), tool wear, and tool breakage. Several requirements must be met in order to implement an on-line monitoring system in industry. It is necessary to use the signal information from sensors already provided in the CNC system or industry-friendly sensors that can be easily installed on production machines. The methods need to be robust enough to work in various machining operations.

Past literature showed the utilization of CNC inherent data to predict machining states as an alternative to externally installed sensors. For instance, spindle motor and/or feed drive currents were used to predict machining states such as cutting force and torque. Any signal that can be related to force can also be indirectly used in the process monitoring methods. As a result, spindle current has been suggested to be used in tool wear and breakage detection purposes in this thesis.

Based on reading the digital spindle motor current from the CNC system, monitoring it, and controlling the operation by overriding feedrate and spindle speed, process monitoring system can be built. It is possible, however, to provide additional information to the machining operation by generating reliable simulations of the machining states. In this study, Virtual Machining Software MACHpro™ [1] is used to simulate the cutting process. Instead of adding additional sensors, process monitoring algorithms can use simulated machining states in combination with CNC data, enabling them to detect chatter, tool breakage and tool wear.

A digital twin system consists of a virtual feedback file and a synchronization algorithm with the on-line cutting operation. The virtual machining system simulates the machining process ahead of actual operation and stores it in a file. Synchronization is conducted by tracing simulation positions stored in the virtual data with the actual positions collected during the cutting process. The simulated cutting process states such as torque, force, power, and chip thickness can be accessed during the online cutting process. Therefore, tool wear, tool breakage and chatter detection methods can employ the simulations and CNC data as prior knowledge in monitoring applications.

The schematic of the digital twin system is presented in Figure 1.1. Simulated cutting force, torque, power and etc. from the Virtual Machining Software MACHpro™ [1] is synchronized with CNC system data. The corrective actions are then taken to control the operation by manipulating the feedrate and spindle speed during machining operations.

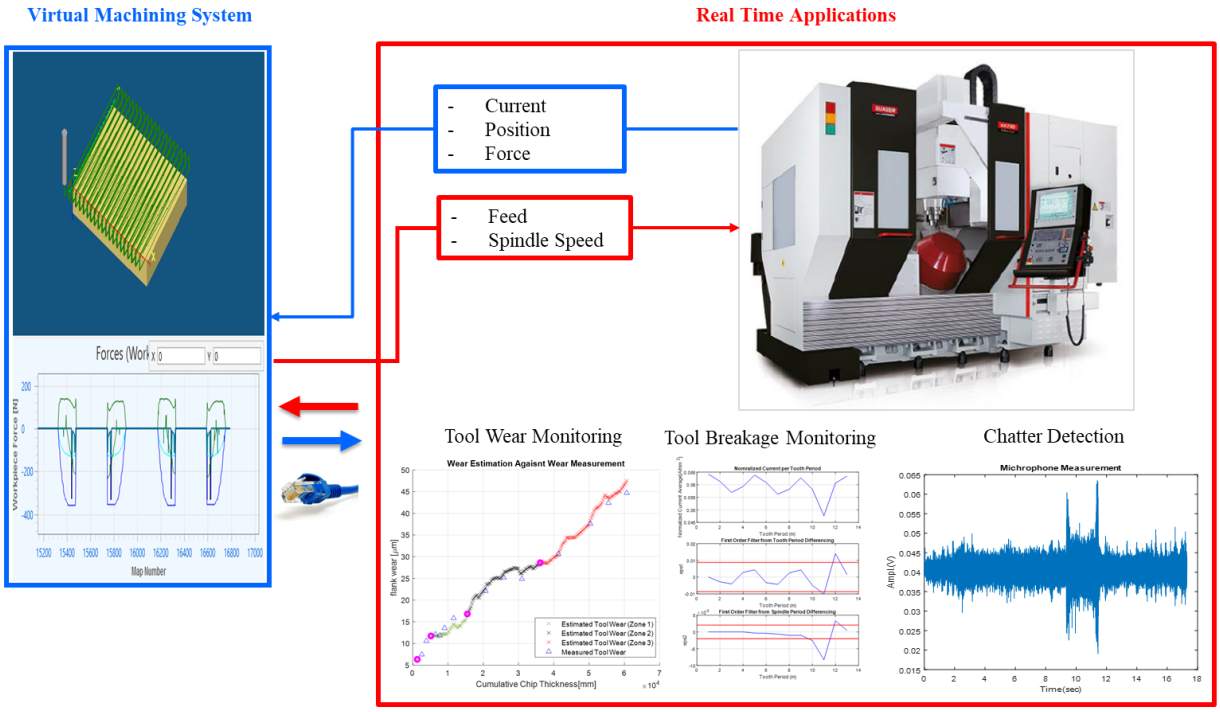

Figure 1.1. Digital twin system schematic. The digital twin system exchanges information between the virtual machining software (MACHpro™ [1]) and CNC data in real-time applications such as tool wear, tool breakage and chatter detection

In the process monitoring algorithms, tool breakage monitoring and chatter detection may yield false alarms at air-cut or transient states. The beginning or end of the tool's engagement with the workpiece is called the transient state. A transient state occurs when the tool transitions from an air-cut state to an in-cut state, exciting the natural frequencies of the machine.

False chatter or tool breakage alarms mostly occur in the transient states which resemble an impact hit. By monitoring spindle load, it is possible to differentiate between air-cut and in-cut states; however, relying solely on CNC data can make it difficult to identify transient states due to the lack of information about the cutting geometry. A cutting state detection algorithm to distinguish all three states (air-cut, transient, in-cut) requires cutter-workpiece engagement conditions from

the virtual machining system. In this case, Digital twin can assist the on-line operation by providing the engagement conditions along the discretized tool path, which helps to reduce false chatter and tool breakage alarms.

Frequent measurement of tool wear is not practiced because it reduces the productivity of costly machine tools. A tool wear monitoring method which requires only a very few measurements to calibrate the relationship between the wear and machining state is needed. Monitoring force coefficients have been proposed as a tool life indicator in the literature. Although monitoring force coefficients have proven to be effective, virtual process simulation can offer an alternative and possibly more simplified approach. In this thesis, commanded spindle motor current extracted from the CNC and simulated cutter - part engagement area and cumulative chip thickness are used to monitor tool wear. There are three regions in the typical wear progression curve, which are characterized by a short and accelerated initial wear zone, slow progression of wear zone, and an accelerated wear zone as the tool life limit approaches.

On-line measurement of cutting force is an important part of process monitoring. The thesis presents a force estimation method that uses a wireless acceleration sensor installed in a tool holder. By compensating for structural dynamics, Kalman Filter predicts the cutting force at the tooltip (see Figure 1.2) from the acceleration data collected from the sensory tool holder during machining.

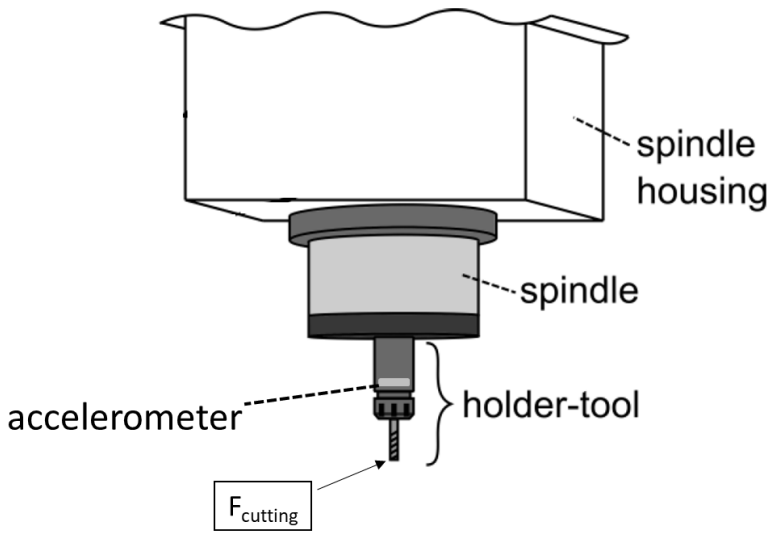

Figure 1.2. Tool holder instrumented with an accelerometer to measure the vibration close to the cutting zone

Hanworth, the thesis is organized as follows; the past literature in monitoring tool wear, chatter detection and tool breakage are reviewed in Chapter 2. The digital twin structure used in the thesis is explained in Chapter 3. Digital twin assisted tool breakage, and chatter detection and avoidance algorithms are presented in Chapter 4 followed by cutting force estimation from vibration sensors embedded in a tool holder in Chapter 5. The thesis is concluded with future research in Chapter 6.

Chapter 2: Literature review

2.1 Overview

The main objective of this thesis is to develop a digital twin system for process monitoring and control of machining operations. The digital twin system consists of virtual feedback generated from a machine simulation system and a structure to bridge its information to the on-line measurements from CNC system or other sensors on the machine. The additional information can be used to further analyze the measurements to detect events such as chatter, tool wear and tool breakage, and consequently control them by sending the required commands to the controller (CNC) system of the machine. This chapter reviews the previous studies related to in-process monitoring and control of machining states (Section 2.2) to detect tool wear (Section 2.2.1), tool breakage (Section 2.2.2), and chatter (Section 2.2.3). Previous research on digital twin development is discussed in Section 2.3. A discussion of direct and indirect approaches to force measurement is presented in Section 2.4. The chapter is concluded in Section 2.5 by outlining the gaps in the reviewed research which forms the basis for this thesis.

2.2 In-process Monitoring and Control of Milling Operation

Intelligent manufacturing systems have been the subject of extensive research and studies in the past. Additionally, there has been an increase in research in this area in recent years since the machining industry has become increasingly dependent on unattended operations. The purpose of this section is to review the studies conducted on tool wear, tool breakage, and chatter detection, in addition to some approaches to be used to avoid these events.

2.2.1 Tool Wear

Wearing or chipping of the tool results in changes in the geometry of the cutting edge and flank contact, resulting in undesirable surface finished. Tool wear monitoring has been extensively studied in the past literature, but a robust and reliable method is still lacking due to difficulties relating the sensor signals with the progression of wear.

Cutting forces have the following general relationship with depth of cut (a), chip thickness (h) and material – tool geometry dependent cutting force coefficients (K_{tc}, K_{te}) as;

$$F_t = K_{tc} a h + K_{te} a \tag{2.1}$$

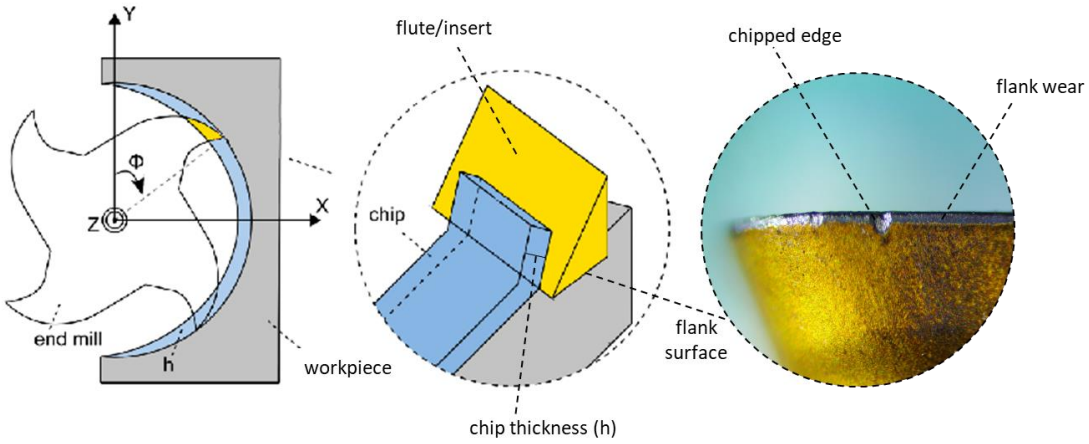

Figure 2.1. Geometry of slot-milling process, the chip formation and end mill's flank wear

The relationship between the cutting force coefficients (K_{tc}, K_{te}) and tool's flank wear has been investigated in [2–4]. The progression of edge force coefficient (K_{te}) resembles the gradual loss of tool material at the cutting edge during machining and used as tool life indicator in [2]–[4]. Nouri et al. [3] demonstrated the relationship between cutting force and tool wear progression using a stationary dynamometer and combined tangential and radial force coefficients Denkena

et al. [4] presented an empirical method based on weighted normalized cutting coefficients over tool life to provide a robust tool wear indicator. Ducroux et al. [2] considered the effect of tool wear by adding wear-dependent coefficients to the mechanistic cutting force model. Liu et al. [5] used both directly measured cutting forces and indirectly estimated cutting forces using the averaged spindle motor current to identify the in-process force coefficients. The edge force coefficients are then monitored as an indicator to detect the transition of wear zones. Xu et al. [6]calibrated the force estimation based on motor spindle power and monitored the cutting coefficients derived from the calibrated force estimation.

2.2.2 Tool Breakage

Tool's cutting edge breaks or chips when it is loaded excessively during machining operations. It is important to detect the tool breakage and stop the process immediately to avoid damage on the workpiece and machine. Consequently, tool breakage detection is studied extensively in the past due to its importance in the manufacturing industry.

Matsushima et al. [7] monitored a sudden change in the residues identified by applying a 28^{th} order autoregressive time series filter on spindle current measurements to detect tool breakage in milling experiments. Similar methods were used by Lan et al. [8], but they used a 15^{th} order time series filter on the cutting force. Rather than complex, high order time series, Altintas [9], [10] applied a tooth and spindle period differentiation on the average cutting force at each tooth period followed up by a 1^{st} order time series filter. As a result, two residues were obtained which allows the detection of tool breakage. The tool breakage threshold was obtained by a scale factor of the maximum residues at the first 5 spindle revolution assuming that the tool is not broken.

Additionally, Altintas [11] used the same method on the average cutting force estimation from feed drive current measurement as an alternative to the direct measurement of forces from the dedicated sensors which are hard to implement in the production environment.

Similarly, Aslan [12] utilized the same 1st order time series on average cutting torque from the spindle current but with the aid of virtual feedback provided by the machining simulation system. The cutting operation is simulated in the virtual machining environment [1] so that the process geometry and chip load are identified throughout the operation. Therefore, the tool breakage threshold is selected as a function of the varying cutter – workpiece engagement (CWE) conditions.,

2.2.3 Chatter Detection

Chatter occurs due the self-excited unstable vibrations during the generation of chip thickness and results in poor surface finish, excessive force on tool and workpiece, hence may damage the machine, cutting tool and workpiece. Stability lobe diagram [13] theoretically predicts the combinations of critically stable depth of cuts and spindle speeds, which is used by process planners in selecting chatter-free cutting conditions in preparing NC tool paths. However, the stability lobes do not always guarantee chatter-free cutting operation due to uncertainties in the structural dynamics of machine tools. The natural frequencies of the spindle may change at high speeds due to thermal loading of bearings, or dynamics may be dependent on the tool position within the workspace of the machine tool.

Delio et al. [14] compared different sensors and suggested a microphone as a practical instrument to detect chatter. They eliminated chatter by matching the identified chatter frequency with the

tooth passing e frequency in milling. Aslan et al. [15] estimated cutting torque using spindle motor current from the closed loop transfer function between cutting torque at the tooltip and digitally commanded current extracted from the CNC. The forced vibrations at spindle and tooth passing frequency harmonics are removed from the frequency spectrum of the signal using a comb filter. Chatter was detected if the remaining peaks in the frequency domain were higher than a threshold. Caliskan et al. [16] proposed an energy-based method to separate the forced vibration and chatter components of the signal and monitored their energy ratio to detect chatter. Rahimi et al. [17] proposed a hybrid chatter detection model on microphone signal. The mentioned energy-based method [16] as a physics-based method was combined with a trained Machine Learning network to avoid the false alarm detected at transient states.

2.3 Digital Twin System

Most of the mentioned chatter, tool breakage and tool wear detection algorithms in Section 2.2.1 to Section 2.2.3 generally use the on-line machining states measured directly from the CNC controller or the sensors installed on the machine. However simulated machining states from a virtual system can assist these algorithms in detecting the events. Van Houten and Kimura [18] designed a Virtual Maintenance System to relate predicted and measured process states to support machining maintenance such as tool failure diagnosis.

Furthermore, Kritzinger et al. [19] provide a definition and classification of digital models, digital shadows and digital twins in the context of manufacturing. Altintas and Aslan et. al [20] the first detailed virtually assisted process monitoring and control system. The MACHpro™ Virtual Machining Software [1] is used to simulate the machining state once the system is provided with

the desired toolpath. Aslan [12] also proposed a method to synchronize the simulated machining states with the on-line operation. The synchronized digitally predicted and on-line measured forces along the tool path helped to detect tool breakage and apply adaptive force control along the path.

2.4 Cutting Force Prediction in Milling

Teti et al. [21] reviewed a number direct and indirect sensing techniques to identify cutting forces. Klocke et al. [22] implemented machining position-oriented monitoring and measuring force from rotary or table dynamometers. Möhring et al. [23] developed a sensory fixture on the spindle to measure force for process monitoring. Altintas et al. [24] used spindle integrated force sensor and compensated the effect of the structural dynamics of the system by using a Kalman Filter, thereby increasing the bandwidth of the sensor. In the mentioned studies, cutting forces were directly measured.

There are also indirect approaches to estimate cutting forces. Altintas [25] used feed drive motor currents to estimate the cutting forces by modeling the feed drive control system. Aslan et al. [26] also presented a force estimation method in 5-axis milling operation using the digital commanded feed drive motor current from the CNC controller. The structural dynamics of the system are compensated using a Kalman Filter and therefore the structural dynamics modes do not limit the bandwidth of the force prediction method. Postel et al. [27] installed a number of accelerometers on the stationary spindle housing away from the tooltip. The cutting forces at the tooltip were estimated indirectly using the accelerometers. The estimation was conducted using a Kalman Filter designed based on the FRF between the displacement at the accelerometer location and force at

the tooltip. Then a data fusion from the multiple installed accelerometers was applied to reinforce the force estimation at the tooltip and reduce the maximum error. Additionally, Xi et al. [28] estimated cutting forces using a smart tool holder system equipped with capacitive sensor in milling and drilling processes.

2.5 Summary

Several in-process monitoring methods were reviewed in the chapter. Since an intelligent machining system is built upon process monitoring methods, the limitations in these methods need to be addressed and if needed new methods be proposed.

The algorithms used to monitor tool wear primarily focused on identifying in-process force coefficients and monitoring them as an indicator of tool health. Furthermore, there is a gap in the literature regarding the estimation of tool wear by using other indicators. These gaps are addressed in Chapter 3 in which a method is presented to monitor and estimate tool wear using the feedback from virtual machining system. In reviewing other studies on tool breakage and chatter detection, it becomes evident that the rich research background of these topics provides implementable methods that can be applied to the complex toolpaths. The only gap that is filled in this study is to distinguish the in-cut state from transient and air-cut states, and apply these methods only during in-cut states along the tool path (Chapter 4).

Chapter 3: Synchronization of Virtual Feedback Model and On-line Operation and Its Application to Tool Wear Monitoring

3.1 Overview

This chapter introduces a virtually assisted on-line tool wear monitoring system for milling operations. Using the digital twin system, a virtual machining software communicates with an on-line cutting process. The simulated machining states such as cutting forces, torque, and engagement along the tool path are bridged into the on-line operation which is conducted by synchronizing the tooltip center positions in virtual and actual machines. Therefore, the on-line operation has access to additional information that can aid in identifying chatter, tool breakage, tool wear, and other events. This chapter presents tool wear monitoring application of the digital twin system.

Tool health indicators are typically constructed based on edge force coefficients [29], [30]. This study introduces an alternative indicator that can be obtained by directly measuring the motor current and using the area of cut and engagement as virtual feedback. This indicator is then monitored throughout an end mill's service life as an alternative for the tool wear monitoring method.

The rest of the chapter is organized as follows; Section 3.2 discusses the development of virtual feedback and its integration into online operations. In Section 3.3, the tool wear monitoring algorithm and in Section 3.4 its estimation is described. Experimental validation is presented in Section 3.4, and the chapter is summarized in Section 3.5.

3.2 Integration of Virtual Feedback Model and On-line Operation

The part machining process is simulated using MACHpro™ virtual Machining System [1] to calculate cutter-workpiece engagement, area of cut, cumulative chip thickness, the envelope of cutting forces, and other machining states along the toolpath. The machining process is simulated before the physical cutting operation. The simulated machining states are stored and later accessed by online machining process monitoring as virtual feedback to assist in detecting events such as tool wear, tool breakage, and chatter.

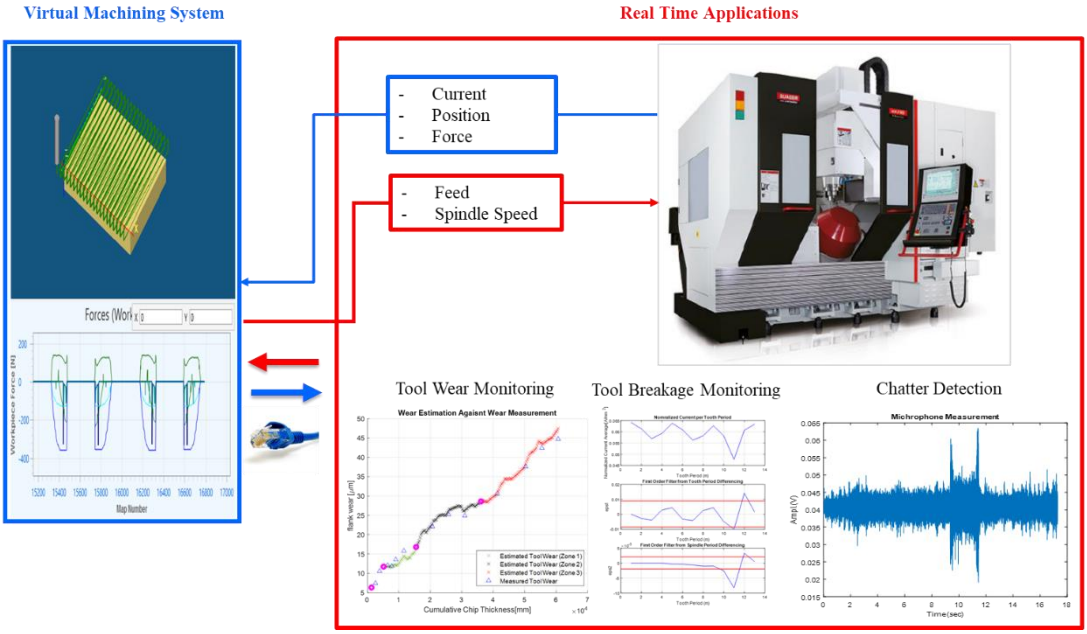

Figure 3.1. Communication between the virtual feedback model and the on-line operation

3.2.1 The Development of Virtual Feedback Model

An in-house developed MACHpro™ Virtual Machining System [1] is used to simulate the machining states and generate the virtual feedback file which is explained as follows.

3.2.1.1 Generating Virtual Feedback file

The main window of MACHpro™ with the corresponding part used in the next sections is given in Figure 3.2. Each bullet-points are explained in Table 3.1. The first step is to choose the CNC machine type which is milling in this study. After that, the solid block geometry and work material are selected. The toolpath file is then provided to the software. The software extracts the tool geometry from the toolpath file automatically, but there is also an option to manually select the tool geometry. It is then necessary to select the toolpath sampling distance at which the software calculates the engagement maps between the tool and the workpiece at the corresponding discrete tool center positions. Finally, the process states such as force, torque, area, and volume of material removal and other needed states are selected and simulated at given sampling distances along the tool path. The software is also capable of optimizing the toolpath by changing the feed rate concerning machine tools and process constraints. As it is not part of the scope of the present study, only the simulation aspect of the software is being used in this study.

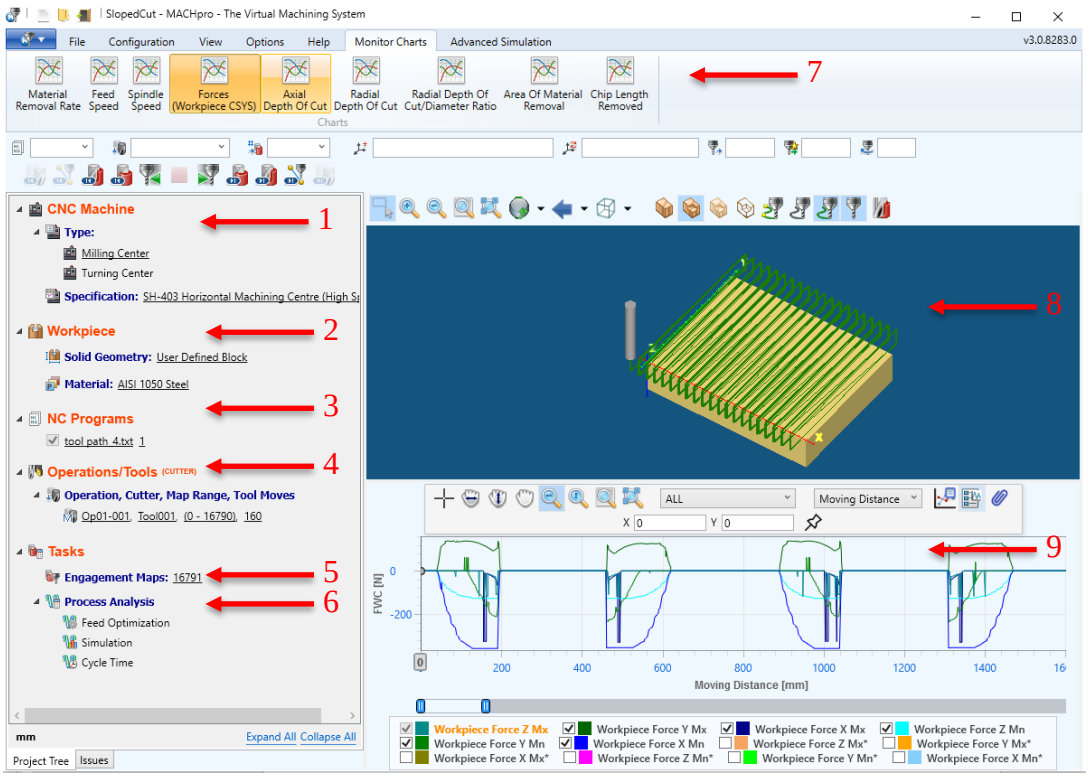

Figure 3.2. MACHpro™ Virtual Machining System [1] user interface

Once the part machining is simulated, the machining parameters are stored in a file to be later accessed by the digital twin system. The simulated states that are extracted from MACHpro™ [1] are X, Y and Z tool tip center positions, the envelope of cutting forces in X, Y and Z directions in workpiece coordinate system (Workpiece CSYS), cutter-workpiece engagement boundaries, area of cut, and cumulative chip thickness. Other machining parameters like feed rate, spindle speed, and tool geometries are also stored. The stored file is then post-processed to synchronize the tooltip position and subsequently other process states which forms the digital twin system.

Table 3.1. Explanation of bullet-points shown in Figure 3.2 [12]

Point#	Module Name	Explanation
1	CNC Machine	Specifying type of CNC machine
2	Workpiece	Selecting the raw workpiece geometry in the form of STL file and material from the database
3	NC program	Uploading NC toolpath in the form of APT file
4	Operations/Tools	Reviewing/Editing tool geometry
5	Engagement Maps	Selecting engagement map sampling distance
6	Process Analysis	Simulation of process states (Force, Torque, etc.)
7	Monitor Charts	List of simulated process states to be plotted
8	Parts and Toolpath Visual	Visualization of final machined part with the corresponding toolpath
9	Graph Monitor	Graph of selected process states

3.2.1.2 Cutting States Detection

Once the virtual model is generated using MACHpro™, it can be used to detect the cutting states. The term "cutting states" refers to three different states of the tool during the machining process. These states are air-cut, transient and in-cut states which need to be distinguished from one another. As the name implies, an air cut refers to the part of an operation where a tool is not engaged with the workpiece and rotates in the air. A transient state occurs when a tool enters or leaves the

workpiece, referred to as entrance and exit during an operation. This state indicates that the tool is not in its full engagement with the workpiece, and it is similar to an impact excitation. Consequently, the machine is excited to vibrate at its natural frequencies. Finally, the in-cut state is when the tool is fully engaged with the workpiece. The mentioned cutting states are depicted in Figure 3.3.

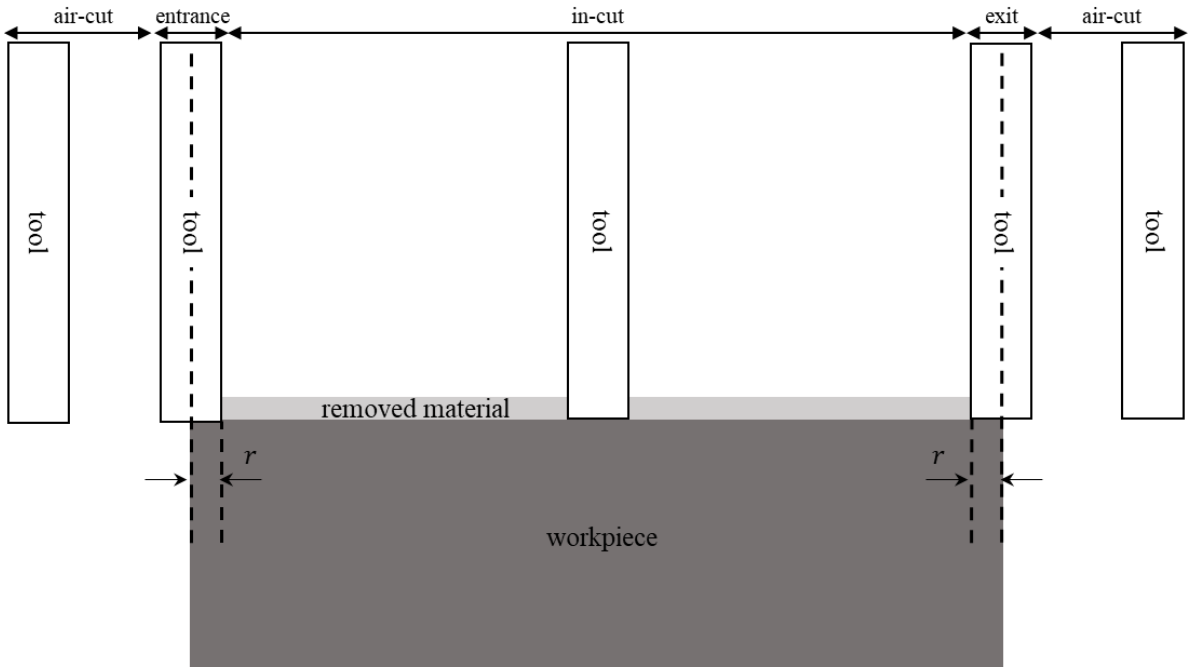

Figure 3.3. Cutting State (air-cut, entrance, in-cut, exit) along the toolpath

It is important to separate these states from each other which is accomplished using the extracted engagements stored in the virtual file. Once the engagement is zero it means that there is no engagement between tool and workpiece, and the tool is in an air-cut state.

$$engagement_{tool-workpiece} = 0 \rightarrow \text{Cutting State : air-cut} \tag{3.1}$$

To find transient states (entrance and exit), the period of time for which each of these states last is evaluated. This period ($t_{transient}$) is equal to the time that the radius of the tool travels inside or outside of workpiece in the feed direction as follows;

$$t_{transient} = \frac{r}{f} \tag{3.2}$$

where r is the tool radius in [mm] and f is feedrate in [mm/s]. Once the transient time period is calculated, the starting position of the entrance state can be obtained by considering the first non-zero engagement sample which is the first engagement sample where its previous sample is zero, but the current sample is non-zero. This is where the tool enters the workpiece. The index for this sample is stored as the starting point for the entrance state as follows;

$$\begin{cases} engagement_{tool-workpiece}(i) \neq 0 \\ engagement_{tool-workpiece}(i-1) = 0 \end{cases} \rightarrow p_{start\_entrance} = i \tag{3.3}$$

where $p_{start\_entrance}$ is the index of starting point for the entrance state. Following this step, the time that the tool travels in each iteration is calculated as follows;

$$\begin{aligned} L_i &= \sqrt{(X_i - X_{i-1})^2 + (Y_i - Y_{i-1})^2 + (Z_i - Z_{i-1})^2} \\ t_i &= L_i / f_i \end{aligned} \tag{3.4}$$

where X_i, Y_i and Z_i are the tool center positions at each discrete engagement interval along the tool path, f_i is the feedrate and i is the iteration number, L_i is the distance in that the tool travels in feed direction in each iteration and consequently t_i is its corresponding time. The total time value is

summed up going forward from the start point and once it is equal to the transient period, the index is stored as the ending point for entrance.

$$\sum_{p_{start\_entrance}}^{j} t_i = t_{trasnient} \rightarrow p_{end\_entrance} = j \tag{3.5}$$

As a result, the start and the end of the entrance states are obtained and distinguished from the rest. A similar procedure is repeated to find the exit state where this time the end point is obtained as follows;

$$\begin{cases} engagement_{tool-workpiece}(i) \neq 0 \\ engagement_{tool-workpiece}(i+1) = 0 \end{cases} \rightarrow p_{end\_exit} = i \tag{3.6}$$

To find the start point, the distance that the tool travels in the feed direction in each iteration and the corresponding time is calculated as in.(3.4) The total time value is summed up going backward from the endpoint until it is equal to the transient time period.

$$\sum_{j}^{p_{end\_exit}} t_i = t_{trasnient} \rightarrow p_{start\_exit} = j \tag{3.7}$$

Once air-cut and transient states are found the remaining part is the in-cut state. The whole method is summarized as follows;

$$\left.\begin{cases} engagement(i) = 0 \rightarrow \text{Cutting State : air-cut} \\ p_{start\_entrance} \leq i \leq p_{end\_entrance} \rightarrow \text{Cutting State : entrance} \\ p_{start\_exit} \leq i \leq p_{end\_exit} \rightarrow \text{Cutting State : exit} \end{cases}\right\} \rightarrow \text{transient states} \tag{3.8}$$
$$\text{none of the above} \rightarrow \text{Cutting State : in-cut}$$

By using this method, the number of cuts in one toolpath can also be identified and distinguished. Identifying each cut in one toolpath will be further discussed in the following sections.

Having determined the cutting states, each cutting state is assigned a number corresponding to its state which is represented in Table 3.2. This parameter is added to the virtual file and used accordingly.

Table 3.2. Corresponding value of cutting states in the virtual feedback file

State	Air-cut	Transient State	In-cut
Value	0	1	2

3.2.2 Synchronization of the Virtual Feedback File and the On-line Operation

Once the virtual file is generated and uploaded to the digital twin system, the next step is to establish synchronization between the on-line operation on the machine and the virtual feedback file, so that both can work in parallel to exchange information.

The synchronization between the virtual feedback file and the online operation is achieved by tracing tooltip center positions. The X, Y and Z position of the tooltip in the workpiece coordinate system along the toolpath is obtained from the virtual feedback model with the engagement map sampling distance set as 1 [mm] here. The nominal X, Y and Z position of the tooltip is then measured from the CNC. Upon measuring the tooltip positions, the positions are searched in the virtual file position columns. The tolerance to trace the positions between the measured and simulated ones is set to be ±0.5 [mm] for X, Y and Z axis so that no sample is lost. Once each position is found in the virtual feedback file, its index number is stored. Then the operation is

repeated, and the new positions are searched from the following iteration. The flowchart of the explained method is represented in Figure 3.4.

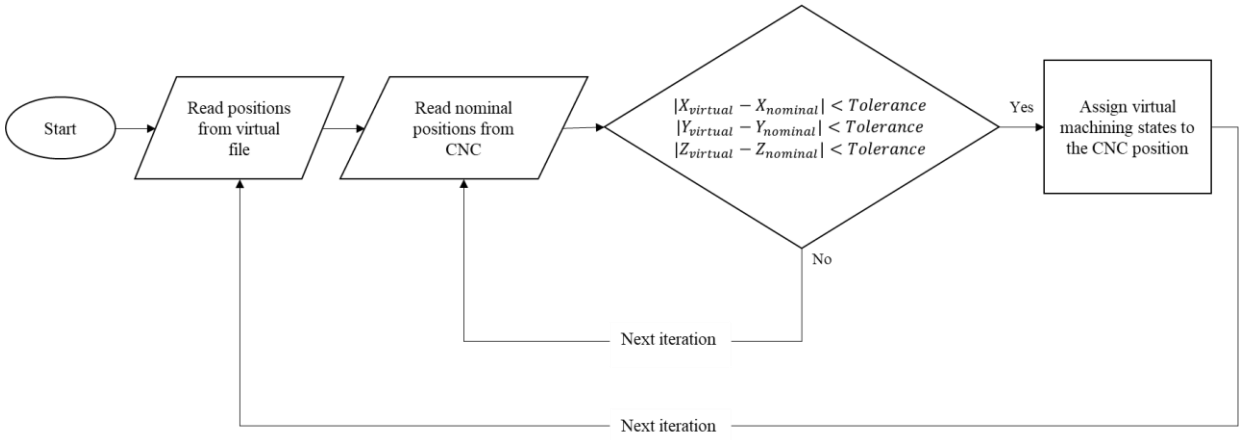

Figure 3.4. Flowchart of the overall synchronization procedure

By synchronizing the online operation with the virtual feedback file, the simulated machining states such as engagement, area of cut, and the cutting forces can be accessed online. This information is then used to enhance the process or detect events like chatter, tool breakage, and tool wear.

3.3 On-line Tool Wear Detection via Spindle Current Measurements Monitoring

The first application to the digital twin system which consists of the virtual feedback file from MACHpro™ is tool wear monitoring. The typical tool life curve characterized by flank wear can be divided into three wear zones [10]. In the beginning, the cutting-edge wears rapidly. The second phase involves gradual and steady wear until the critical limit is reached. When the critical limit is exceeded, aggressive flank wear will occur, ultimately resulting in tool breakage.

The cutting torque and therefore the cutting force are proportional to the measured motor current. The spindle motor torque and tangential cutting force is calculated as follows;

$$\tau_t = K_{ts} I_{nom,spindle}$$
$$F_t = \frac{1}{D/2}\tau_t = \frac{K_{ts}}{D/2} I_{nom,spindle} \tag{3.9}$$

where $I_{nom,spindle}$ $[A]$ is the nominal spindle current measured from the spindle motor, K_{ts} [Nm/A] is the spindle's motor constant, τ_t [Nm] is the spindle torque, D $[m]$ is the tool diameter and F_t $[N]$ is tangential cutting force.

In this study, the spindle current measured from the specified CNC machine is used and processed. The spindle current is preferred over X, Y and Z motor drive current due to the high level of noise usually present in these drives [31] but in general, they can also be used in this method.

The synchronization between the on-line operation and the virtual feedback file can add extra knowledge of the cutting operation. Through the use of cutting state detection and synchronization, the cutting states of the operation and the area of the cut are identified. Using the cutting states, the spindle current corresponding to the in-cut state is distinguished from the rest. For the next step, the distinguished spindle current samples are divided over their corresponding area of the cut as follows;

$$I_{Normalized} = \frac{I_{in\text{-}cut} - \bar{I}_{air-cut}}{A} \tag{3.10}$$

where $I_{in\text{-}cut}$ is the distinguished spindle current, A is the synchronized area of cut in $[mm^2]$, and $I_{Normalized}$ is the normalized spindle current in $[\frac{A}{mm^2}]$. Additionally, the average air-cut spindle current ($\bar{I}_{air-cut}$) is subtracted from the measurements to isolate the current related to the cutting torque.

Depending on the toolpath, the repetitive part of the operation can be identified. For example, for the toolpath shown in Figure 3.5, the repetitive part of the cutting operation consists of a sloped cut and a cleaning cut. In other words, the repetitive part consists of two consecutive cuts which can be selected by the user.

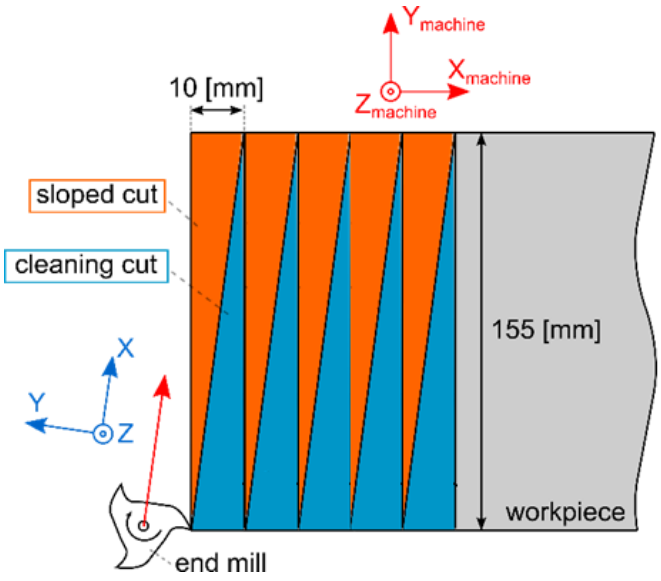

Figure 3.5. A designed toolpath consists of a repetitive sloped and cleaning cut [31]

Finally, the normalized spindle current parameters calculated in Eq. (3.10) for each cut are attached during one repetitive part of the operation which forms the normalized spindle current throughout one repetitive cut. The average normalized current is then monitored during the cutting operation

to detect the transition of flank wear zones. The tool wear monitoring process is summarized in Figure 3.6.

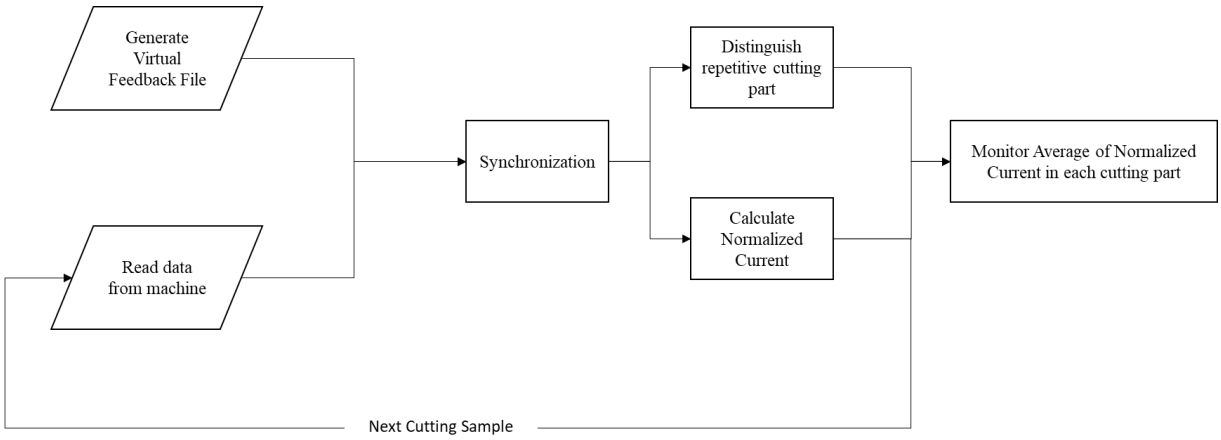

Figure 3.6. Flowchart of overall tool wear monitoring process

3.4 On-line Tool Wear Estimation

Since normalizing the average current with engagement area makes it independent of the variations in the tool-workpiece engagements along the tool path, it can be directly monitored to identify the three different wear zones. However, sometimes it is extremely useful to estimate the flank wear while the operation is in progress, thereby eliminating the need to measure flank wear several times. In the present study, the tool flank wear is estimated using cumulative chip thickness or using an average of normalized current. The relationship between these two parameters and flank wear is assumed to be linear during the entire tool life. The linear relationship is calibrated by having 2 or more wear measurements and applying a linear regression. The cumulative chip thickness and the average of normalized current are combined to monitor tool wear.

3.4.1 Method 1: Using Cumulative Chip Thickness

In this method, tool flank wear is only estimated using cumulative chip thickness. It is assumed that there is a linear relationship between these two parameters as follows;

$$w_{estimated_c} = a_{c_0} + a_{c_1} c \tag{3.11}$$

where c [mm] is cumulative chip thickness and $w_{estimated_c}$ [μm] is the corresponding estimated flank wear. a_{c_0} [μm] and a_{c_1} [$\frac{\mu m}{mm}$] coefficients are calibrated by applying linear regression [32]. Since the progression of wear vs. cumulative chip thickness presents three different zones, Eq. (3.11) is different for each wear zone. In this case, 2 wear measurements should be taken in each wear zone to identify the slope and intercept of the tool wear line. Tt is assumed that the relationship between tool wear and cumulative chip thickness is linear during the whole cutting operation. Therefore, two wear measurements are needed for the estimation method at first. 1 or 2 more wear measurements can be provided depending on the length of the cutting operation to update a_{c_0}, a_{c_1} coefficients.

3.4.2 Method 2: Using Average of Normalized Current

In the second method, the average of normalized current is used, and it is assumed that there is a linear relationship between it and flank wear as follows;

$$w_{estimated_I} = a_{I_0} + a_{I_1} \bar{I}_{Normalized} \tag{3.12}$$

where $\bar{I}_{Normalized}$ $[\frac{A}{mm^2}]$ is the average of normalized current and $w_{estimated_I}[\mu m]$ is the corresponding estimated flank wear. a_{I_0} $[\mu m]$ and a_{I_1} $[\frac{\mu m}{A/mm^2}]$ are calibrated using linear regression. Since wear versus average of normalized current is linear during the length of the cutting operation, two wear measurements are enough to estimate tool wear. Additional wear estimation can also be provided at any time by the operator to update the coefficient used in Eq. (3.12).

3.4.3 Method 3: Using Cumulative Chip Thickness and Average of Normalized Current

The cumulative chip thickness and average of normalized current are both used in this method. These two parameters are combined as follows;

$$w_{estimated_{c,I}} = a_{c,I_0} + a_{c,I_1} c + a_{c,I_2} \bar{I}_{Normalized} \tag{3.13}$$

where $w_{estimated_{c,I}}[\mu m]$ is the corresponding estimated flank wear. a_{c,I_0} $[\mu m]$, a_{c,I_1} $[\frac{\mu m}{mm}]$ and a_{c,I_2} $[\frac{\mu m}{A/mm^2}]$ are calibrated using MATLAB's multiple linear regression function [32]. Eq. (3.13) is for a plane rather than a line. The values of cumulative chip thickness and average of normalized current at any point during the cutting operation is known. By replacing them in Eq. (3.13), the tool flank wear can be estimated.

3.4.4 Method 4: Using Weighted Linear Combination of Flank Wear Estimation from Method 1 and 2

The estimated flank wear (w_c) from the cumulative chip thickness (Eq. (3.11)) and the wear (w_I) estimated from the average of normalized current (Eq. (3.12)) are combined by applying a weights p_c and p_I to each as follows;

$$w_{estimated_{c,I}} = \begin{bmatrix} w_c & w_I \end{bmatrix} \begin{Bmatrix} p_c \\ p_I \end{Bmatrix} \tag{3.14}$$

The weights are calibrated by solving Eq. (3.14) with least square function [32]. The same wear measurements that were taken to estimate tool wear in Eq. (3.11) and Eq. (3.12) are used to calibrate the weights. In this way, the estimation errors from each method are weighted to obtain an improved tool wear prediction.

3.5 Experimental Verification

The proposed tool wear monitoring with the digital twin is experimentally verified in milling tests conducted on the 5-axis Quaser UX600 CNC machine tool. The real-time data are collected using in-house developed monitoring software, INTELCUT, which communicates with the HEIDENHAIN CNC controller via TNC Ethernet connection. The tool center positions are collected at 333 [Hz] sampling frequency and nominal digital motor current, feedrate and spindle speed are collected at 10 [kHz] sampling frequency but reduced to 333 [Hz] to synchronize with current data.

The virtual feedback file is first generated for each toolpath. The real-time data are also collected and stored. The tool wear monitoring and detection algorithm are implemented on MATLAB [32], where virtual file is first uploaded, and the stored data are fed to the software. The tool wear monitoring algorithm is then applied and verified by regularly inspecting the end mill's flank surface (w_{flank}) under the microscope. This algorithm is currently incorporated into the INTELCUT software for on-line tool wear monitoring.

3.5.1 Case 1: Sloped Cutting Experiment

A sloped cutting test was performed where a 12 [mm] diameter end mill with 3 flutes was used to cut an AISI 1050 steel workpiece. The toolpath consists of a sloped cut with increasing radial immersion. Following this, a cleaning cut is made to remove the excess material before the next cut. In this experiment, the sloped cut and the cleaning cut are selected as a repetitive cut which is repeated 235 times. The toolpath is provided to MACHpro™ as illustrated in Figure 3.1 and the virtual feedback file is generated. The test setup and the corresponding toolpath used in this cutting operation are presented in Figure 3.7 and further details for this cutting experiment is documented in Table 3.3.

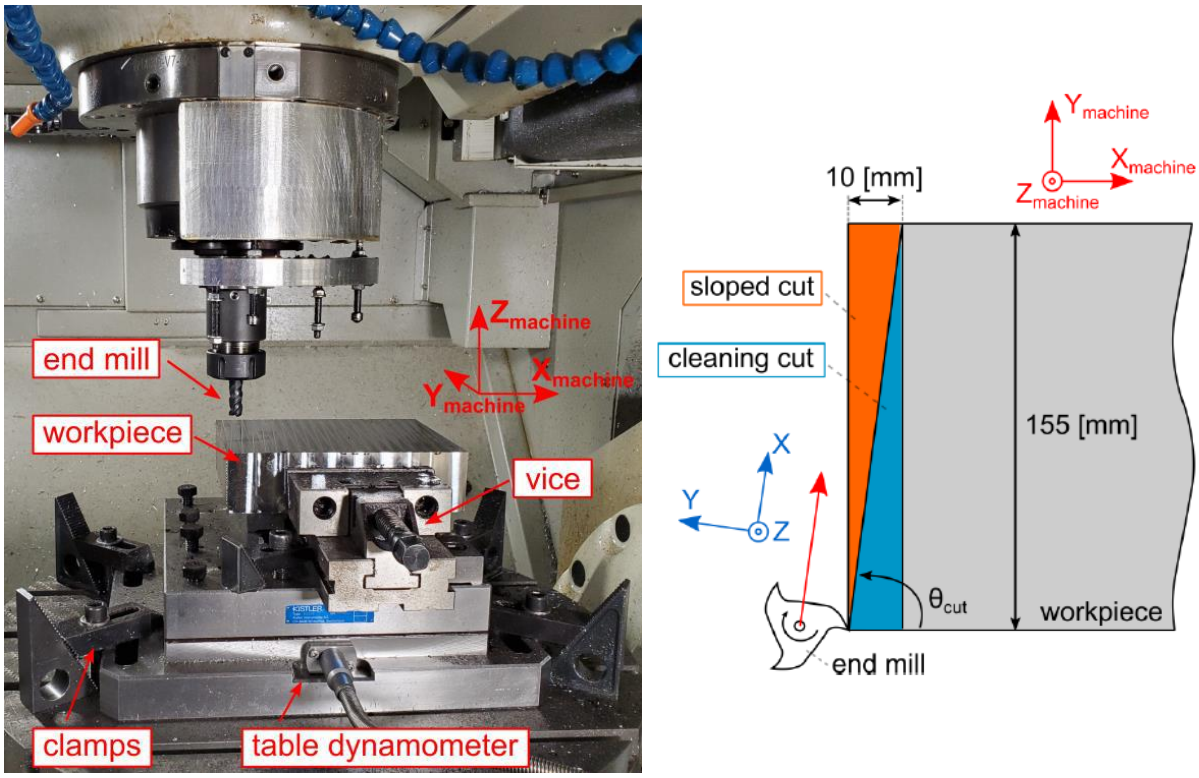

(a) (b)

Figure 3.7. (a) Overview of the test setup and (b) Overall view of the designed toolpath for one iteration of the cutting operation. The red coordinate is $\boldsymbol{XYZ_{Machine}}$ frame and the blue coordinate is defined as a local frame in the feed, normal and axial directions of the cut [adopted from 35]

Table 3.3. Specifications of the cutting experiment [adopted from 35]

Tool	Diameter: 12 [mm]	Rake angle: 8 [deg]
	Corner radius: 0.5 [mm]	Helix Angle: 48 [deg]
	Number of flutes: 3	
Workpiece Material	AISI 1050 Steel	
Cutting Conditions	Spindle Speed: 8000 [rev/min]	
	Feedrate: 0.1 [mm/flute/rev]	
	Depth of Cut: 2 [mm]	

First, the X, Y, Z tool positions collected from the CNC machine are synchronized with the X, Y, Z simulated positions stored in virtual feedback file. The synchronization results can be seen for 5 consecutive cuts in Figure 3.8.

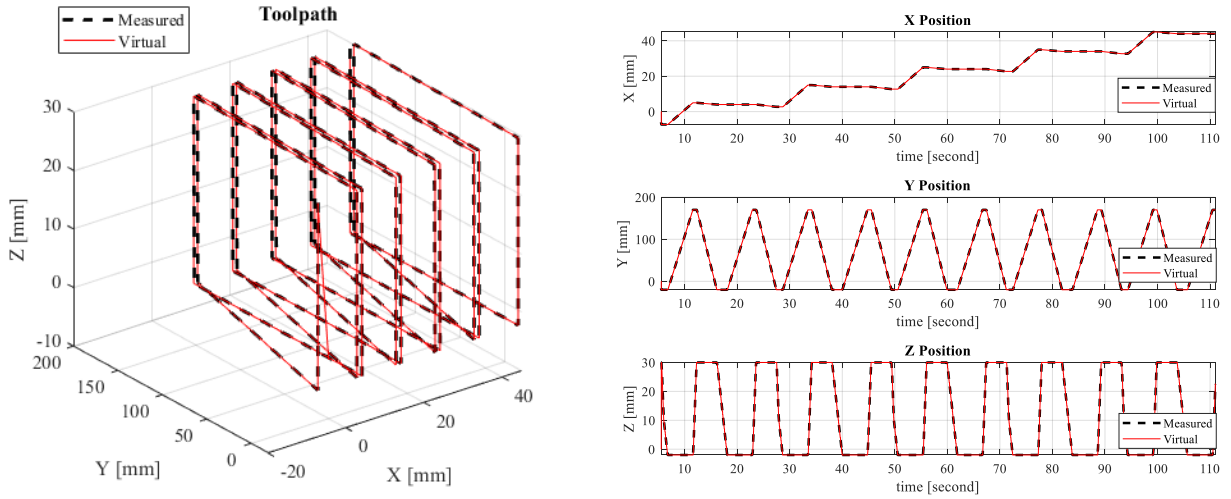

(a) (b)

Figure 3.8. (a) Simulated and real-time collected toolpath synchronization and (b) Simulated and real-time collected tool center positions synchronization in an experiment in which a sloped cut is repeated five times

Synchronization being conducted, the engagement for each cutting sample, the in-cut state and the number of repetitive cuts is identified. The spindle motor current corresponding to each in-cut state is distinguished. The spindle current and the synchronized cutting states over time in the span of the first cut are presented in Figure 3.9.a and the distinguished spindle current is presented in Figure 3.9.b for the same cut. The in-cut spindle current between the beginning cut and the end cut are compared to each other in Figure 3.10. Due to the increased cutting forces which is caused by the tool wear and the direct relationship between cutting force and current as explained in Eq. (3.9) , this observation was expected.

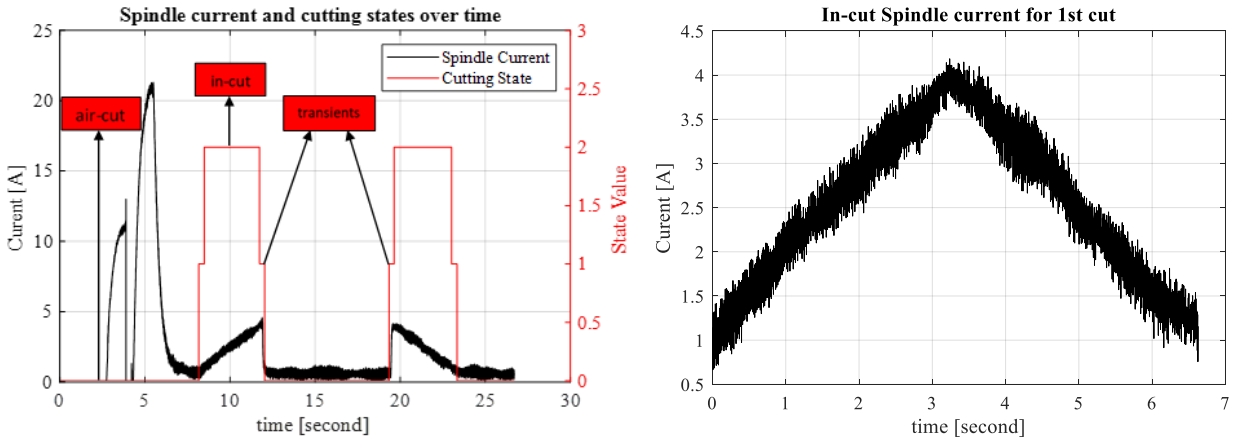

(a) (b)

Figure 3.9. Spindle Current on top of synchronized cutting states and (b) In-cut spindle current for 1st cutting part

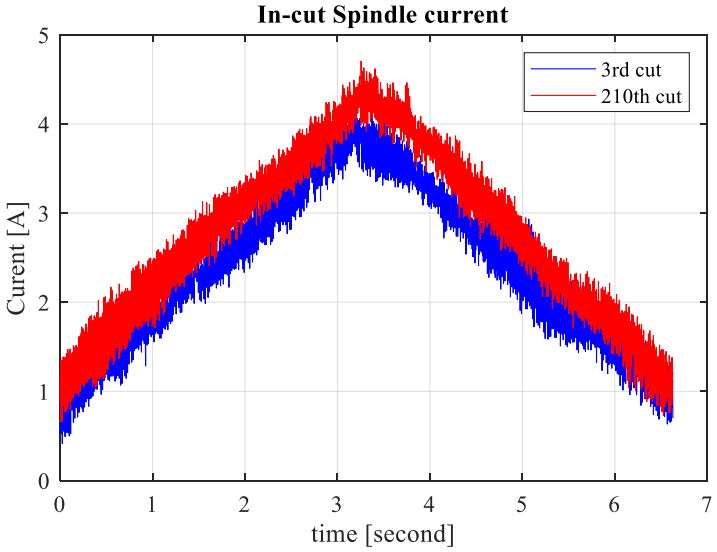

Figure 3.10. Comparing in-cut spindle current for 3rd and 210th cut

The average of normalized current over cumulative chip thickness is shown in Figure 3.11. In the X axis, the number of cuts is replaced with the cumulative chip thickness which represents the progress in the cutting operation. The linear fitting of the data shows three different rates. To verify

this result, the end mill's flank surface was regularly measured under the microscope. Figure 3.12 illustrates the progression of flank wear averaged across all flutes.

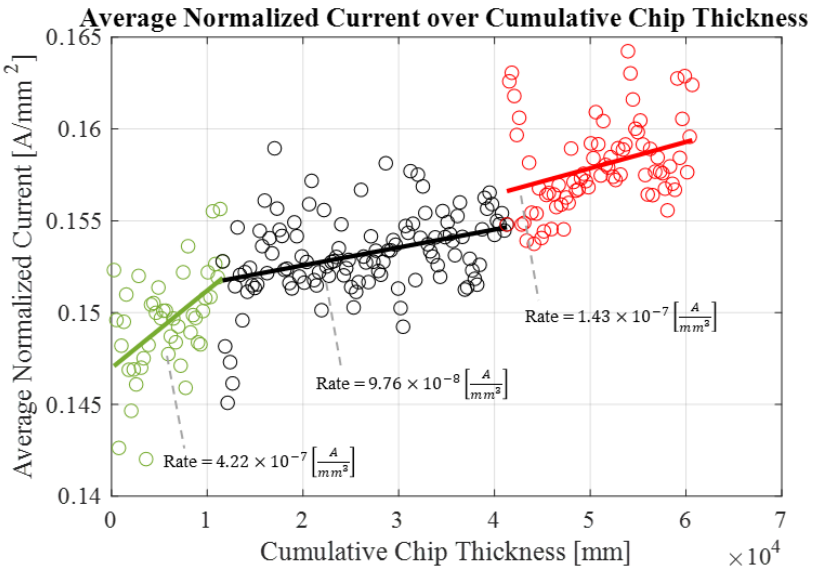

Figure 3.11. Average of normalized current over cumulative chip thickness during the sloped cutting experiment

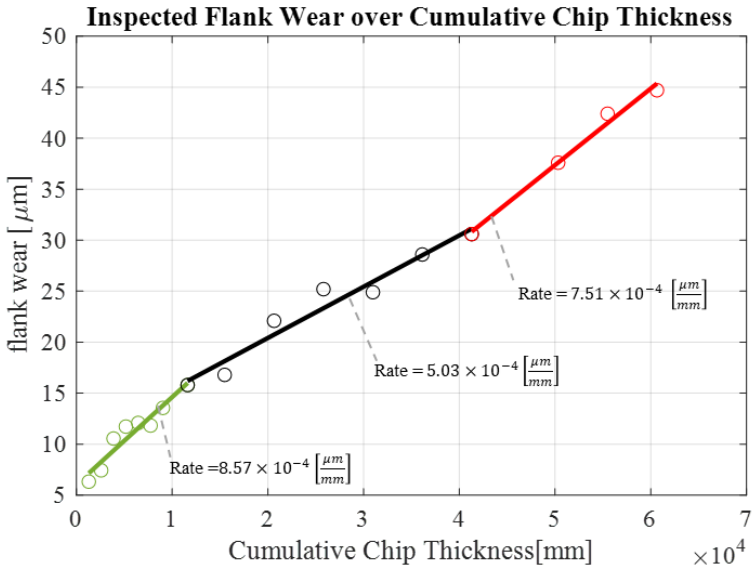

Figure 3.12. Inspected flank wear over cumulative chip thickness during the sloped cutting experiment [31]

Additionally, the rate of change in the flank wear $d(w_{flank})/d(c)$ and the average of the normalized current $d(\bar{I}_{Normalized})/d(c)$ under three wear zones are tabulated in Table 3.4 where c is cumulative chip thickness. The percentage variations from one wear zone to the next are also shown. It can be observed that the transition of wear zones for $d(\bar{I}_{Normalized})/d(c)$ and $d(w_{flank})/d(c)$ are similar from zone two to three but they are a bit exaggerated from zone one to two which can happen because of the noise in the measured spindle current and fast wear of fresh-sharp cutting edge in the beginning of the cut. Overall, the average spindle current is a suitable indicator for tool health monitoring.

Table 3.4. A comparison of the rates of change in flank wear and the average normalized current for the three wear zones. A percentage variation from the transition of wear zones is also shown.

Wear Zone	$d(w_{flank})/d(c)[\frac{\mu m}{mm}]$	$d(\bar{I}_{Normalized})/d(c)\ [\frac{A}{mm^3}]$
#1 initial	8.57×10^{-4}	4.22×10^{-7}
#2 Steady	5.03×10^{-4} ↓ 41 [%] from zone #1	9.76×10^{-8} ↓ 76 [%] from zone #1
#3 accel.	7.51×10^{-4} ↑ 49 [%] from zone #2	1.43×10^{-7} ↑ 47 [%] from zone #2

Although the average normalized current can be used directly to estimate flank wear, due to present noise in data, a moving average is applied in each wear zones that are already classified. Therefore, a set of new points are obtained which can be replaced with the previous points. The obtained points on top of the previous points are illustrated in Figure 3.13. Since a waiting time is needed

before applying the moving average, a gap is seen in the obtained points at the beginning of the cutting operation.

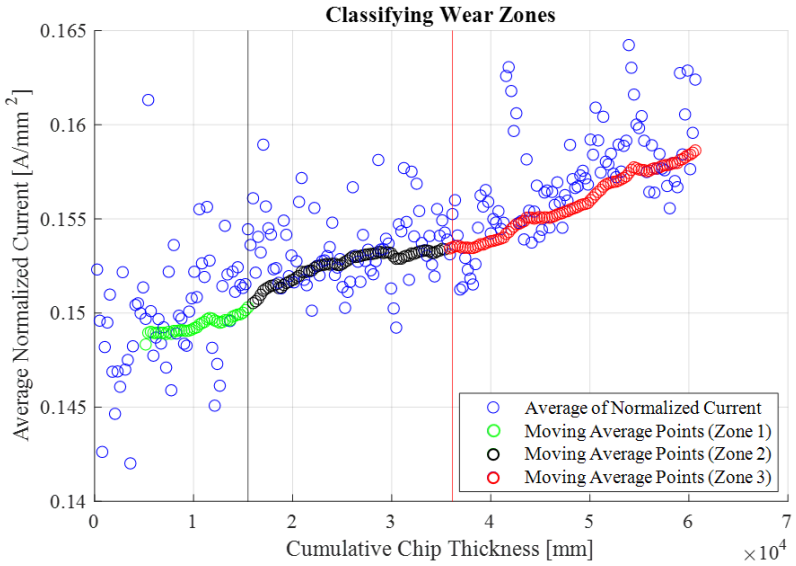

Figure 3.13. Applying moving average in each wear zone

Finally, the flank wear is estimated using four different methods as described in Section 3.4. Figure 3.14 to Figure 3.17 illustrate the estimated and measured flank wear for methods 1 to 4 respectively. The green, black and red points are estimated tool flank wear by using 2, 3, 4 wear measurements (purple points) respectively. The blue points are the regularly inspected tool wear measurements to verify the estimations. Moreover, the coefficients used in method 1 to 3 are given in Table 3.5 to Table 3.7 and the weights used in method 4 are given in Table 3.8.

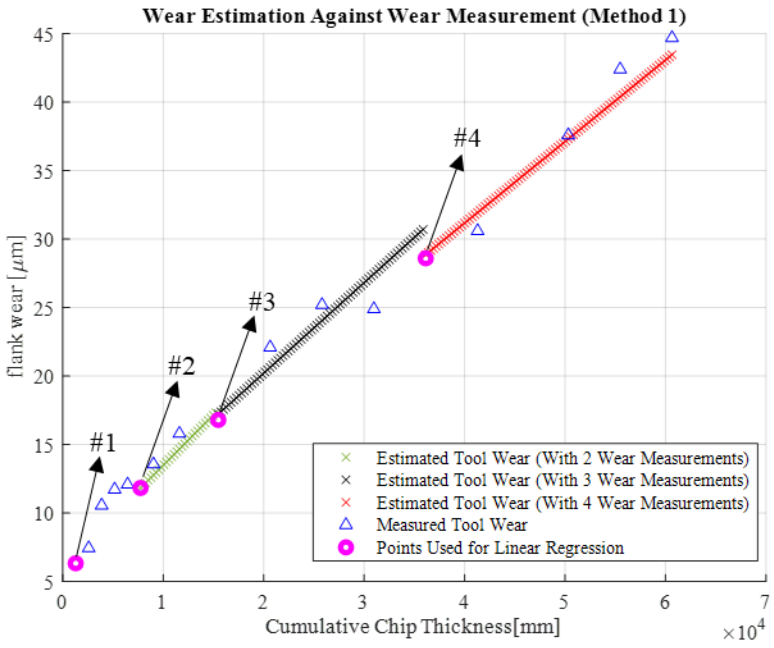

Figure 3.14. In-process estimation of flank wear using cumulative chip thickness (method 1) in sloped cutting experiment

Table 3.5. Coefficients for tool flank wear as a linear function of cumulative chip thickness calibrated by different number of wear measurements in sloped cutting experiment

	a_{c_0} $[\mu m]$	a_{c_1} $[\frac{\mu m}{mm}]$
2 Wear Measurements (update 1)	6.14	7.35×10^{-4}
3 Wear Measurements (update 2)	6.99	6.61×10^{-4}
4 Wear Measurements (update 3)	7.36	5.95×10^{-4}

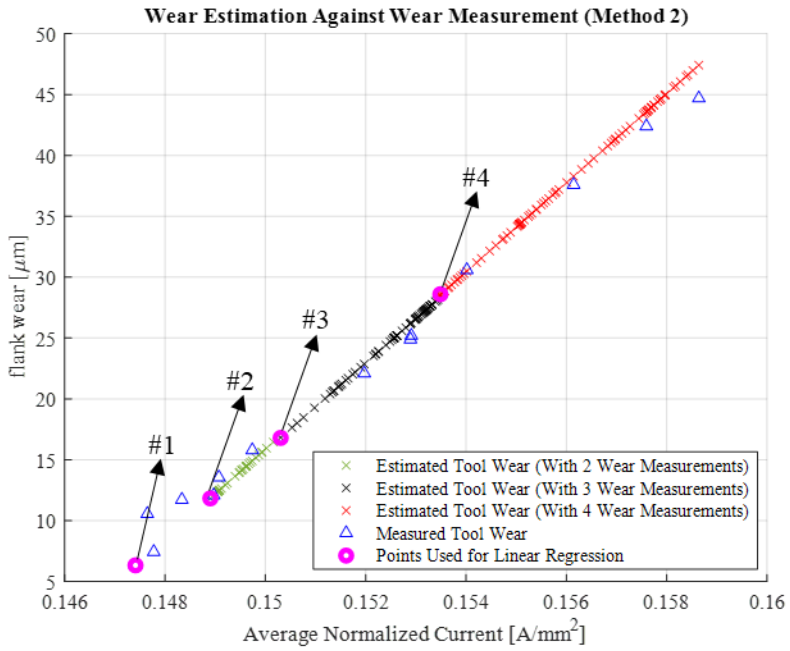

Figure 3.15. In-process estimation of flank wear using average of normalized current (method 2) in sloped cutting experiment

Table 3.6. Coefficients for tool flank wear as a linear function of average of normalized current calibrated by different number of wear measurements in sloped cutting experiment

	$a_{I_0}\ [\mu m]$	$a_{I_1}\ [\frac{\mu m}{A/mm^2}]$
2 Wear Measurements (update 1)	-537.2	3.69×10^3
3 Wear Measurements (update 2)	-527.0	3.62×10^3
4 Wear Measurements (update 3)	-533.4	3.66×10^3

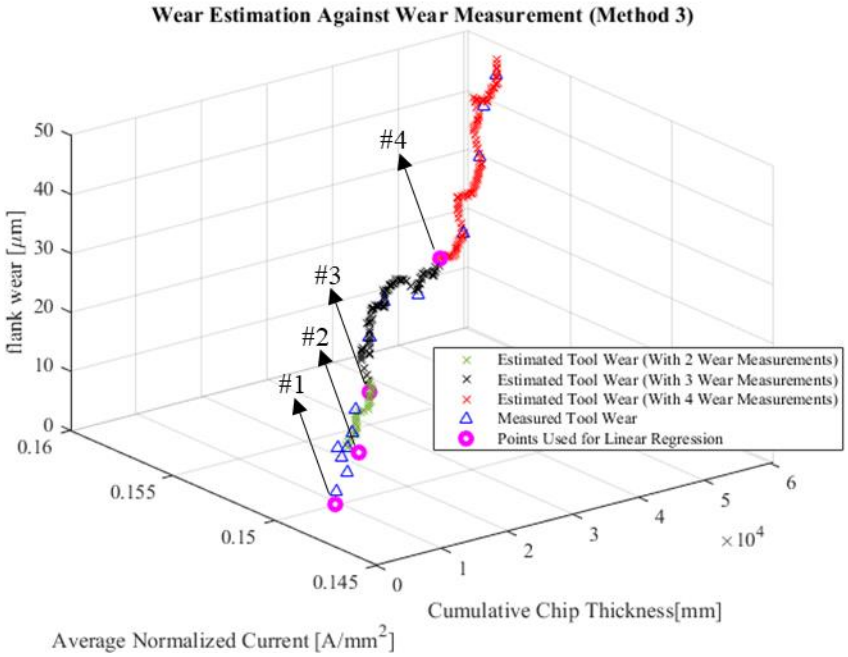

Figure 3.16. In-process estimation of flank wear using cumulative chip thickness and average of normalized current (method 3) in sloped cutting experiment

Table 3.7. Coefficients for tool flank wear as a function of cumulative chip thickness and average of normalized current calibrated by different number of wear measurements in sloped cutting experiment

	$a_{I,c_0}\ [\mu m]$	$a_{I,c_1}\ [\frac{\mu m}{mm}]$	$a_{I,c_2}\ [\frac{\mu m}{A/mm^2}]$
2 Wear Measurements (update 1)	5.23	8.52×10^{-4}	0
3 Wear Measurements (update 2)	-613.5	-1.20×10^{-4}	4.21×10^{3}
4 Wear Measurements (update 3)	-507.4	3.03×10^{-5}	3.49×10^{3}

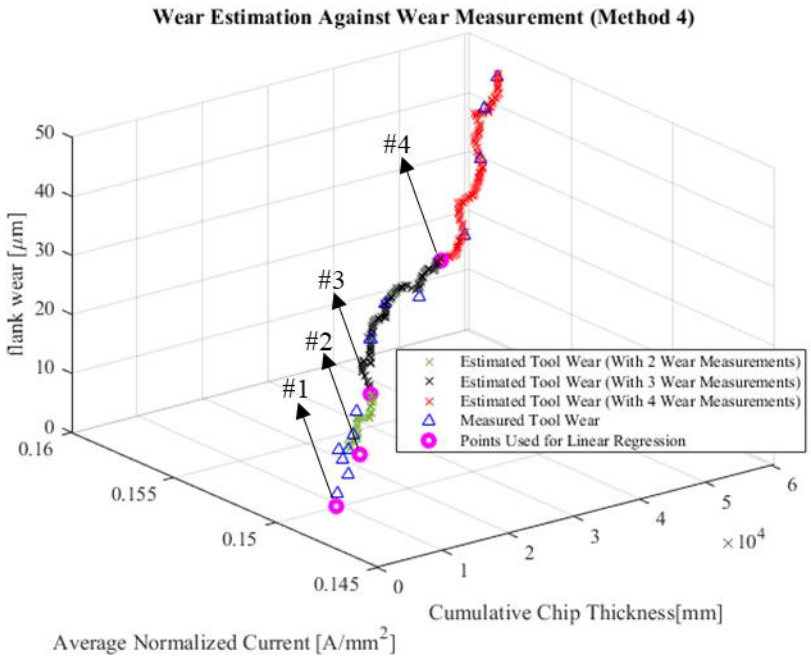

Figure 3.17. In-process estimation of flank wear using estimated flank wear from cumulative chip thickness and average of normalized current (method 4) in sloped cutting experiment

Table 3.8. Assigned weights to estimated flank wear from method 1 and 2 calibrated by different number of wear measurements in sloped cutting experiment

	w_c	w_I
2 Wear Measurements (update 1)	0.50	0.50
3 Wear Measurements (update 2)	0.49	0.49
4 Wear Measurements (update 3)	0.49	0.49

Finally, the error between the estimated tool flank wear and the measured tool wear is calculated for each method and is given in Table 3.9. The errors are calculated by comparing the regularly inspected tool wear measurements (blue points) with the estimations. The errors are under 10 percent. Method 3 has the lowest error among others.

Table 3.9. Error between estimated and measured tool flank wear for method 1 to 4 in sloped cutting experiment

Method	Error [%]
1. Cumulative Chip thickness	4.6
2. Average of Normalized Current	3.5
3. Cumulative Chip thickness & Average of Normalize Current	3.8
4. Weighted linear combination of methods 1 & 2	2.6

3.5.2 Case 2: Pocket Cutting Experiment

In the second case, a pocket machining experiment is conducted where a 25 [mm] indexable end mill with 4 inserts is used to cut an AISI 1050 steel workpiece. It should be noted that the end mill used in this case is different from the tool used in the first cutting experiment. The toolpath consists of two identical but mirrored pockets. Machining each pocket was divided into four sections and each insert's flank wear was measured at the end of each section under a microscope. The toolpath for each pocket consists of 25 repetitive cuts. Since the toolpath of the two pockets is mirrored, a total number of 50 similar cuts are conducted. The test setup is illustrated in Figure 3.18.a and the final machined part can be seen in Figure 3.18.b. Figure 3.18.c presents the simulation of the cutting operation in MACHpro™. Based on this model, the needed machining states are selected,

and the virtual feedback file is generated. Further details for this cutting experiment are tabulated in Table 3.10.

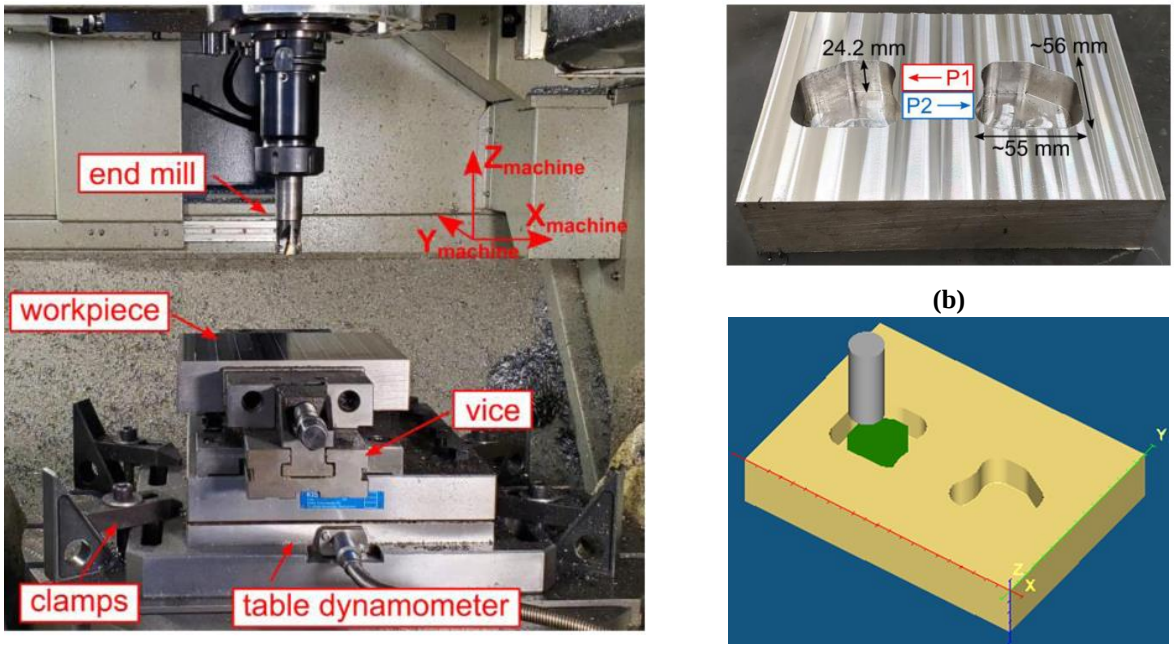

Figure 3.18. (a) Pocket machining experiment test setup [adopted from 37] (b) machined part with overall dimensions. Pocket P1 and P2 are identical and mirrored and their dimension is 55 [mm] × 56 [mm] × 24.2 [mm] [adopted from 37] (c) Virtual machining of the pocket machining experiment

Table 3.10. Specifications of the cutting experiment [adopted from 37]

Tool	Diameter: 25 [mm]	Rake angle: 18 [deg]
	Corner radius: 0.4 [mm]	Number of inserts: 4
Workpiece Material	AISI 1050 Steel	
Cutting Conditions	Spindle Speed: 4500 [rev/min]	
	Feedrate: 0.1 [mm/flute/rev]	

The synchronization results for the first section of machining the left pocket (see Figure 3.18.b), which consists of 6 consecutive cuts, are shown in Figure 3.19. Same as in the previous case, the in-cut state is distinguished from the rest of the cutting operation. The repetitive cut of the pocket machining toolpath engaged with the workpiece twice. This number can be selected by the user so that the algorithm attaches the two consecutive in-cut spindle currents together and considers it as one cut. Then it can compare it to the following cuts. Figure 3.20.a show the spindle motor current and the corresponding cutting states, and Figure 3.20.b shows the in-cut spindle current throughout first cutting part. As it is observed in these two figures, in-cut states are identified twice consecutively, and the two in-cut spindle currents are attached together.

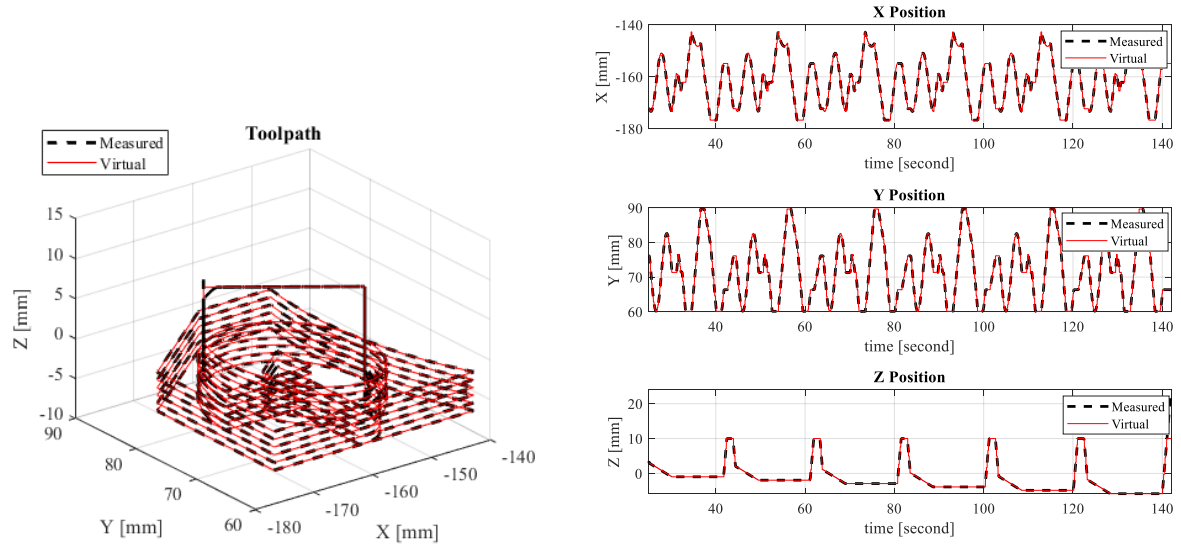

(a) (b)

Figure 3.19. (a) Simulated and real time collected toolpath synchronization and (b) Simulated and real time collected tool center positions synchronization in the pocket machining for 6 consecutive cutting parts

The in-cut spindle current for the first and last cuts during the machining of both pockets is depicted in Figure 3.21. The expected gradual increase in in-cut spindle currents due to the increased cutting forces is evident in this figure.

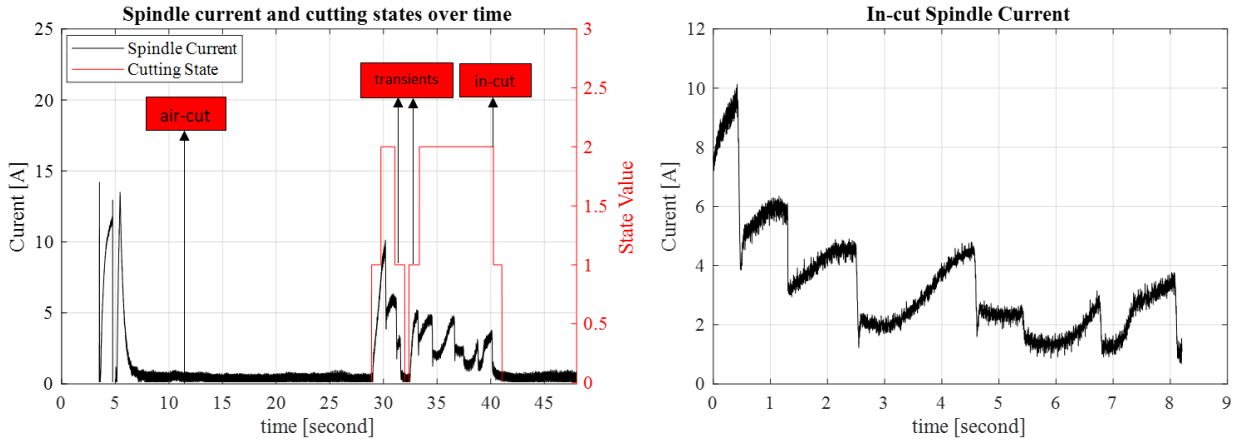

(a) (b)

Figure 3.20. (a) Spindle Current on top of synchronized cutting states and (b) In-cut spindle current for 1st cut

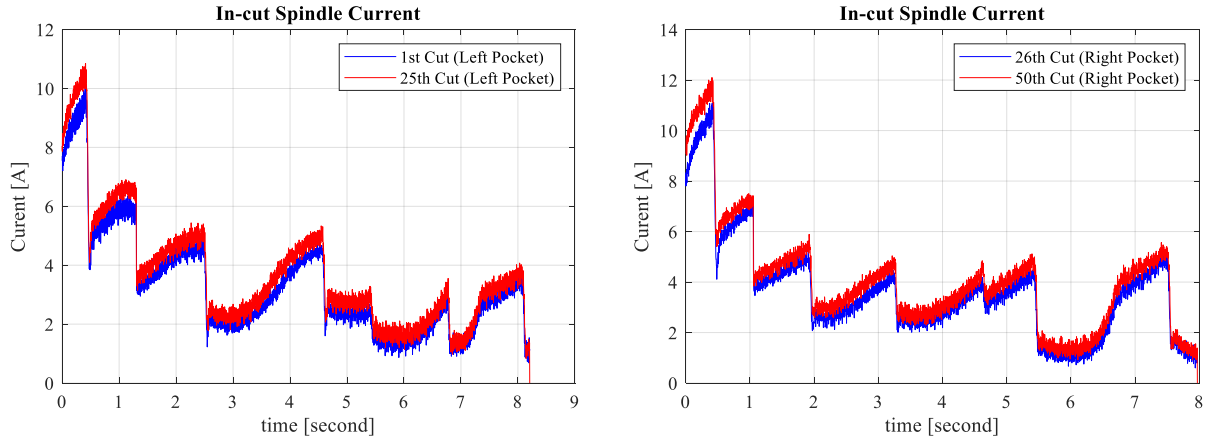

(a) (b)

Figure 3.21. Comparing in-cut spindle current for first and last cut of left and right pocket

Average of normalized current over cumulative chip thickness is shown in Figure 3.22. The linear fitting is applied to the points and the rate of change is demonstrated. The end mill's flank surface was regularly inspected under the microscope. Figure 3.23 illustrates the progression of flank wear averaged across all inserts. As it is observed, only one wear zone is present and confirms the result obtained from the average of normalized current.

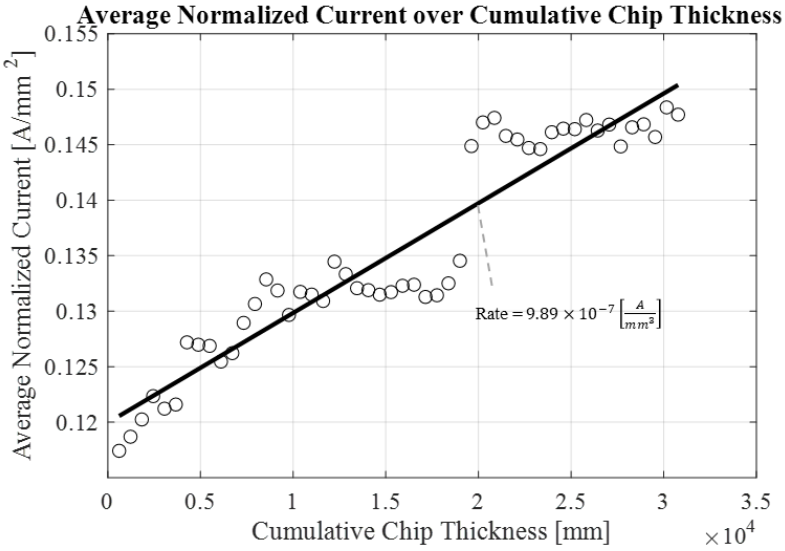

Figure 3.22. Average of normalized current over cumulative chip thickness in the pocket machining experiment

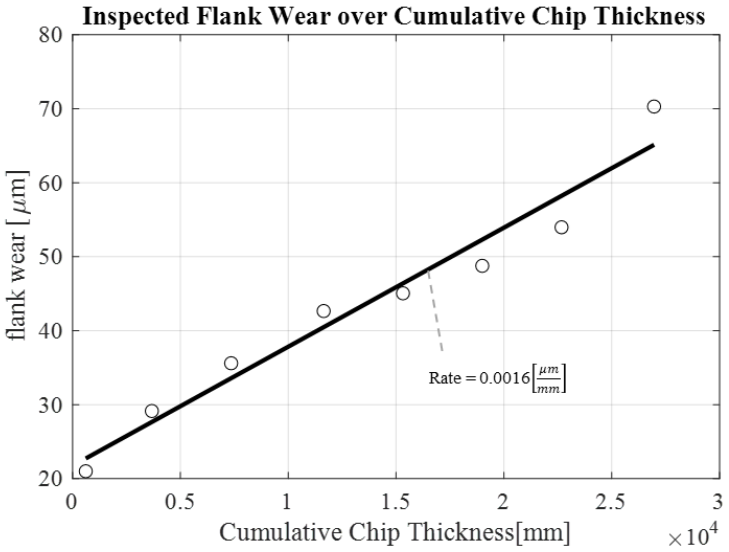

Figure 3.23. Inspected flan wear over cumulative chip thickness in the pocket machining experiment

Same as the previous case, to estimate the end mill's in-process flank wear the wear zones identification method is applied and one wear zone is detected. A backward moving average is followed up, and the filtered points can be seen in Figure 3.24.

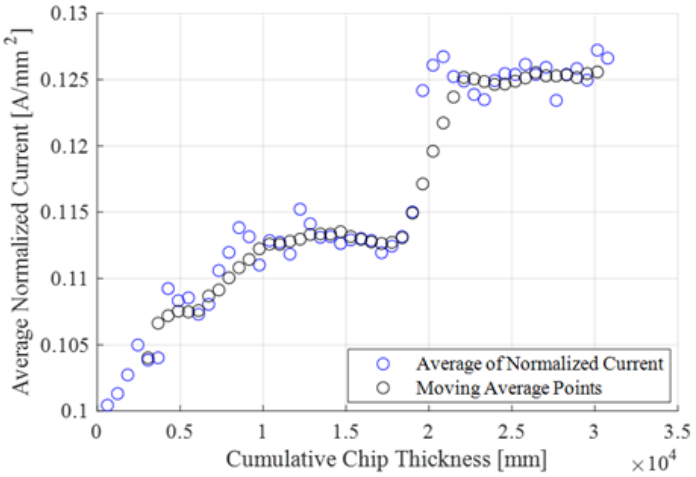

Figure 3.24. Applying moving average

Finally, the flank wear estimation using method 1 to 4 are shown in Figure 3.25 to Figure 3.28 respectively. The coefficients used in method 1 to 3 are shown in Table 3.11 to Table 3.13 and the assigned weights in method 4 is given in Table 3.14. In this experiment, tool wear is estimated using 2-3 wear measurements (purple points). The blue points are the regularly inspected tool wear under the microscope during the cutting operation for verification of the estimation methods. The flank wear estimations are shown on top of the flank wear measurement. Based on their comparison, it is evident that the estimation methods are reliable in this case as well.

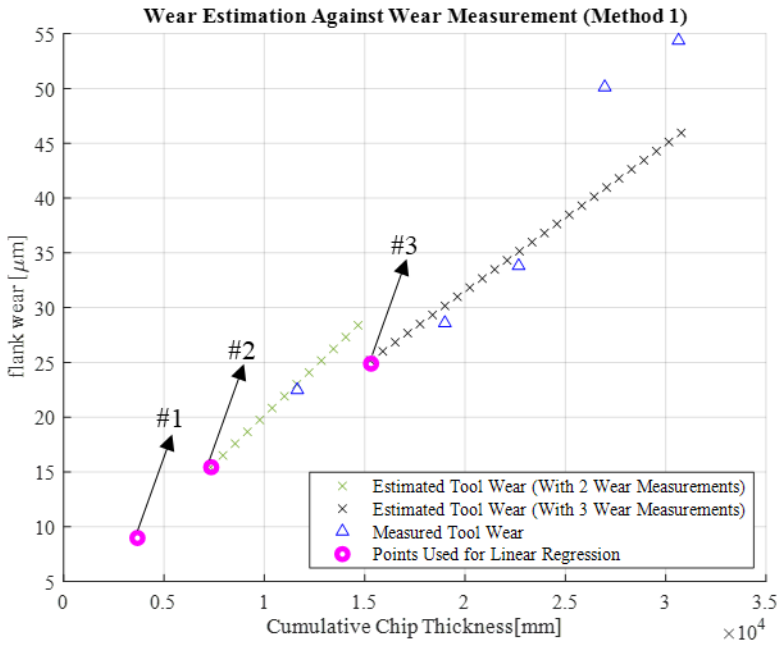

Figure 3.25. In-process estimation of flank wear using cumulative chip thickness in pocket cutting experiment

Table 3.11. Coefficients for tool flank wear as a linear function of cumulative chip thickness calibrated by different number of wear measurements in pocket cutting experiment

	$a_{c_0}\ [\mu m]$	$a_{c_1}\ [\frac{\mu m}{mm}]$
2 Wear Measurements (update 1)	2.50	1.8×10^{-3}
3 Wear Measurements (update 2)	4.69	1.3×10^{-3}

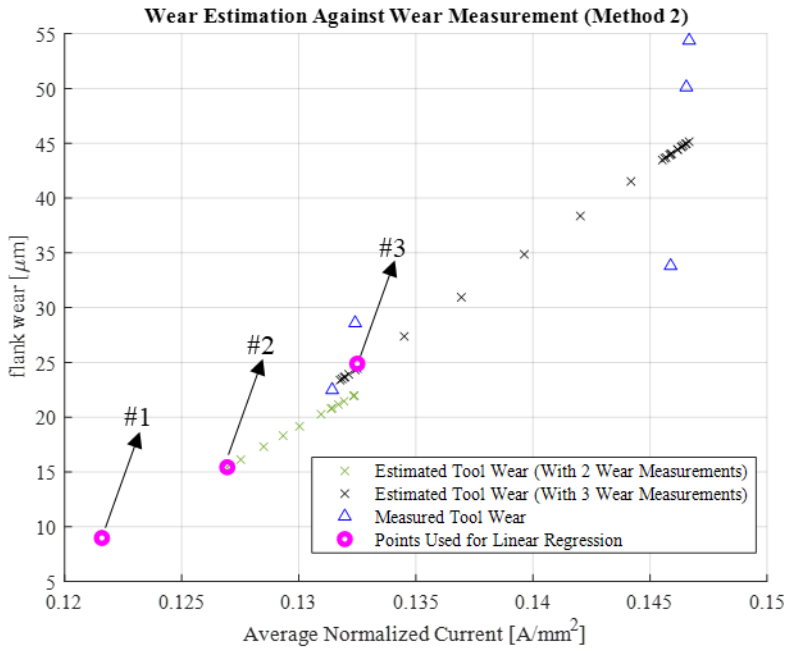

Figure 3.26. In-process estimation of flank wear using average of normalized current in pocket cutting experiment

Table 3.12. Coefficients for tool flank wear as a linear function of the average of normalized current calibrated by different number of wear measurements in a pocket cutting experiment

	$a_{I_0}\ [\mu m]$	$a_{I_1}\ [\frac{\mu m}{A/mm^2}]$
2 Wear Measurements (update 1)	-137.7	1.21×10^3
3 Wear Measurements (update 2)	-169.1	1.46×10^3

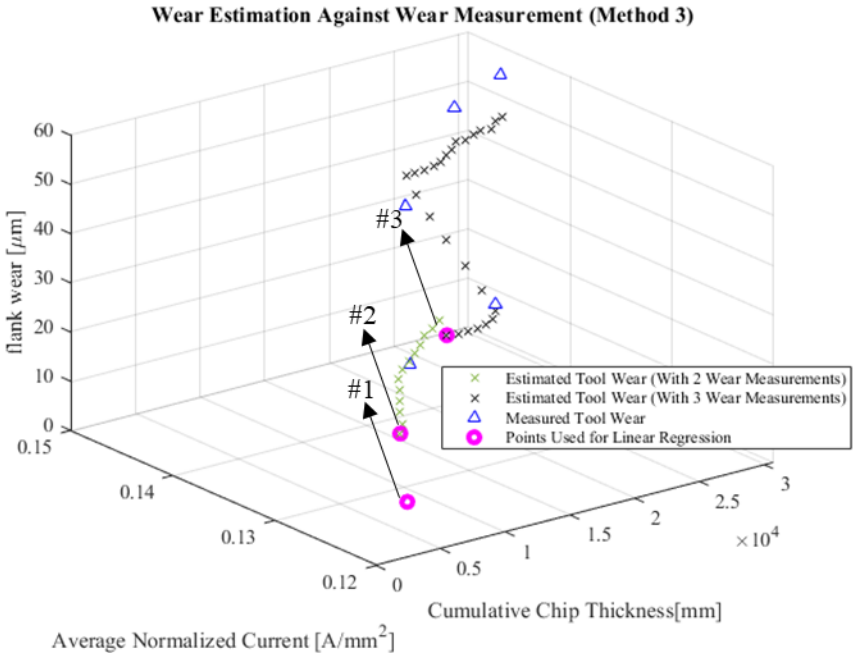

Figure 3.27. In-process estimation of flank wear using cumulative chip thickness and average of normalized current in the pocket cutting experiment

Table 3.13. Coefficients for tool flank wear as a function of cumulative chip thickness and average of normalized current calibrated by different number of wear measurements in pocket cutting experiment

	a_{I,c_0} $[\mu m]$	a_{I,c_1} $[\frac{\mu m}{mm}]$	a_{I,c_2} $[\frac{\mu m}{A/mm^2}]$
2 Wear Measurements (update 1)	2.50	1.8×10^{-3}	0
3 Wear Measurements (update 2)	-85.02	6.63×10^{-4}	753.07

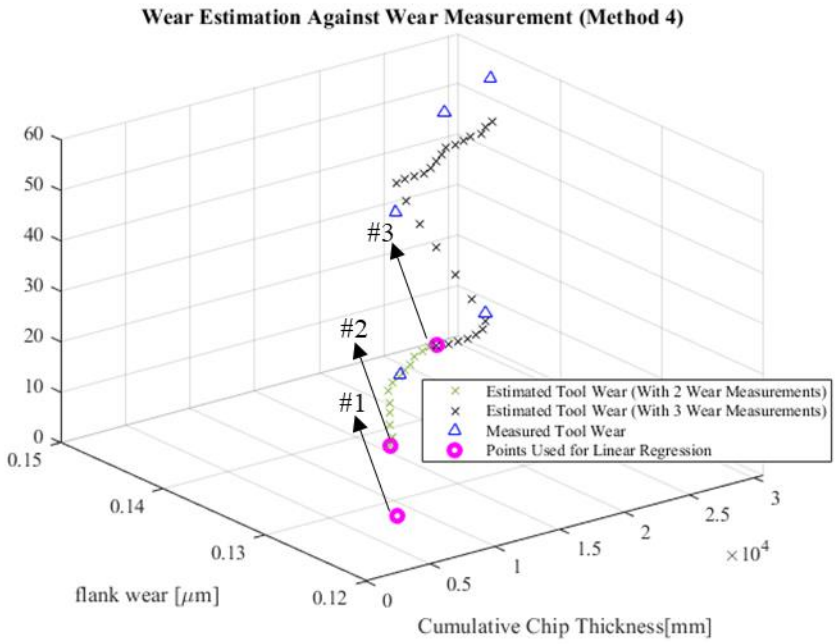

Figure 3.28. In-process estimation of flank wear using estimated flank wear from cumulative chip thickness and average of normalized current in pocket cutting experiment

Table 3.14. Assigned weights to estimated flank wear from methods 1 and 2 calibrated by different numbers of wear measurements in a pocket cutting experiment

	w_c	w_I
2 Wear Measurements (update 1)	0.5	0.5
3 Wear Measurements (update 2)	0.49	0.51

Finally, the estimated flank wear from each method is compared to the measured tool wear and the error is given in Table 3.15. The errors are all under 20 percent, so the flank wear estimation methods have been verified to be suitable candidates for use. By doing so, the operator can reduce the number of wear measurements to only four, thereby saving time from removing the tool from the spindle and measuring flank wear under a microscope. If spindle motor current measurements

are noisy, Table 3.15 shows that the cumulative chip thickness can be used to track tool wear with 7.7% error.

Table 3.15. The error between estimated and measured tool flank wear for method 1 to 4 in pocket cutting experiment

Method	Error [%]
1. Cumulative Chip thickness	7.7
2. Average of Normalized Current	13.6
3. Cumulative Chip thickness & Average of Normalize Current	9.0
4. Weighted linear combination of method 1 & 2	9.2

3.5.3 Case 3: Stacked Cutting Experiment

In case 3, a down milling experiment is conducted where a 25 [mm] indexable end mill with 4 inserts is used to cut an AISI 1050 steel workpiece. The tool used in this experiment is the same as the tool used in case 2. The toolpath consists of 5 stacks (see Figure 3.29.b) and the toolpath for each stack is divided into 4 sections. Each stack is 10 [mm] high which means the axial depth in each section of the cuts is 2.5 [mm]. The test setup is illustrated in Figure 3.29.a. Final machined part can be seen in Figure 3.29.b. As it is obvious the tool removes less material as it goes downward to the next stack. The virtually machined part is presented in Figure 3.29.c. The simulated machining states are selected using this model and stored. Further details for this cutting experiment are given in Table 3.16.

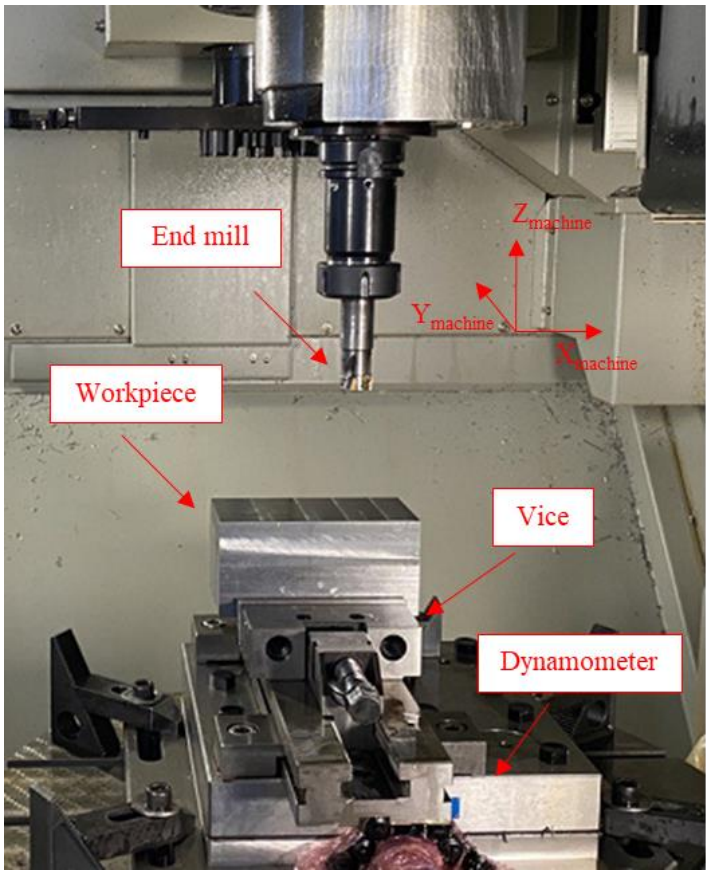

(a)

(b)

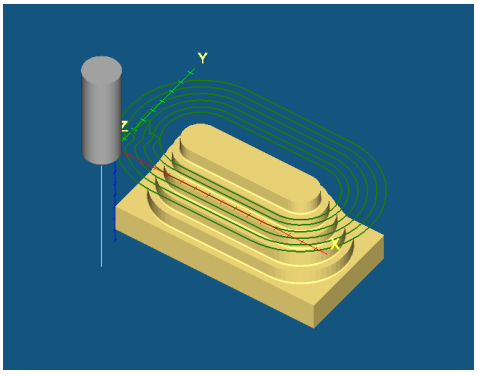

(c)

Figure 3.29. (a) Machining experiment test setup (b) Machined part (c) Virtual machining of the part

Table 3.16. Specifications of the cutting experiment

Tool	Diameter: 25 [mm]	Rake angle: 18 [deg]
	Corner radius: 0.4 [mm]	Number of flutes: 4
	Tool Length: 70.1 [mm]	
Workpiece Material	AISI 1050 Steel	
Cutting Conditions	Spindle Speed: 3360 [rev/min]	Axial Depth of Cut: 2.5 [mm]
	Feedrate: 0.1 [mm/flute/rev]	Radial Depth of Cut: 5 [mm]

The synchronization between the collected and virtual tool center positions for machining the first section of the first stack is shown in Figure 3.30. The spindle current on top of the synchronized cutting states and the distinguished in-cut spindle current from the rest of the measured spindle current can be seen in Figure 3.31.a and Figure 3.31.b respectively. Additionally, the gradual increase of in-cut spindle current due to tool wear can be seen in Figure 3.32.

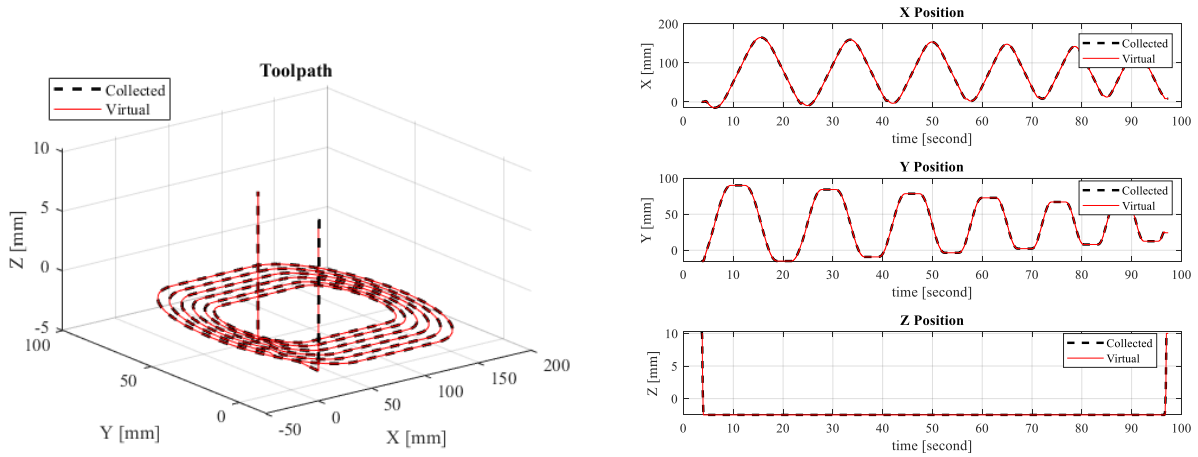

(a) (b)

Figure 3.30. (a) Simulated and real time collected toolpath synchronization (b) Simulated and real time collected ***X***, ***Y***, ***Z*** tool center positions synchronization for the first section of first stack

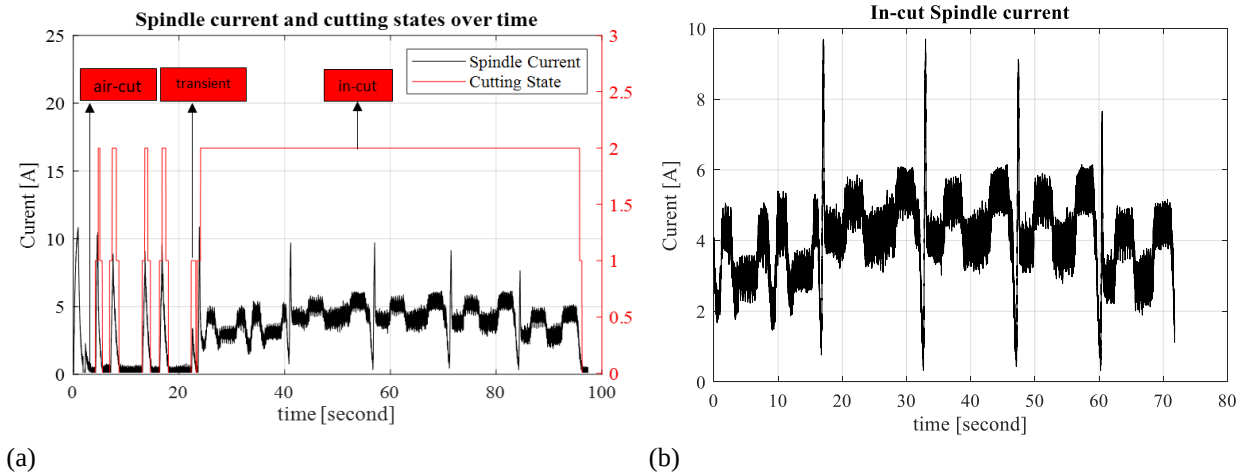

(a) (b)

Figure 3.31. (a) Spindle Current on top of synchronized cutting states and (b) In-cut spindle current for first section of first stack

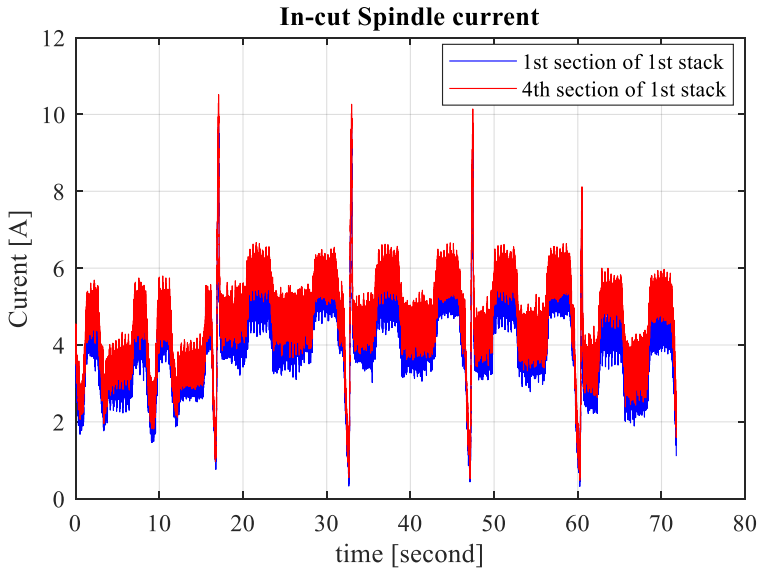

Figure 3.32. Comparing in-cut spindle current for the first and fourth sections of stack

The in-cut spindle current is divided by the area of cut to obtain an average of normalized current. The progression of the average of normalized current is presented in Figure 3.33. The progression of tool wear across all inserts is presented in Figure 3.34. The wear zones are identified in both of these figures and a green, black and red line is passed from the points in zone 1, 2 and 3 respectively. The rate of change in the flank wear $d(w_{flank})/d(c)$ and average of the normalized current $d(\bar{I}_{Normalized})/d(c)$ under three wear zones are tabulated in Table 3.17. Similar to case 1, It can be observed that the transitions from zone 1 to 2 and zone 2 to 3 for $d(w_{flank})/d(c)$ comparing to $d(\bar{I}_{Normalized})/d(c)$ is about 20% exaggerated. However, this experiment still confirms the average of normalized current is an appropriate indicator for tool health monitoring.

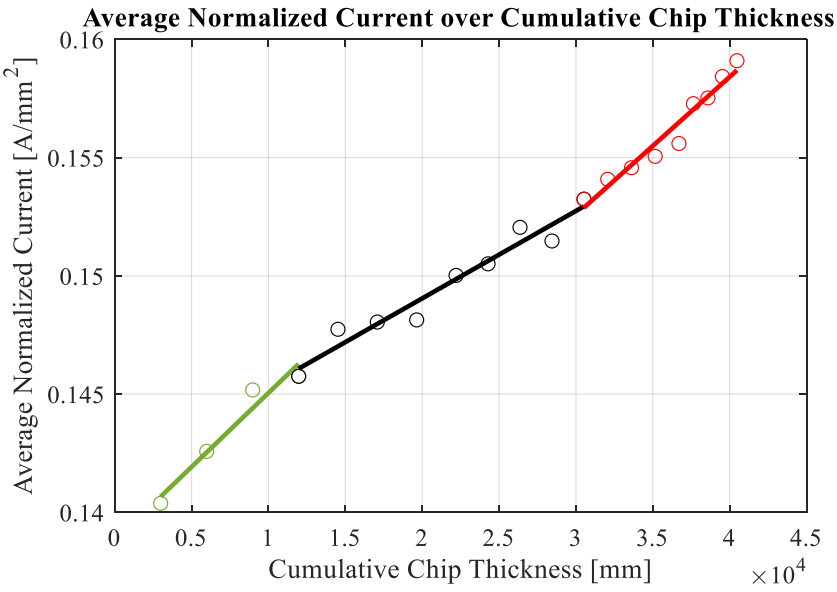

Figure 3.33. Average of normalized current over cumulative chip thickness in stacked cutting experiment (green: zone 1, black: zone 2, red: zone 3). The progression of average of normalized current is steep at first, then decreases and is accelerated again

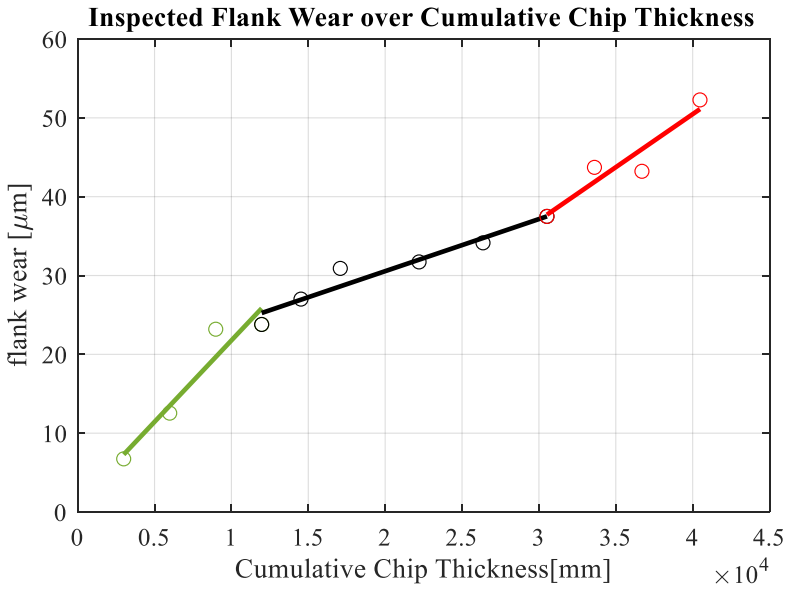

Figure 3.34 Inspected flank wear over cumulative chip thickness in stacked cutting experiment (green: zone 1, black: zone 2, red: zone 3). The progression of inspected flank wear is steep at first, then decreases and is accelerated again

Table 3.17. A comparison of the rates of change in flank wear and the average normalized current for the three wear zones in stacked cutting experiment. A percentage variation from the transition of wear zones is also shown.

Wear Zone	$d(w_{flank})/d(c)[\frac{\mu m}{mm}]$	$d(\bar{I}_{Normalized})/d(c)\ [\frac{A}{mm^3}]$
#1 Initial	2.07×10^{-3}	6.25×10^{-7}
#2 Steady	7.23×10^{-4} ↓ 65 [%] from zone #1	3.70×10^{-7} ↓ 41 [%] from zone #1
#3 Accel.	1.26×10^{-3} ↑ 74 [%] from zone #2	5.84×10^{-7} ↑ 58 [%] from zone #2

Finally, end mill's flank wear estimation is shown in Figure 3.35 to Figure 3.38 using the 4 methods explained in Section 3.4. The coefficients used in method 1 to 3 are shown in Table 3.18 to Table 3.20 and the assigned weights in method 4 is given in Table 3.21. The estimated flank wear is obtained using 2-4 wear measurements (purple points). The error between the estimated and measured tool wear is given in

Table 3.22. It can be concluded that all errors are below 10%, which confirms the effectiveness of these methods in the third cutting case.

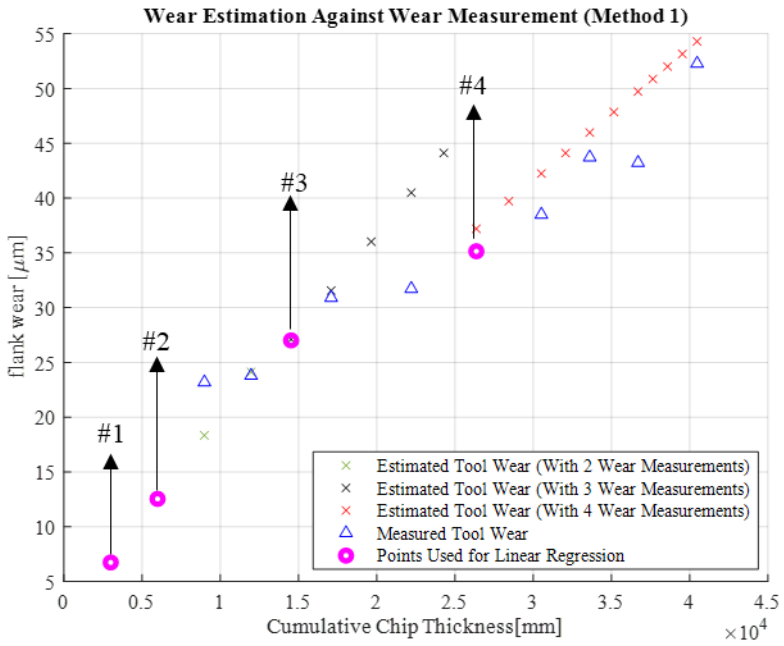

Figure 3.35. In-process estimation of flank wear using cumulative chip thickness in stacked cutting experiment

Table 3.18. Coefficients for tool flank wear as a linear function of cumulative chip thickness calibrated by different number of wear measurements in stacked cutting experiment

	$a_{c_0}\ [\mu m]$	$a_{c_1}\ [\frac{\mu m}{mm}]$
2 Wear Measurements (update 1)	0.94	1.9×10^{-3}
3 Wear Measurements (update 2)	1.77	1.7×10^{-3}
4 Wear Measurements (update 3)	5.53	1.2×10^{-3}

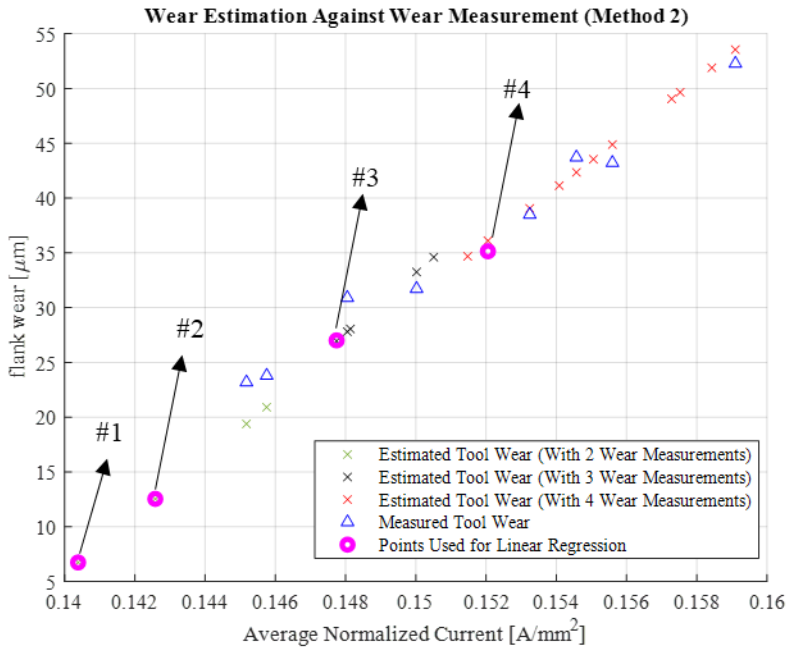

Figure 3.36. In-process estimation of flank wear using average of normalized current in stacked cutting experiment

Table 3.19. Coefficients for tool flank wear as a linear function of average of normalized current calibrated by different number of wear measurements in stacked cutting experiment

	$a_{I_0}\ [\mu m]$	$a_{I_1}\ [\frac{\mu m}{A/mm^2}]$
2 Wear Measurements (update 1)	-363.6	2.64×10^3
3 Wear Measurements (update 2)	-381.2	2.76×10^3
4 Wear Measurements (update 3)	-340.3	2.47×10^3

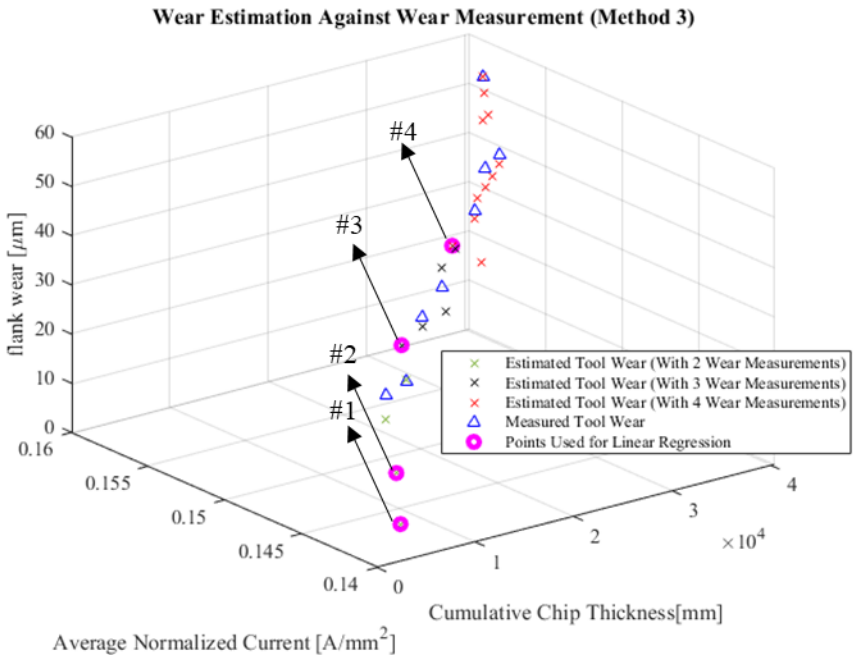

Figure 3.37. In-process estimation of flank wear using cumulative chip thickness and average of normalized current in stacked cutting experiment

Table 3.20. Coefficients for tool flank wear as a function of cumulative chip thickness and average of normalized current calibrated by different number wear measurements in stacked cutting experiment

	$a_{I,c_0}\ [\mu m]$	$a_{I,c_1}\ [\frac{\mu m}{mm}]$	$a_{I,c_2}\ [\frac{\mu m}{A/mm^2}]$
2 Wear Measurements (update 1)	0.94	1.9×10^{-3}	0
3 Wear Measurements (update 2)	-257.5	5.64×10^{-4}	1.87×10^{3}
4 Wear Measurements (update 3)	-576.3	-8.97×10^{-4}	4.17×10^{3}

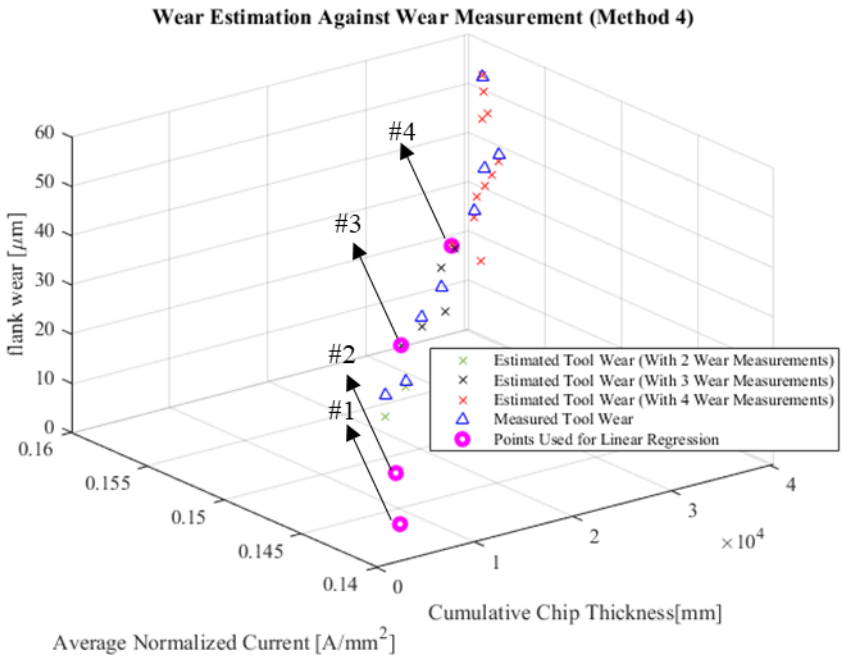

Figure 3.38. In-process estimation of flank wear using estimated flank wear from cumulative chip thickness and average of normalized current in stacked cutting experiment

Table 3.21. Assigned weights to estimated flank wear from method 1 and 2 calibrated by different number of wear measurement in stacked cutting experiment

	w_c	w_I
2 Wear Measurements (update 1)	0.5	0.5
3 Wear Measurements (update 2)	0.32	0.68
4 Wear Measurements (update 3)	-0.55	1.55

Table 3.22. Error between estimated and measured tool flank wear for method 1 to 4 in stacked cutting experiment

Method	Error [%]
1. Cumulative Chip thickness	9.2
2. Average of Normalized Current	5.7
3. Cumulative Chip thickness & Average of Normalize Current	5.8
4. Weighted linear combination of method 1 & 2	5.9

3.6 Summary

A detailed description of the structure of the digital twin and its use to monitor and estimate tool flank wear is presented in this chapter. The machining states are simulated and stored in a virtual feedback file. The simulated machining states are synchronized with the on-line positions of the CNC machine tool. Commanded spindle current is collected from the CNC during machining, normalized against the engagement area provided by the simulation engine, and combined with the simulated cumulative chip thickness to track the tool wear.

The study continues and estimates the in-process tool wear using four different methods. The estimation is conducted by using either cumulative chip thickness in the first method or average of normalized current in the second method. Additionally, both of these parameters are combined in method 3 and 4. The estimations are verified with the measured flank wear and the error for each method is calculated. The error for all of the method in all three cases are under 20 percent. However, the operator may decide to use either one of these methods based on the specified cutting operation. By estimating tool wear based on the average spindle current, the need to stop the operation many times is eliminated. Instead, flank wear is only required to be measured 3 or 4

times. By doing so, it is possible to increase the speed of cutting operations while maintaining information about the flank wear on the tool surface.

Chapter 4: Tool Breakage and Chatter Detection Applications in Digital Twin System

4.1 Overview

This chapter focuses on improving chatter and tool breakage detection by utilizing the cutting states detection method introduced in Chapter 3.

Occasionally, chatter detection and tool breakage methods may produce false alarms in transient states which excites natural modes of the structure. By separating transient entry – exist states from the rest the number of false alarms can be reduced in machining parts.

Here, the spindle motor current obtained from the CNC is utilized as a sensor measurement for tool breakage detection. The tool breakage method is explained in 4.2 with an experimental verification. The chatter detection is presented in Section 4.3 and the chapter is summarized in Section 4.4.

4.2 Tool Breakage Detection

4.2.1 In-process Tool Breakage Detection Using Spindle Current and Virtual Feedback

In-process tool breakage algorithm using average resultant cutting force per tooth period is explained in [10]. Other sensor measurements can be analyzed using the same algorithm if they can be correlated with the cutting forces at the machine tool's operating frequency. The feed drive motor current measurements at tooth passing frequency under 20 [Hz] or in other words at low cutting speeds have been used to detect tool failure in [11]. In this section, spindle current is employed similarly.

Spindle current is related to tangential cutting force as shown in Eq. (3.9) The commanded spindle current is collected from the CNC controller at 10 [kHz] sampling frequency. The average spindle current per tooth period I_a is calculated as follows;

$$I_a(m) = \sum_{i=1}^{n} \frac{I_{nom,spindle}(i)}{n} \tag{4.1}$$

where $I_{nom,spindle}$ is the commanded spindle current in [A], n is the number of spindle current samples collected at tooth period (m). Providing the cutter workpiece engagement (CWE) geometry is not changing and there is no tooth breakage or run-out on the cutter, the average spindle torque per tooth period must remain constant. Since the average spindle current is equal in every tooth period, the first differences in the average spindle currents are zero [10].

$$\Delta I_a = I_a(m) - I_a(m-1) = (1 - z^{-1}) I_a(m) \tag{4.2}$$

If the CWE changes, a tooth is damaged or a run-out exists on the cutter, the chip load changes. Chip load changes are reflected in the average current per tooth period. The average current profile will follow the geometric trend if the cutter experiences a transient geometry (entrance and exit states) along the toolpath. To eliminate the slow varying DC trend caused by varying CWE, a first-order adaptive time series filter is used as [34];

$$\varepsilon_1(m) = \left(1 - \hat{\phi}_1 z^{-1}\right)\left[I_a(m) - I_a(m-1)\right] = \left(1 - \hat{\phi}_1 z^{-1}\right)\Delta I_a(m) \tag{4.3}$$

where $\hat{\phi}_1$ is estimated from measurements $\Delta I_a(m)$ by applying standard recursive least squares (RLS) algorithm at each tooth period as explained in [34]. Moreover, the tool run-out can still produce high-amplitude residuals which can be removed by differentiating the average spindle current at every tooth period from one spindle period before [9];

$$\Delta^N I_a = I_a(m) - I_a(m-N) \tag{4.4}$$

where N is the number of flutes on the tool. The first-order adaptive times series filter is applied again on the resulting differences as follows;

$$\varepsilon_2(m) = \left(1-\hat{\phi}_2 z^{-1}\right)\left[I_a(m) - I_a(m-N)\right] = \left(1-\hat{\phi}_2 z^{-1}\right)\Delta^N I_a(m) \tag{4.5}$$

where $\hat{\phi}_2$ is estimated in similar way as $\hat{\phi}_1$. In previous studies [10], [11], the two residuals are obtained at every tooth period. During the first few revolutions of spindle, the maximum residuals of both filters are measured based on the assumption that the cutter is not broken during this period. The breakage thresholds are set by scaling the obtained maximum residuals by a user-defined factor (α_1 and $\alpha_{2`}$) as follows;

$$\begin{aligned} LIMIT_1 &= \alpha_1 \max\left(\varepsilon_1(m=1),\ldots,\varepsilon_1(m=N\times \#Sr)\right) \\ LIMIT_2 &= \alpha_2 \max\left(\varepsilon_2(m=1),\ldots,\varepsilon_2(m=N\times \#Sr)\right) \end{aligned} \tag{4.6}$$

where $\#Sr$ is the number of spindle revolutions required to calibrate the thresholds using the initial residues. In [10], [11] threshold factors are usually chosen intuitively between 2 and 3. The initial

calibration is therefore an essential step in identifying tool breakage and if done incorrectly, may result in false warnings of tool breakage.

To identify the maximum residues at the first few spindle revolutions of the cut, it is important to identify when the cutter is engaged with workpiece or is in an in-cut state. The literature [10], suggests measuring the maximum residues when the cutting forces increase from the level of air machining. In this case, the transient state (entrance) will be included in the first few spindle revolutions to find the maximum residues. Although the effect of transient geometry is removed when the time series filter is applied for the second time (ε_2), the effect may still be present in the first residue (ε_1) after the filtering.

As explained in Section 3.2.1.2, the cutter has three different cutting states, namely air-cut, in-cut, and transient (entrance and exit) states. These states can be identified by providing the toolpath to Virtual Machining system [1]. The cutting states are identified using the cutting states detection algorithm explained in Section 3.2.1.2. The virtual feedback contains machining states such as cutting states, cutter-workpiece engagements, simulated cutting forces, torque, etc. at the tool center positions along the tool path.

To bridge the information provided by virtual feedback to the online cutting operation, the tool center positions collected from the CNC system are synchronized with the virtual feedbacks explained in Section 3.2.2.

Once the cutter is in an in-cut state, the tool breakage algorithm starts calculating the residues. The maximum residues are obtained at the first few spindle revolutions of the identified in-cut state and the threshold is calibrated accordingly.

As a result of utilizing virtual feedback, the tool breakage algorithm can find the maximum residues at the start of the in-cut state rather than the start of the cutting operation. The proposed method is summarized in Figure 4.1.

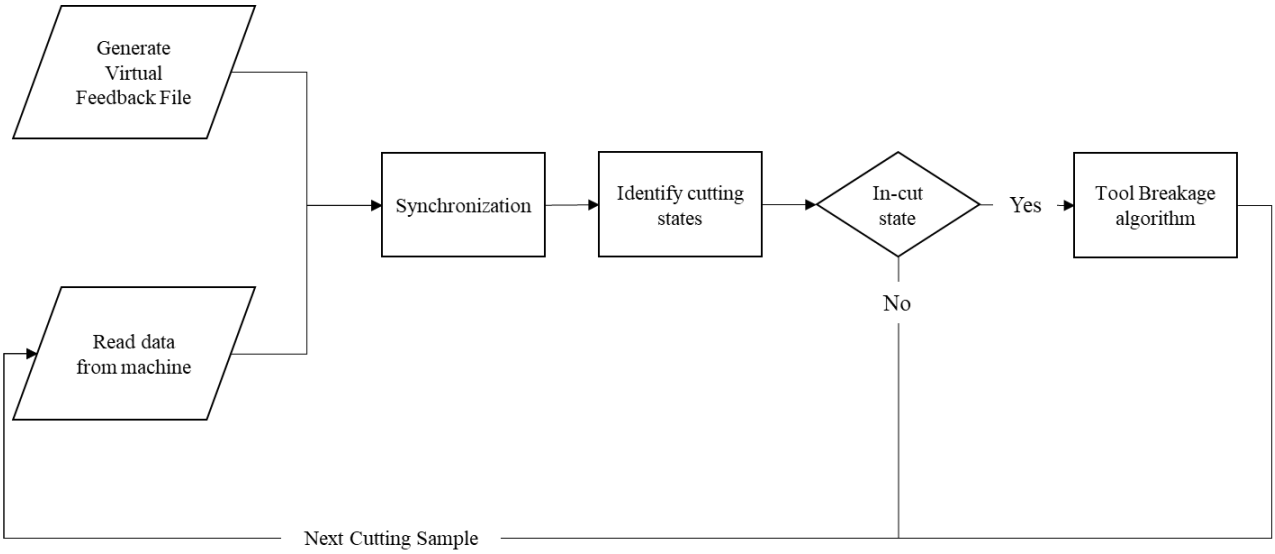

Figure 4.1. Flowchart of the overall proposed tool breakage detection procedure

4.2.2 Experimental Verification

The tool breakage detection algorithm using commanded spindle current is experimentally verified through a milling test experiment where a 25 [mm] indexable tool with 4 insert cuts an Aluminum 7075 workpiece. The milling test experiments is conducted using Quaser UX600 CNC machine tool with the HEIDENHAIN CNC controller.

The milling test is conducted along the toolpath shown in Figure 4.2. The toolpath reflects an increasing radial immersion in the cutter-workpiece engagement. The axial depth of cut in this toolpath is selected as 2 [mm] and the spindle speed is 6000 [rev/min] which means the tooth passing frequency (spindle frequency times number of flutes) is 400 [Hz]. The cutting conditions are tabulated in Table 4.1.

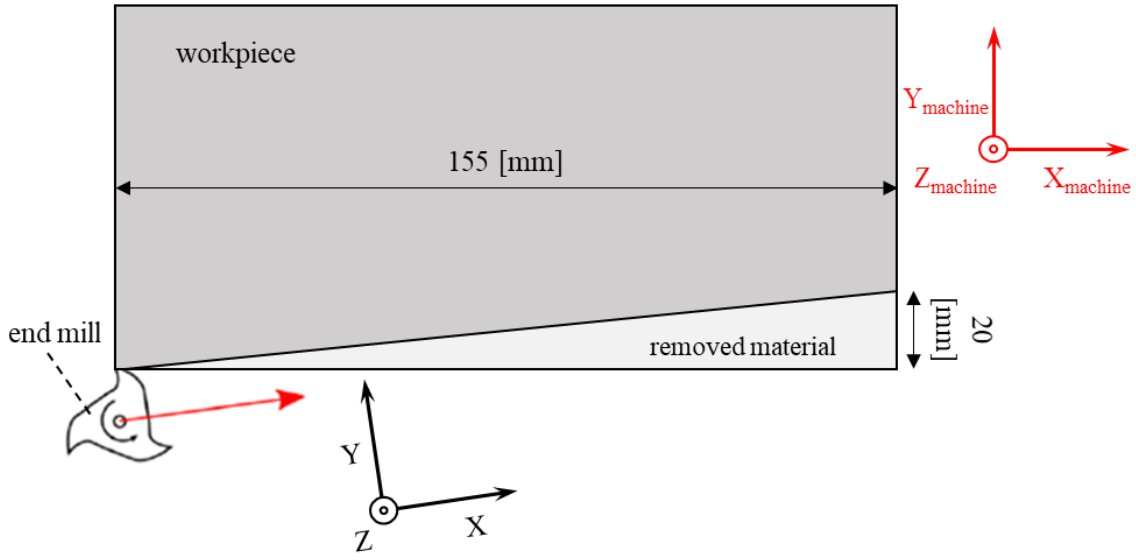

Figure 4.2. Overall view of the designed toolpath for the tool breakage experiment. The red coordinates are XYZ_{Macine} frame and the black coordinates are defined as a local frame in the feed, normal and axial directions of the cut

Table 4.1. Specifications of the tool breakage milling experiment on Quaser UX600 CNC machine

Tool	Diameter: 25 [mm]	Rake angle: 18 [deg]
	Corner radius: 0.4 [mm]	Number of inserts: 4
Workpiece Material	7050 Aluminum	

Cutting Conditions	Spindle Speed: 6000 [rev/min]
	Feedrate: 0.1 [mm/flute/rev]
	Axial Depth of Cut: 2 [mm]
	Radial immersion: increasing from 0 at the beginning to 20 [mm] at the end of the cut

The real-time data including tool center positions and spindle current are collected using the in-house built software, INTELCUT, which communicates with the HEIDENHAIN CNC controller via TNC Ethernet connection. The tool center positions are collected at 333 [Hz] and nominal digital motor current is sampled at 10 [kHz].

The virtual feedback is generated by running the toolpath on the Virtual Machining Software [1] and the virtually machined workpiece is presented in Figure 4.3. The sampling distance is selected as 1 [mm] in the software. This means that the machining states can be accessed at 1 [mm] intervals along the tool path. The tool center positions and simulated engagements are stored in a virtual feedback file. Additionally, the cutting states (air-cut, transient, in-cut) are identified using the engagements and are added to the virtual feedback data file.

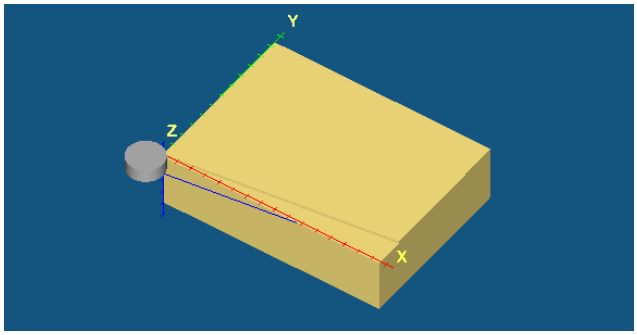

Figure 4.3. Virtually machined workpiece under the sloped toolpath with the cutting conditions given in **Table** 4.1 in MACHpro™ software [1]

When the virtual feedback is generated, the collected real-time tool center positions are synchronized with the tool center position in the virtual feedback with ±0.1 [mm] tolerance. The toolpath synchronization result is presented in Figure 4.4.

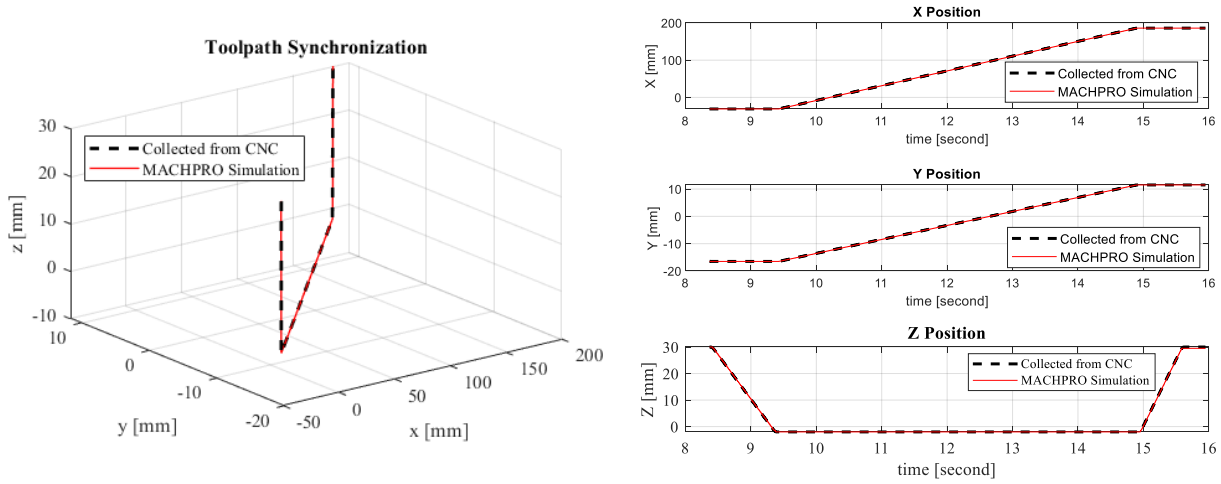

(a) (b)

Figure 4.4. (a) Simulated and real-time collected toolpath synchronization and (b) Simulated and real-time collected tool center positions synchronization in tool breakage experiment

In the next step, the cutting states are identified online (see Figure 4.5) which leads the obtaining the spindle current in the in-cut state. The distinguished in-cut spindle current is shown in Figure 4.5.

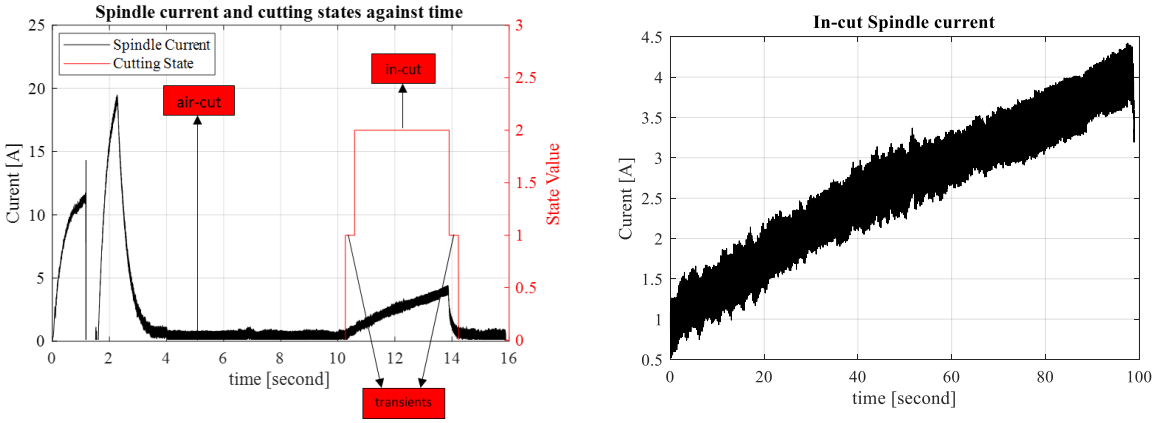

a) (b)

Figure 4.5. Spindle Current on top of synchronized cutting states and (b) In-cut spindle current in tool breakage experiment with healthy inserts

The sloped cutting test is once conducted with 4 healthy inserts and the spindle current is collected. To imitate tool breakage one of the inserts in the cutter is removed and the test is repeated with the same cutting conditions. The cutter has one fewer insert, so the spindle load or current is expected to increase on the next insert. This is because the insert removes more material in the absence of its previous insert. The in-cut spindle current for both cases are presented in Figure 4.6.a. The in-cut spindle current is zoomed at 242nd to 250th tooth periods or 2 full spindle periods as presented in Figure 4.6.a. At 242nd and 243rd tooth periods, the spindle currents for broken and healthy tools are almost equal. However, a drop occurred in the 244th tooth period for a broken tool. This is followed up by an increase in the 245th tooth period. 242nd to 245th tooth periods represent one spindle period and the same behavior is repeated in the following spindle periods.

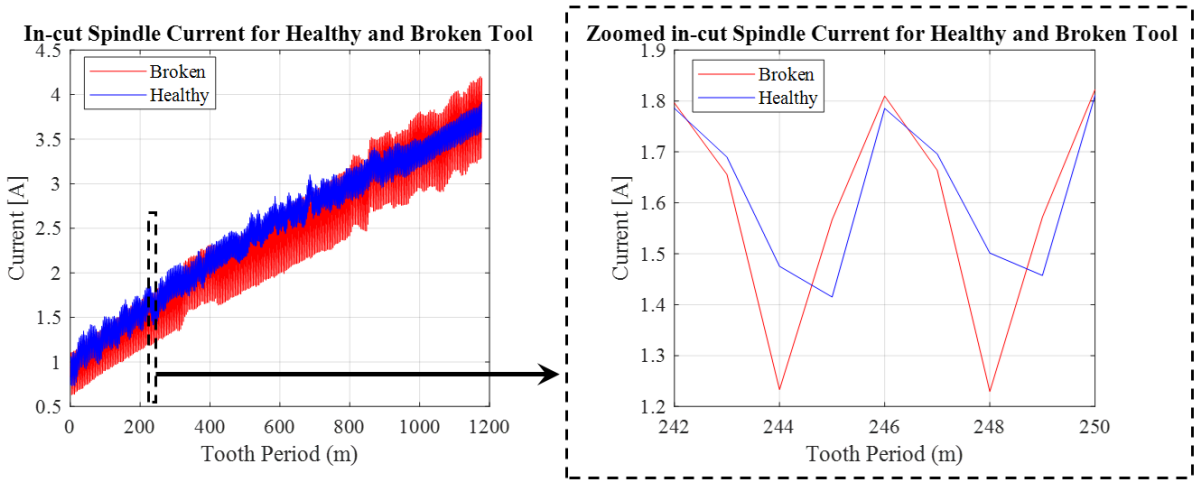

(a) (b)

Figure 4.6. (a) In-cut spindle current with healthy and broken insert under sloped toolpath at tooth periods (b) Zoomed in-cut spindle current at tooth period 242 to 250

The collected spindle current with healthy and broken tools are assembled at the 600th tooth period to resemble the breakage of the cutter in the middle of the cut. The residual thresholds for tool breakage are calibrated at the first 5 spindle revolutions and the threshold factors α_1 and α_2 in Eq. (4.6) are chosen as 2 and 3 respectively which corresponds to $LIMIT_1 = 0.40\ [\mathrm{A}]$ and $LIMIT_2 = 0.15\ [\mathrm{A}]$.

The assembled spindle currents and first and second residues are given in Figure 4.7. The tool failure is detected at 602th tooth period since both residues exceed their thresholds and ε_1 exceeds its threshold thereafter ($m = 602$). Since the tool breakage event is at 600th tooth period, the spindle current is assembled to the healthy one, the experiment verifies the algorithm performance. Additionally, the monitoring system can stop the feed motion within 150-200ms when the tool breakage event is detected.

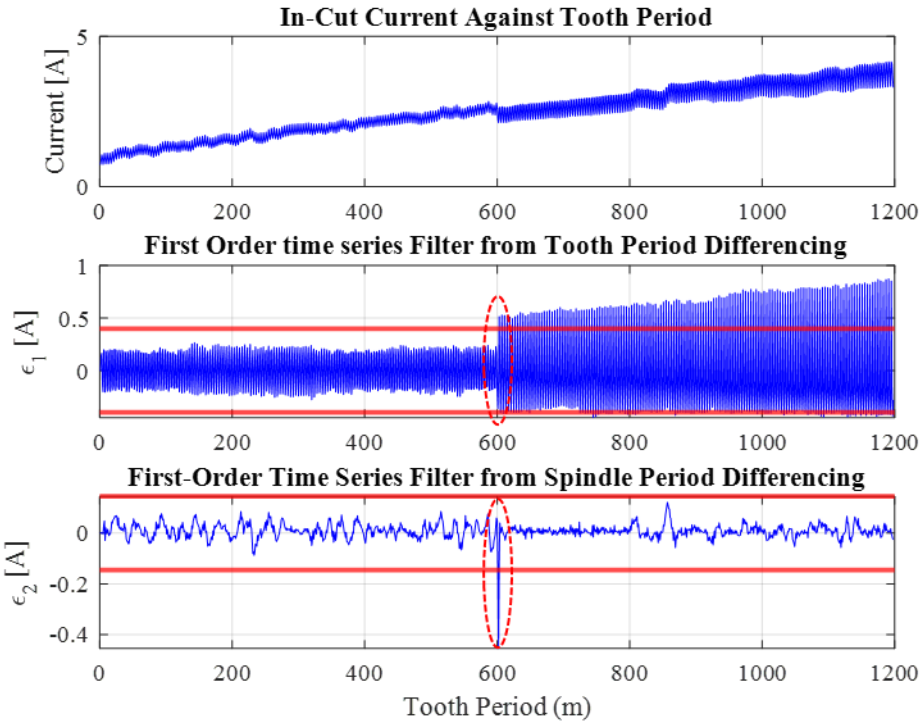

Figure 4.7. $\mathcal{E}_1$ and $\mathcal{E}_2$ exceeding their threshold limits and tool breakage detected at 600th tooth period using the distinguished spindle current by the assist of virtual feedback.

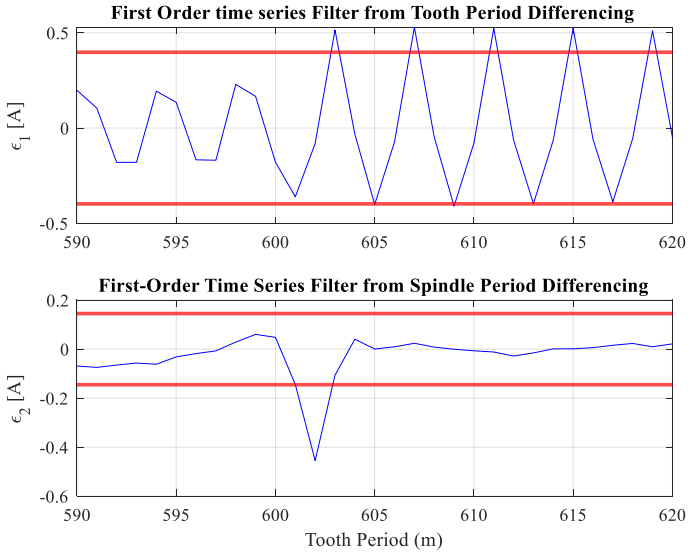

Figure 4.8. Zoomed Window of tool breakage thresholds at 590th to 620th tooth period. Tool breakage event detected at 602nd tooth period.

4.3 Chatter Detection

Two different chatter detection algorithms are modified here to run with the digital twin system: energy-based chatter detection [16]and FFT-based chatter detection [10].

4.3.1 Energy-base and FFT-base Chatter Detection

Energy-based chatter detection explained in [16] is based on monitoring the vibration energy. It finds periodic forced vibration components and removes them from the measurements with a Kalman Filter to isolate the chatter component. Then chatter amplitudes and frequencies are identified using the nonlinear energy operator (NEO). This algorithm monitors the ratio of the energy of the chatter component to the total vibration energy as the chatter indicator. Chatter can be predicted with different signals such as force, acceleration and sound. While this method can predict the chatter when the cutter is in-cut state, it gives false alarms at transient states (entrance and exit). In transient states an impact excitation occurs, machine vibrates at its natural frequencies and the vibration is falsely considered as chatter.

FFT-based chatter detection [10] computes a moving FFT window of the vibration signal. This algorithm detects the peak amplitudes around the spindle and tooth passing frequencies and determines which peak is the highest. In order to detect chatter, the highest peak in the entire FFT window must exceed the highest peak coming from the spindle or tooth passing frequencies. Air cutting is detected at the beginning of the algorithm by finding the highest peak of the FFT window at the first few milliseconds (e.g. 200 [ms]) to avoid false chatter alarms. Similar to the energy-based methods, this method can also misunderstand the impact hit excitation frequency as chatter in the transient states.

To show the false chatter alarm in FFT-based method as an example, a milling test is conducted while collecting sound with a microphone at 10 [kHz]. An indexable tool with 4 inserts and a diameter of 25 [mm] cuts a 7050 Aluminum workpiece. The spindle speed is selected as 5300 [rev/min] and the axial and radial depth of cut are 2.5 and 25 [mm], respectively. Chatter detection result is shown in Figure 4.9. Chatter is falsely detected during the transient state (entrance) and the detected frequency is 1070 which probably is close to one of the natural frequencies of the system. Also, chatter is detected after the transient at 915 [Hz]. This false alarm could be avoided by providing the identified cutting states to the chatter detection methods and avoid false alarms at entry or other non-in-cut states.

The cutting states detection can therefore be utilized for chatter detection in both of the above methods, thereby utilizing the in-cut portion of the measured signal and eliminating false alarms in other cutting states.

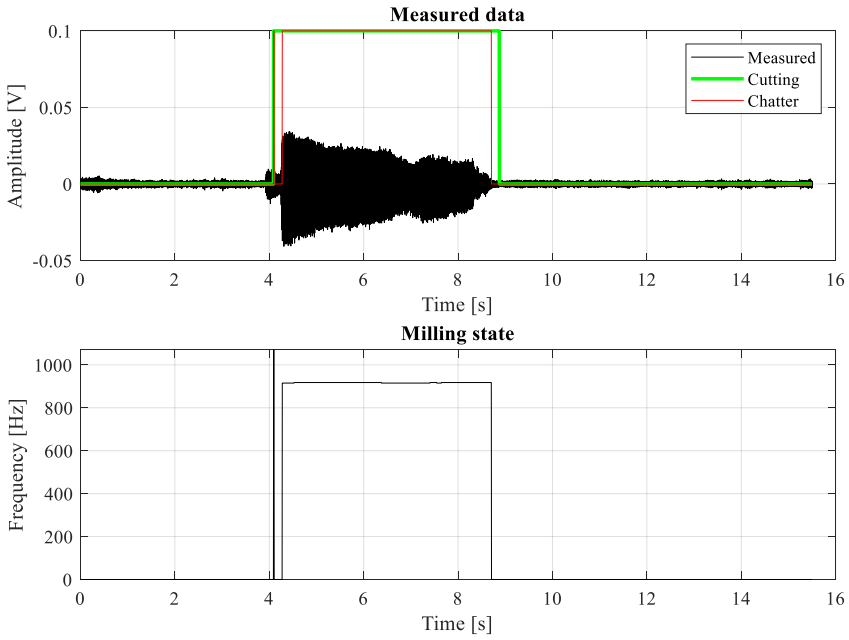

Figure 4.9. FFT-base chatter detection method applied in an unstable slot-cutting test. Spindle speed is 5300 [rev/min] and axial depth of cut is 2.5 [mm].

4.3.2 Chatter Avoidance

When chatter is detected by either energy-based or FFT-based methods, a chatter avoidance algorithm changes the spindle speed. This is conducted by matching the tooth and chatter frequency. The tooth passing frequency [10], [14] is matched by the integer divisions of chatter frequency as follows;

$$\omega_{updated} = \begin{cases} \text{Lower Spindle Frequency:} & \dfrac{\omega_{chatter}}{N \times \left\lceil \dfrac{\omega_{chatter}}{\omega_{initial} \times N} \right\rceil} \\ \text{Upper Spindle Frequency:} & \dfrac{\omega_{chatter}}{N \times floor\left\lfloor \dfrac{\omega_{chatter}}{\omega_{initial} \times N} \right\rfloor} \end{cases} \tag{4.7}$$

where N is number of teeth on the cutter, $\omega_{chatter}$ is the detected chatter frequency, $\omega_{initial}$ is the initial spindle frequency of the cutting operation and ceil and floor function rounds values to the nearest integer toward positive and negative infinity respectively. There are two spindle speeds calculated which are the closest to the initial spindle speed. One of them is lower and the other is higher. As each CNC machine has its own spindle override limit, the lower spindle frequency is selected in the event that the upper spindle frequency cannot be reached. Once the spindle speed has been updated, the remainder of the cutting operation is monitored to see if chatter is eliminated. If chatter is detected again, the same procedure is repeated.

The chatter avoidance algorithm is tested in a 3-axis milling experiment. A 25 [mm] indexable end mill with 4 inserts is used to cut an Aluminum 7050 workpiece under a straight-line toolpath with a full radial immersion or slot cutting. The axial depth of cut was 2.5 [mm] and the spindle speed was 5250 [rev/min]. The cutting conditions are tabulated in Table 4.2. The test was conducted on Quaser UX600 CNC milling machine.

Sound is collected using INTELCUT software from the microphone. Additionally, XYZ positions in tool coordinates, feed rate and spindle speed are collected from the CNC controller. The sampling frequency was 10 [kHz].

Table 4.2. Specifications of the chatter avoidance milling experiment on Quaser UX600 CNC machine

Tool	Diameter: 25 [mm]	Rake angle: 18 [deg]
	Corner radius: 0.4 [mm]	Number of inserts: 4
Workpiece Material	7050 Aluminum	
Cutting Conditions	Spindle Speed: 5250 [rev/min]	Axial Depth of Cut: 2.5 [mm]
	Feedrate: 0.1 [mm/flute/rev]	Radial Depth of Cut: 25 [mm]

The chatter avoidance result is shown in Figure 4.10. Chatter is detected at 2.5 [s] in the microphone data and the detected chatter frequency $\omega_{chatter}$ =898.70 [Hz]. When chatter is detected, the stop command is sent to the CNC controller to stop the feed drive motion. the feedrate goes to zero at 3.1 [s]. CNC takes 0.6 seconds to stop the feed motion. In this position, the spindle is still rotating but the cutter has no engagement with the workpiece.

The detected chatter frequency is passed to the avoidance function to determine the new spindle speed. The lower and upper spindle speeds are obtained using Eq. (4.7) as 4494 and 6740 [rev/min], respectively. Since the spindle speed override limit in Quaser machine is 150 [%], the higher spindle speed can be reached ($\frac{6740}{5250} = 1.28 < 1.50$). Therefore, spindle override is equal to 1.28. The new spindle speed is calculated accordingly and is set to $1.28 \times 5250 = 6720$ [rev/min]. The feed is equal to 0.1 [mm/flute/min] corresponds to $0.1 \times 4 \times 6720 = 2688$ [mm/min] feed speed. Chatter avoidance function outputs and the updated cutting conditions are tabulated in Table 4.3 and Table 4.4 respectively.

The cutting conditions are updated, and the cutting operation is resumed at 7.1 [s]. No chatter is detected during the rest of the operation which verifies the performance of the algorithm.

Table 4.3. Specifications of chatter avoidance function

Chatter Avoidance function Outputs	$\omega_{chatter} = 898.70$ [Hz]
	$\omega_{updated} = \begin{cases} \text{Lower Spindle Frequency:} & 4494 \text{ [rev/min]} \\ \text{Upper Spindle Frequency:} & 6740 \text{ [rev/min]} \end{cases}$
	$\text{Spindle/feedrate override} = \begin{cases} \text{Lower:} & 0.86 \\ \text{Upper:} & 1.28 \end{cases}$

Table 4.4. Updated cutting conditions using chatter avoidance function outputs

Updated Cutting Conditions	Spindle Speed: 6720 [rev/min]	Feedrate: 2688 [mm/min]

The stability lobe of the end mill is identified using CUTPRO™ [35]. An accelerometer is attached to the tooltip and an impact test is conducted with a hammer. The measured impact force and acceleration are provided to the software to obtain the frequency response functions of the system in X and Y directions. The FRFs are then used to identify the stability lobes diagram of the milling operation (see Figure 4.11). As it is shown in this figure, the initial cutting conditions are in an unstable area, however the suggested lower and upper spindle speeds provide stability while keeping the gain of cutting operation or chip load.

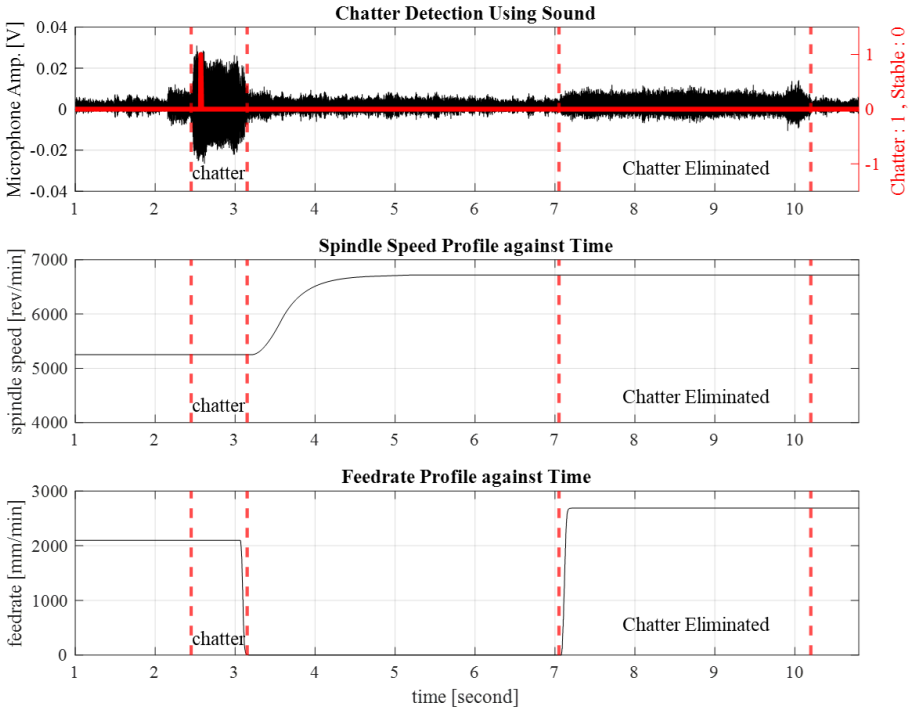

Figure 4.10. Chatter avoidance experiment result. Chatter is detected at 2.5 [s]. The cutter's feedrate and spindle speed is updated, and chatter is eliminated.

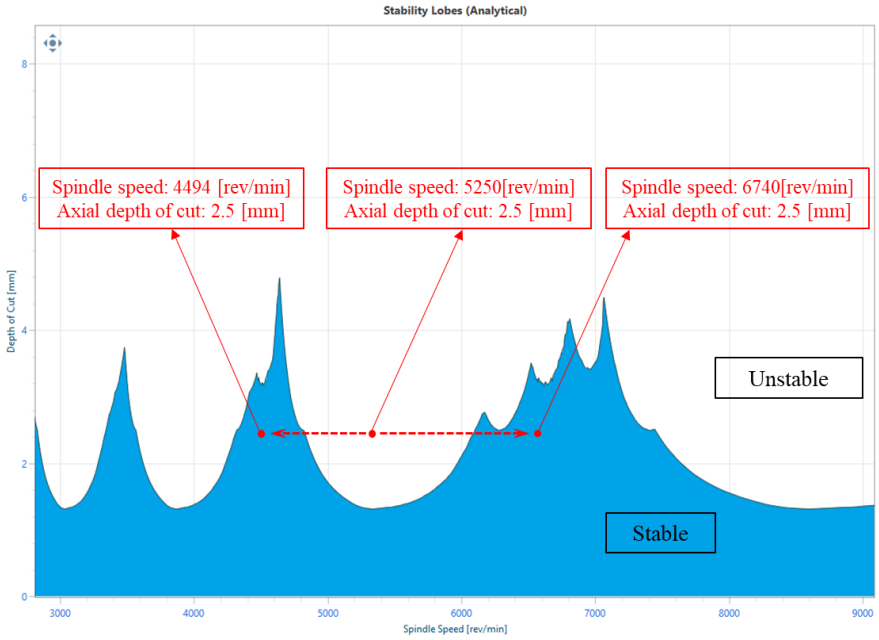

Figure 4.11. Stability lobe for the indexable end mill given in Table 4.2

The machined workpiece used in this experiment has two slot cuts, see Figure 4.10. In the left cut, avoidance is activated, which explains why chatter marks are present at the beginning but are eliminated afterward. However, chatter marks are evident throughout the entire operation in the right cut where the chatter avoidance was not activated.

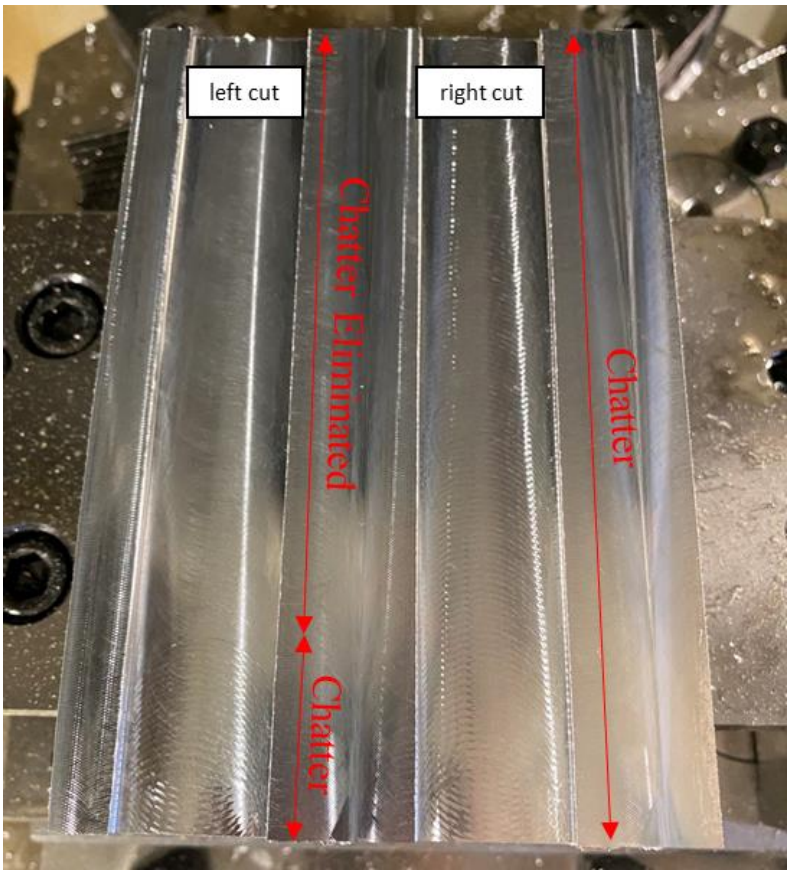

Figure 4.12. Machined workpiece under two slot cutting experiments with the same cutting conditions at the beginning. Chatter avoidance is activated for left channel, therefore changing the cutting condition after chatter is detected to eliminate it. Cutting condition does not change in right channel, therefore chatter marks are visible for the entire cut.

4.4 Summary

This chapter examines how a digital twin system can improve the accuracy of detecting chatter and tool breakage in machining. To detect tool breakages, a previously employed method has been modified to work with a digital twin. At each tooth period, the spindle current is averaged, and tooth and spindle period differencing are applied. Next, a first-order time series is applied, which produces two residues that can be monitored to indicate the tool failure. Once tool failure is detected the CNC machine is stopped and a tool change is required. To detect chatter, previously developed energy and FFT-based methods are modified to work with the digital twin. Upon chatter detection. The chatter avoidance algorithm updates the spindle speed and relocates the cutting condition to the stable part of the stability lobe.

Chapter 5: Cutting Force Prediction using Tool Holder Acceleration Sensor

5.1 Overview

The cutting forces are the most reliable state that represents the machining process. Tool wear and tool breakage, machining load, surface finish and dimensional quality of the part are all mainly determined by cutting forces at the tool tip. However, the available cutting force sensors are either designed for laboratory use such as dynamometers or force sensors integrated into spindle housing which is away from the tool tip.

This chapter presents a method to monitor the force at the tooltip using a tool holder with an integrated accelerometer [36]. The transfer function between the force at the tool tip and vibrations measured by the accelerometer is modeled. A Kalman filter is used to estimate the radial forces at the tooltip by compensating the disturbances caused by the transmission of signals from the tooltip to the accelerometer position [27].

The proposed method is experimentally demonstrated to estimate radial cutting force at the tool tip in milling experiments. A good agreement was found between cutting force estimation and actual cutting forces measured with a dynamometer.

5.2 Sensory Tool Holder

The tool holder has an acceleration sensor that measures tool vibrations as shown in Figure 5.1 which was developed at the Institute of Production Engineering and Laser Technology of the Technical University of Vienna [36].

Figure 5.1. Sensory tool holder [adopted from 36]

The structure of the sensory tool holder is represented in Figure 5.2.a. The tool holder consists of a single acceleration MEMS-sensor (±100 g radial) with a vibratory mass utilized in a standard HSK-A 63 tool holder. The accelerometer in the tool holder has a linear frequency response range under 11 [kHz]. The acceleration signal is sampled at 9524 [Hz] by the embedded processor which is within the linear frequency range of the sensor. The other parts of the tool holder are the battery and wireless communication link which transfers the digital data to a mounted transceiver and from there to an external computer for process monitoring as shown in Figure 5.2.b.

(a) **(b)**

Figure 5.2. (a) Structure of sensory tool holder [adopted from 41], (b) Communication structure of sensory tool holder system [adopted from 41]

5.2.1 Kinematic model of the Sensory Tool older

Based on rotational acceleration measurements obtained from the accelerometer located inside the tool holder, the following model was presented for milling applications by Bleicher et al. [38]. The tool holder is assumed to rotate at a constant rotational speed ω_{sp} around the z-axis. The acceleration sensor is modeled as a frictionless spring-mass-damper system as shown in Figure 5.3. Newton's second law is applied on the system as follows;

$$\sum F = m\frac{d^2\Delta x}{dt^2} = -c\frac{d\Delta x}{dt} - k\Delta x - m\frac{v^2}{r} \tag{5.1}$$

where m [kg] is the accelerometer mass, c [Ns/m] is the damping constant and k [N/m] is the spring constant, v [m/s] is the tangential speed of the rotating mass and r [m] is its radial distance

from the spindle axis in the inertial spindle frame of reference (x_{IS}, y_{IS}). The linear speed and radial distance are written as;

$$v = r\frac{d\theta}{dt} = r\omega_{sp} \quad \leftarrow \quad r = r_A + x_0 + \Delta x \tag{5.2}$$

The center of the accelerometer mass shown in Figure 5.3 is designed in a way so it is near the spindle axis A. Due to the finite accuracy of assembly, the center of mass is never aligned with the center of gravity which results in a static eccentricity x_0.

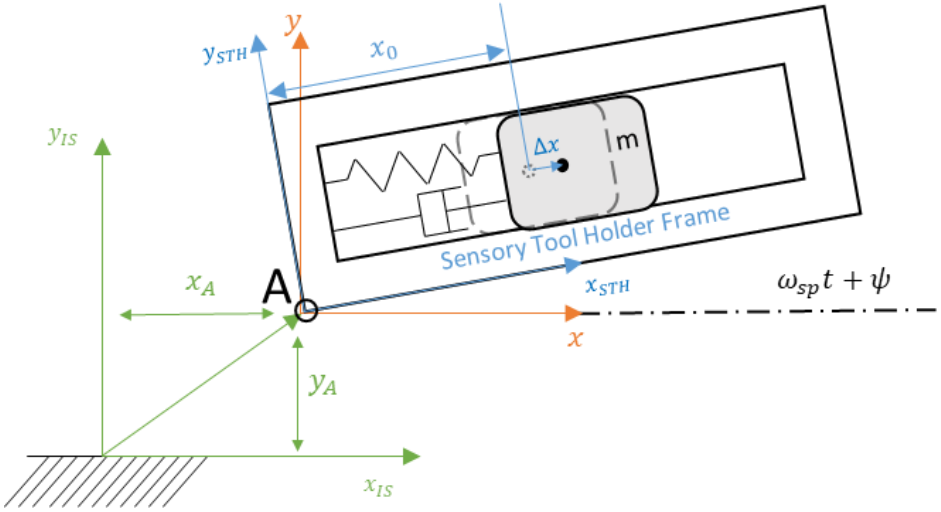

Figure 5.3. Mechanical model of the accelerometer instrumented inside the tool holder [38]

The time-variant radial deflection of the holder (r_A) is due to the vibration (x_A, y_A) caused by cutting forces (F_x, F_y) shown in Figure 5.4. Considering the tool and the tool holder as an elastic cylindrical beam that is cantilevered from the spindle, the time-variant deflections in x, y directions are expressed as follows [10]:

$$x_A = \frac{F_x v_A{}^2}{6EI}(3l - v_A)$$
$$y_A = \frac{F_y v_A{}^2}{6EI}(3l - v_A) \tag{5.3}$$

where $v_A = l - z$, l is the total length of tool and tool holder, z is the distance between point A and the tool tip, E is the Young's Modulus and I is the area moment of inertial of the tool and tool holder.

The radial deflection can be found by considering the angular position (θ) of the mass as;

$$r_A = x_A \cos(\theta + \psi) + y_A \sin(\theta + \psi) = x_A \cos(\omega_{sp} t + \psi) + y_A \sin(\omega_{sp} t + \psi) \tag{5.4}$$

where ψ is the initial angle of the tool holder. Substituting Eq. (5.2) and (5.4) in Eq. (5.1) results in;

$$\sum F = m \frac{d^2 \Delta x}{dt^2} = -c \frac{d\Delta x}{dt} - k\Delta x + m\left[\frac{r^2 \omega_{sp}{}^2}{r}\right]$$
$$m \frac{d^2 \Delta x}{dt^2} + c \frac{d\Delta x}{dt} + k\Delta x = m\omega_{sp}{}^2 \left[x_A \cos(\omega_{sp} t + \psi) + y_A \sin(\omega_{sp} t + \psi) + x_0 + \Delta x\right] \tag{5.5}$$

Since the vibration is caused by harmonic cutting forces, the following relationship is obtained:

$$x(t) = Xe^{j\omega_{sp} t}, \frac{d^2}{dt^2} x(t) = \ddot{x}(t) = -\omega_{sp}{}^2 Xe^{j\omega_{sp} t} \tag{5.6}$$

Considering Eq. (5.6), Eq. (5.5) can be further simplified as [38];

$$\Delta\ddot{x} + \frac{c}{m}\Delta\dot{x} + \left(\frac{k}{m} - {\omega_{sp}}^2\right)\Delta x = x_0{\omega_{sp}}^2 - \ddot{x}_A\cos(\omega_{sp}t + \psi) - \ddot{y}_A\sin(\omega_{sp}t + \psi) \tag{5.7}$$

From the left-hand side of Eq. (5.7), the spindle speed reduces the system's stiffness hence the sensor's natural frequency. The inherent frequency of the sensor must be substantially higher than the rotational speed as a requirement. In addition, both the centripetal acceleration ($x_0{\omega_{sp}}^2$) and the modulation caused by rotation in x and y on the right-hand side of Eq (5.7) affect the vibration (Δx). The modulation is due to cutting forces which cause an acceleration at point A (x_A, y_A). This effect is illustrated with time variant trigonometric functions. The centripetal acceleration is the results of the constant offset in x direction due to static eccentricity (x_0) which is negligibly small. This equation serves as the basis for further time and frequency-domain analysis of the sensor signal.

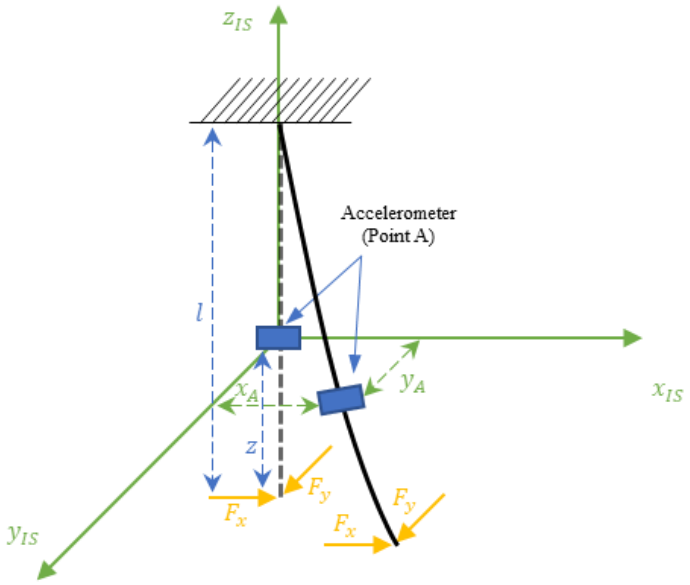

Figure 5.4. Deflection of the tool and tool holder due to cutting forces

5.2.2 Pre-processing of Acceleration Data

The acceleration signals collected from the sensory tool holder need to be sanitized first. The acceleration signal is sent to an external computer through the use of wireless communication where signal losses can occur. Since the continuous sampling of the signal's components is one of the very key elements to monitoring real-time data, the data losses need to be fixed. To remove any possible time gap in the signal, a preliminary data pre-processing procedure is conducted.

The acceleration sensor provides a message counter which can indicate whether the signal transmission is lost. Monitoring this value, time can be rescaled by filling in each lost point with either a so-called "NaN" (Not-a-Number-Value) or the last valid data (sample and hold). The sanitized signal now consists of all the samples required to comply with a constant sampling frequency. The pre-proccing procedure is depicted in Figure 5.5. Since the acceleration is measured per gravitational constant, it is also rescaled by g value to obtain acceleration in m/s^2.

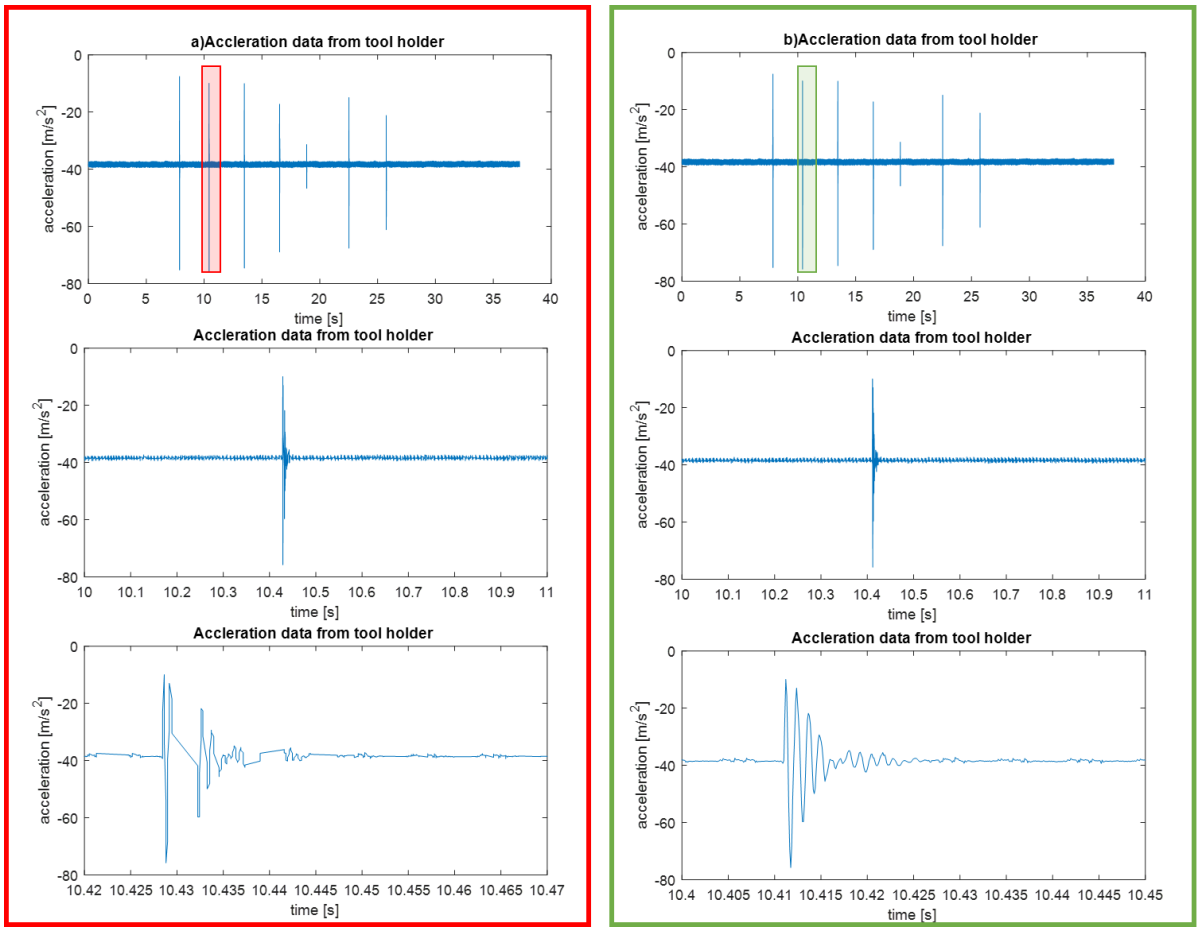

Figure 5.5. a) raw acceleration signal, b) sanitized acceleration data (rescaling time, finding gap and sample and hold)

5.3 Kalman Filter Design

Aslan designed a Kalman filter to estimate the forces from servo drive current commands [12] which is extended to acceleration signals here. A state observer is constructed from the s-domain transfer function of tool holder dynamics. An often-used method for achieving this transformation is to perform a manual curve-fitting technique by selecting modes in the measured FRF and obtaining the s-domain transfer function. However, a simplified method of obtaining s-domain transfer functions using an automated curve-fitting procedure [12] is employed in this study.

5.3.1 The frequency response function of the system at the tool tip

The objective of the dynamic model is to estimate the radial cutting force at the tool tip during machining from the accelerometer instrumented in the tool holder. The transfer function between the cutting force at the tool tip and the measured vibration at the accelerometer location is identified as follows.

Cross FRF of force and vibration between tooltip and the point where the sensor is located inside tool holder (see Figure 5.2.a) is identified through modal tap testing where an instrumented hammer is used to perform the FRF measurements and acceleration data are collected from the sensory tool holder. The impact is applied at the tool tip. The impact force and acceleration signals are then stored and processed. The corresponding displacement signals are obtained by integrating accelerometer measurements twice in frequency domain. Following modal tap testing, the FRF is fed into MALTAB's System Identification Toolbox® [6] which is based on Sanathanan-Koerner (SK) iterations and returns the corresponding modal parameters in the S-domain. Figure 5.6 presents the measured FRF through the modal tap test and the fitted curve. The measurements were very close in both x and y (radial) directions.

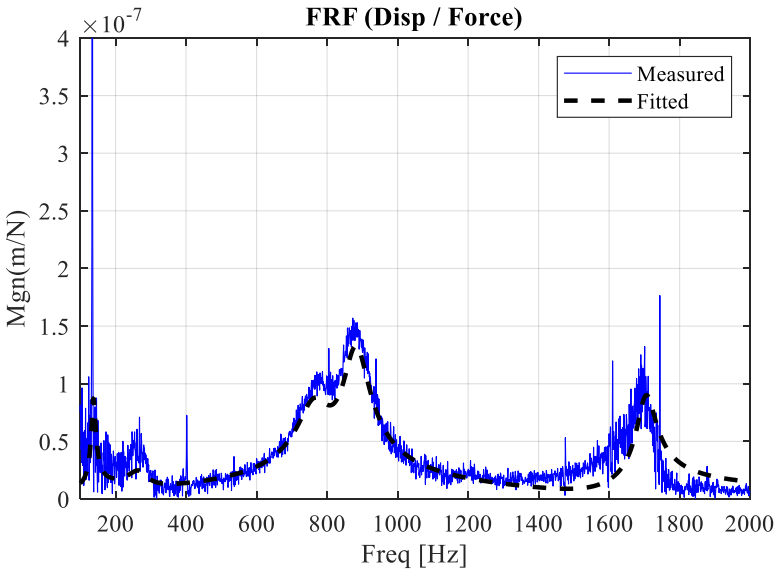

Figure 5.6. FRF of the tool tip and the automated curve fit (X direction)

MATLAB's "modalfit" built-in function [32] is able to provide the modal parameters including the natural frequencies (ω_{nk}), damping ratios (ζ_k) and the residues (α_k, β_k) for a given FRF measurement. Transfer function between input and output can be written in the following form where force at the tool tip is F and displacement is $d_{displacement}$. The transfer function parameters for each mode are listed in Table 5.1.

Table 5.1: Modal parameters of the identified transfer function

Mode	ω_{nk}[Hz]	ζ_k[%]	α_k	β_k
1	137.4	4.2	-0.019	-4.74×10^{-6}
2	268.8	10.7	0.042	1.05×10^{-5}
3	767.2	6.4	-0.173	1.37×10^{-5}
4	881.9	4.3	-0.103	5.10×10^{-5}
5	1703.9	1.6	0.040	2.82×10^{-5}

$$\Phi_{sys}(s) = \frac{X(s)}{F(s)} = \sum_{k} \frac{\alpha_k + \beta_k s}{s^2 + 2\zeta\omega_{nk} s + \omega_{nk}{}^2} \tag{5.8}$$

The transfer function of the system obtained from the curve-fitting is mapped into state-space form;

$$\begin{aligned} \dot{x}_{force}(t) &= A_{force} x_{force}(t) + B_{force} u(t) \\ y_{force}(t) &= C_{force} x_{force}(t) \end{aligned} \tag{5.9}$$

where $x(t)$ and $y(t)$ are state and output vectors, respectively. In continuous time domain, the state-space model includes the normalized state A_{force}, the input B_{force} and the output C_{force}. The state-space models are used to estimate cutting force at the tool tip at higher spindle speeds by dynamically compensating the acceleration signal disturbed by the structural modes of the spindle assembly.

5.3.2 Dynamic Compensation of the System

The cutting force acting on the tool tip is distorted by the structural dynamics of the machine defined by the transfer function given in Eq. (5.8). The aim of the Kalman Filter is to compensate the distortion of the signal transmission from tool to the accelerometer to estimate radial cutting force at the tool tip.

It is important to note that the inversion of the transfer function may cause amplification of low amplitude noise and leads to instability when the system has a non-minimum phase dynamic; therefore, it is not suitable to apply an inverse filter to the command signal. As an alternative, a

disturbance Kalman Filter has been suggested to compensate for the noise caused by the structural dynamics.

5.3.2.1 State Space Representation with the Disturbance Model Expansion

The force signal (F) is separated to its AC (harmonic) and DC (static) components in s domain as follows;

$$F(s) = F_{DC}(s) + F_{AC}(s) \tag{5.10}$$

DC process noise (ω_{DC}) has a constant derivative;

$$\dot{F}_{DC} = w_{DC} \tag{5.11}$$

The AC part of the cutting force is represented as a cosine function with a periodic noise disturbance of (w_{AC}) and a base frequency of spindle revolution per second (ω_{sp-rs}) as;

$$F_{AC}(s) = w_{AC} \frac{s}{s^2 + \omega_{sp-rs}{}^2} \tag{5.12}$$

Eq. (5.12) is converted into state-space form as;

$$\dot{x}_{forceF} = \underbrace{\begin{bmatrix} 0 & -\omega_{sp-rs}{}^2 \\ 1 & 0 \end{bmatrix}}_{A_{forceF}} \underbrace{\begin{bmatrix} F_{AC} \\ \dot{F}_{AC} \end{bmatrix}}_{x_{forceF}} + \underbrace{\begin{bmatrix} 1 \\ 0 \end{bmatrix}}_{B_{forceF}} w_{AC}$$
$$F_{AC} = \underbrace{\begin{bmatrix} 1 & 0 \end{bmatrix}}_{C_{forceF}} \underbrace{\begin{bmatrix} F_{AC} \\ \dot{F}_{AC} \end{bmatrix}}_{x_{forceF}} \tag{5.13}$$

Substituting Eq. (5.10) and (5.13) into Eq. (5.9) results in;

$$\begin{aligned} \dot{x}_{force}(t) &= A_{force} x_{force}(t) + B_{force}(F_{DC} + C_{forceF} x_{forceF}) \\ y_{force}(t) &= C_{force} x_{force}(t) \end{aligned} \tag{5.14}$$

Using Eq. (5.11) to (5.14), the state-space equation is expanded by considering input of the system ($F_{DC} + C_{forceF} x_{force}$) as one of the states;

$$\begin{bmatrix} \{\dot{x}_{force}\} \\ \dot{F}_{DC} \\ \{\dot{x}_{forceF}\} \end{bmatrix} = \underbrace{\begin{bmatrix} A_{force} & B_{force} & B_{force} C_{forceF} \\ 0 & 0 & 0 \\ 0 & 0 & A_{forceF} \end{bmatrix}}_{A_{force\_exp}} \underbrace{\begin{bmatrix} \{x_{force}\} \\ F_{DC} \\ \{x_{forceF}\} \end{bmatrix}}_{x_{force\_exp}} + \underbrace{\begin{bmatrix} 0 \\ \theta_{DC} \\ \theta_{AC} \end{bmatrix}}_{L_{force}} w_{force}$$
$$y_{force-\exp} = \underbrace{\begin{bmatrix} C_{force} & 0 & 0 \end{bmatrix}}_{C_{force\_exp}} \begin{bmatrix} \{x_{force}\} \\ F_{DC} \\ \{x_{forceF}\} \end{bmatrix} + v_{force} \tag{5.15}$$

where $A_{force-exp}$ and $C_{force-exp}$ are the state and output matrices of the expanded state-space model, $w_{force}(t)$ and $v_{force}(t)$ are process and measurement noise terms and L_{force} is noise coupling matrix in which θ_{DC} and θ_{AC} are the noise ratio terms ($\theta_{DC} = \frac{w_{DC}}{w_{force}}$, $\theta_{AC} = \frac{w_{AC}}{w_{force}}$).

5.3.2.2 Kalman Filter Design

The cutting force is estimated as $\hat{F}$ using the following Kalman observer state space system written as;

$$\begin{aligned}
\dot{\hat{x}}_{force_\exp} &= A_{force_\exp}\hat{x}_{force_\exp} + K_{force}\left(y_{force_\exp} - \hat{y}_{force_\exp}\right) \\
&= A_{force_\exp}\hat{x}_{force_\exp} + K_{force}\left(y_{force_\exp} - C_{force_\exp}\hat{x}_{force_\exp}\right) \\
&= \left(A_{force_\exp} - K_{force}C_{force_\exp}\right)\hat{x}_{force_\exp} + K_{force}y_{force_\exp} \qquad (5.16) \\
\hat{y}_{force_\exp} &= \hat{F} = C_{0_force}\hat{x}_{force_\exp} \leftarrow C_{0_force} = \begin{bmatrix} 0 & 1 & C_{forceF} \end{bmatrix}
\end{aligned}$$

K_{force} is the Kalman Filter gain and $\hat{x}_{force\_exp}$ is the estimated state vector. The transfer function of the Kalman Filter is obtained from the state-space as;

$$\frac{\hat{F}}{X} = \left\{ \frac{C_{0\_froce}adj\left[sI - \left(A_{force\_\exp} - K_{force}C_{force\_\exp}\right)\right]}{\det\left[sI - \left(A_{force\_\exp} - K_{force}C_{force\_\exp}\right)\right]} K_{force} \right\} \qquad (5.17)$$

The estimated state vector is discretized at each sampling interval (k) as;

$$\begin{aligned}
\hat{x}_{force_\exp}(k+1) &= \exp\left\{\left(A_{force_\exp} - K_{force}C_{force_\exp}\right)t_d\right\}\hat{x}_{force_\exp}(k) \\
&\quad + \left[\int_0^{t_d} \exp\left\{\left(A_{force_\exp} - K_{force}C_{force_\exp}\right)t_\tau\right\}K_{force}dt_\tau\right] y(k) \qquad (5.18) \\
\hat{F}(k+1) &= C_{0_force}\hat{x}_{force_\exp}
\end{aligned}$$

where t_d is the discrete sampling time and is selected as 0.1 [ms]. By minimizing the state estimation error ($\tilde{x}_{force\_exp}$) between the actual state (x_{force_exp}) and estimated state ($\hat{x}_{force\_exp}$), the Kalman Filter Gain (K_{force}) can be identified;

$$\tilde{x}_{force\_\exp} = \hat{x}_{force\_\exp} - x_{force\_\exp} \tag{5.19}$$

The differential equation for the state estimation error covariance matrix (P) can be written as;

$$\begin{aligned} \dot{P}(t\,|\,t) = {} & A_{force\_\exp}(t)P(t\,|\,t) + P(t\,|\,t)A^T_{force\_\exp}(t) \\ & + L(t)Q(t)L^T(t) - P(t\,|\,t)C^T_{force\_\exp}(t)R^{-1}C_{force\_\exp}(t)P(t\,|\,t) \end{aligned} \tag{5.20}$$

Eq. (5.20) can be solved using the Riccatti Equation [39] for a stable observer when its error approaches zero.

The measurement covariance matrix (R) is tuned from the root mean square (RMS) of the air-cutting fluctuations, whereas the system covariance matrix (Q) is tuned to accommodate the compensations. The Kalman Filter gain is calculated as follows;

$$K_{force}(t) = P(t\,|\,t)C_{force\_\exp}{}^T(t)R^{-1}(t) \tag{5.21}$$

where the measurement covariance matrix (R), system noise covariance matrix (Q), and the noise coupling matrix (L) for the system are obtained as;

$$R = [1], Q = \left[10^{21}\right], L = \begin{bmatrix} 0_{1\times 15} & 1 \end{bmatrix}^T \tag{5.22}$$

Finally, the FRF of the Kalman Filter ($\Phi_{sys_{KL}}$), and the FRF of the compensated system ($\Phi_{sys} \times \Phi_{sys_{KL}}$) for the measured FRF of the uncompensated system Φ_{sys} identified in Figure 5.6 are illustrated in Figure 5.7.

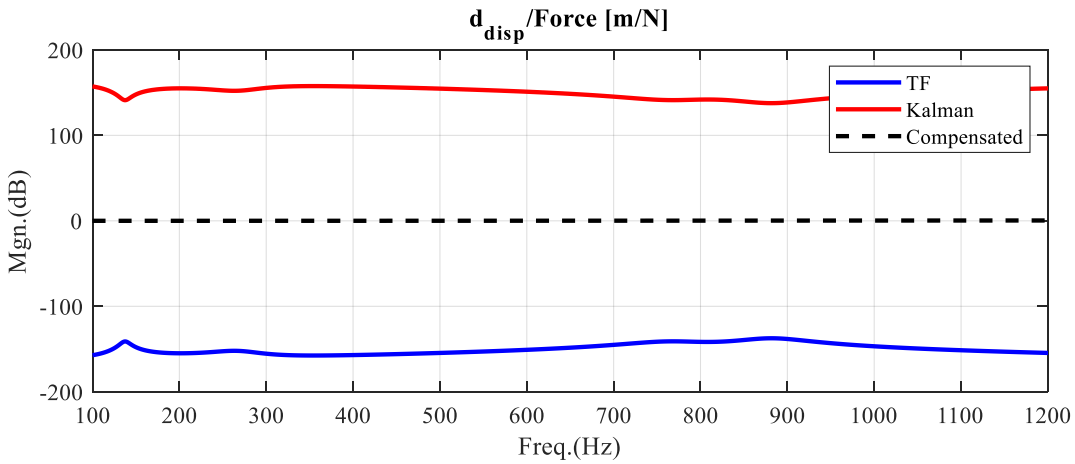

Figure 5.7. Measured (force to displacement - Φ_{sys}), Kalman and Compensated FRFs of the system

5.4 Experimental Verification

The estimation of the radial cutting force at the tool tip from the acceleration sensor is verified through milling test experiments where the workpiece is Aluminum 7075 and tests are conducted with a 20-mm diameter and 2-fluted end mill tool clamped to the sensory tool holder. Spindle speeds are selected as 7500, 9000, and 10500 rev/min to evaluate this method over a wide variety of frequencies. All of the cutting tests are conducted on 5 axis Quaser UX600 CNC machine tool.

At first the cutting forces are measured in X and Y direction with a dynameter of type Kistler 9255B. The bandwidth of the dynamometer installed on the CNC table is identified as 230 [Hz]. Since the tooth passing frequencies (spindle frequency multiplied by the number of flutes) are usually higher than the dynamometer's bandwidth in the high-speed milling experiments, its

dynamic should be considered so that the measurements are still reliable at higher frequencies. Therefore, a Kalman Filter is designed to compensate for the dynamically distorted force signals measured by the dynamometer as well.

The force-to-force FRFs in X in Y direction are measured through tap testing of the dynamometer with an impact hammer. Curve fitting is applied to the measured FRFs to identify the modes as explained in Section 5.3. Figure 5.8 presents the measured and curve-fitted FRFs in X in Y directions of the dynamometer.

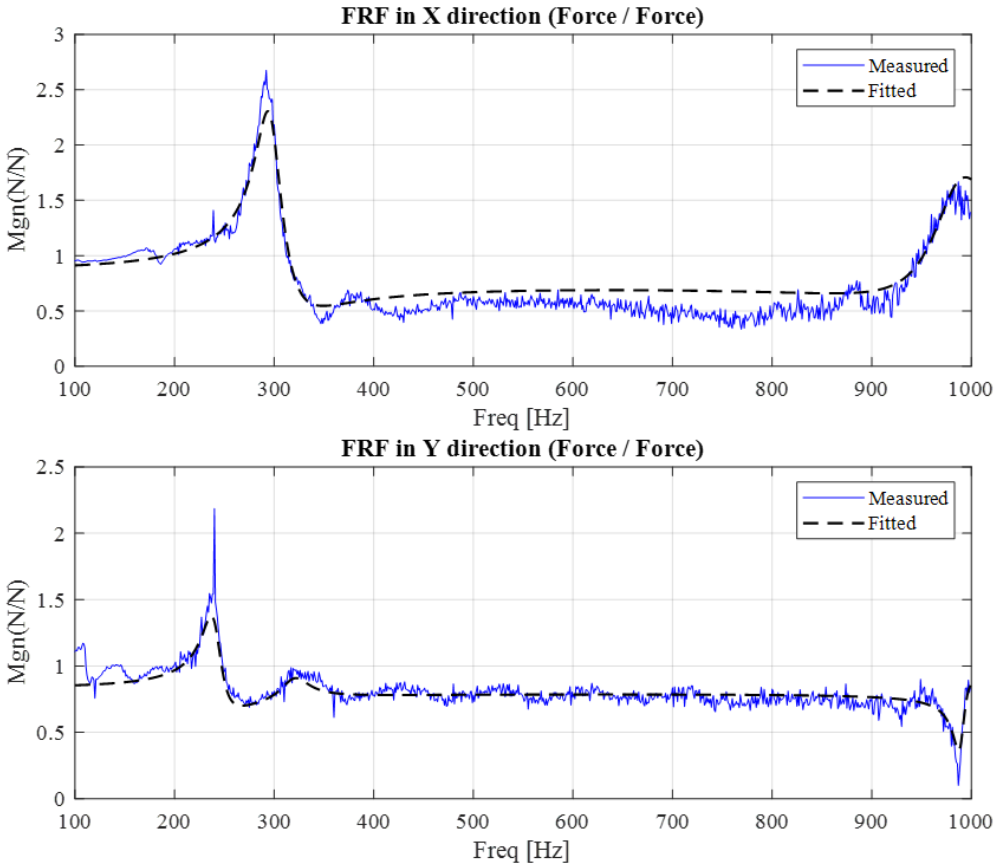

Figure 5.8. Measured and curve fitted FRFs of dynamometer in X and Y direction

The FRFs are then used to design a Kalman Filter to compensate for the dynamically distorted force measurements of the dynamometer. Derivation of the Kalman Filter transfer function is explained in Section 5.3 from Eq. (5.8) to (5.21). The uncompensated measured FRFs, the FRFs of the Kalman Filter, and the compensated FRFs of the dynamometer in X and Y directions of the dynamometer are given in Figure 5.9.

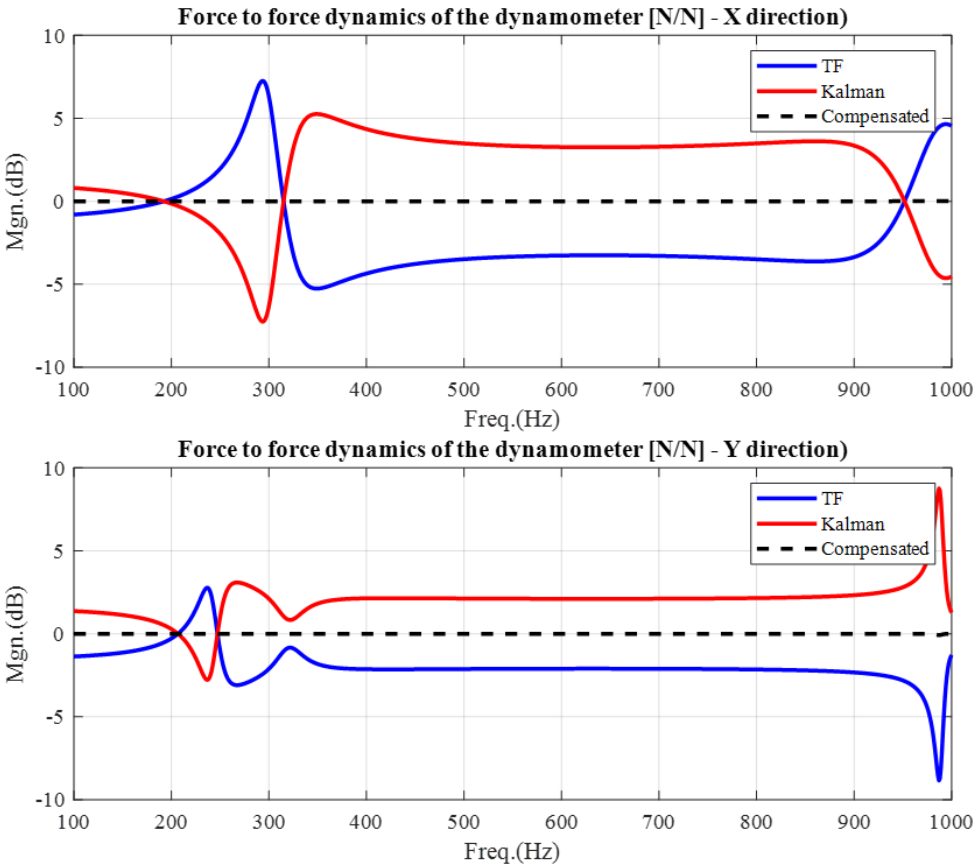

Figure 5.9. Measured force to force FRF of the dynamometer, designed Kalman Filter and compensated FRFs in X and Y direction.

Finally, the radial force at the tool tip is calculated from measured X and Y forces from the dynamometer after compensation as follows;

$$F_r = -F_X \sin(\omega_s t) - F_Y \cos(\omega_s t) \tag{5.23}$$

where ω_s is the spindle frequency. This equation is used to verify the estimated radial force from the sensory tool holder in the next three cases.

5.4.1 Case 1: 20-mm diameter, 2-fluted end mill, 7500 rev/min spindle speed

First cutting experiment is conducted with a 20-mm diameter, 2-fluted tool at 7500 rev/min spindle speed. Axial depth of cut is selected as 2 [mm] and the radial depth of cut is 20-mm (full immersion cut). The federate is 0.1 [mm] per tooth. The vibrations are collected from the accelerometer inside the sensory tool holder with a sampling frequency of 9524 [Hz].

A 12^{th} order Butterworth low-pass filter is applied to the measured forces in X and Y directions to remove the frequency contents above 1000 [Hz]. Then the low-pass filtered forces are compensated using the Kalman Filter. Low pass filtered forces and compensated forces in X and Y directions from the dynamometer are shown in Figure 5.10. The radial force is then calculated from the compensated X and Y forces given in Eq. (5.23).

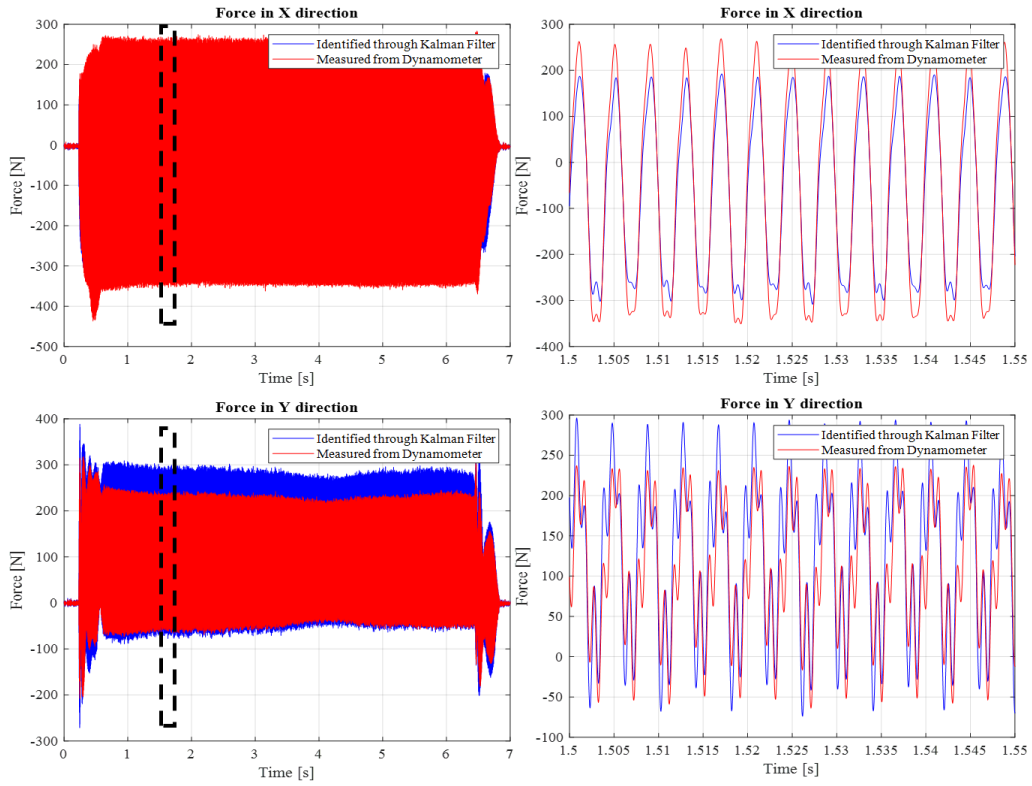

Figure 5.10. Measured and Kalman Filtered forces in X and Y direction from dynamometer for case 1. Spindle speed =7500 rev/min, tool had 2 flutes. The Kalman Filter for estimating radial force is designed based on the displacement to force FRF measurement of this tool (see Figure 5.6). The estimated radial force using an accelerometer inside the tool holder along with the calculated radial force from the measured force in X and Y directions of the dynamometer are illustrated in Figure 5.11. It can be observed that the estimated and measured forces are in an acceptable agreement.

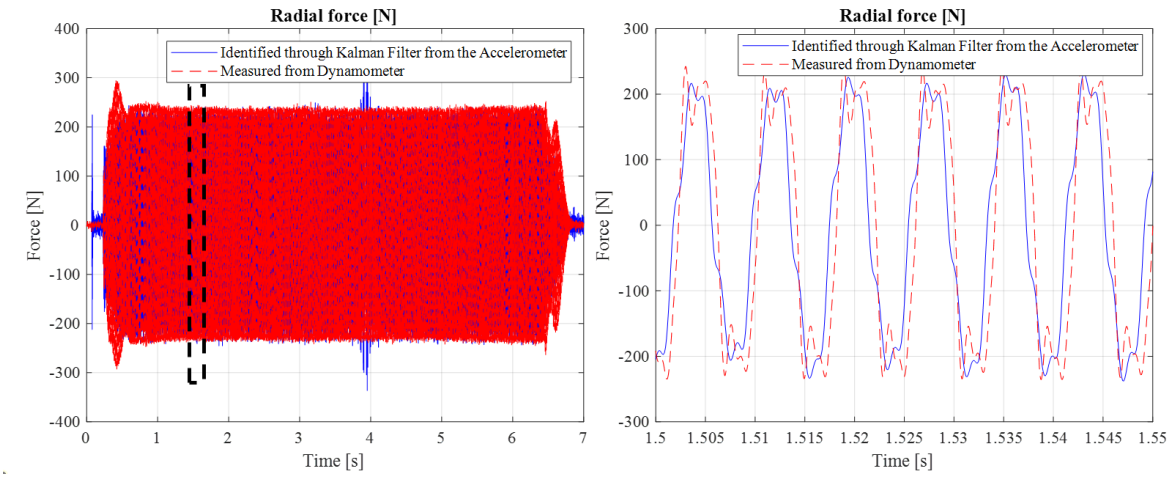

Figure 5.11. Radial force predictions from accelerometer and measured force from dynamometer for case 1. Spindle speed =7500 rev/min, tool had 2 flutes.

5.4.2 Case 2: 20-mm diameter, 2-fluted end mill, 9000 rev/min spindle speed

In this case, the spindle speed is increased to 9000 rev/min and other cutting conditions remained unchanged as the previous case. The spindle and tooth passing frequencies are 150 and 300 [Hz] which are higher than the previous test conducted at 7500 rev/min. Higher tooth passing frequency is selected to show the robustness of the method in higher frequencies. Measured forces in X and Y directions are low-pass filtered and compensated using Kalman Filter (see Figure 5.12) leading to calculating radial force at the tool tip.

The resulting estimated radial forces are illustrated in Figure 5.13 and are verified with the actual radial forces.

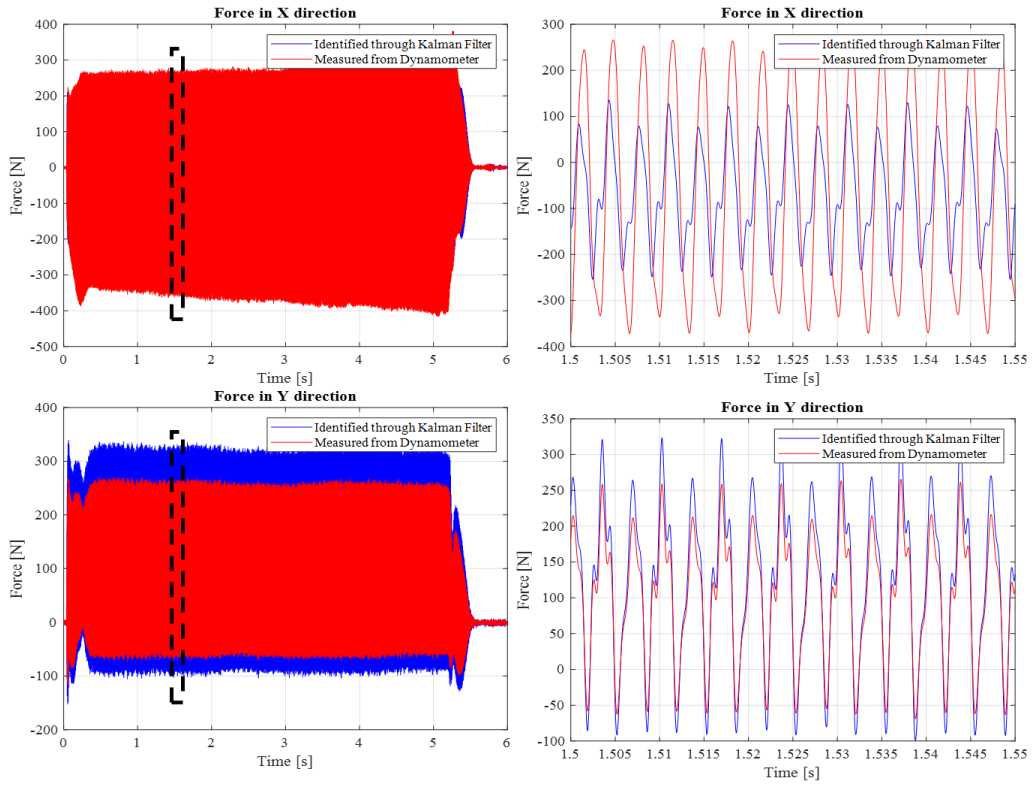

Figure 5.12. Measured and Kalman Filtered forces in X and Y direction from dynamometer for case 2. Spindle speed =9000 rev/min, the tool had 2 flutes

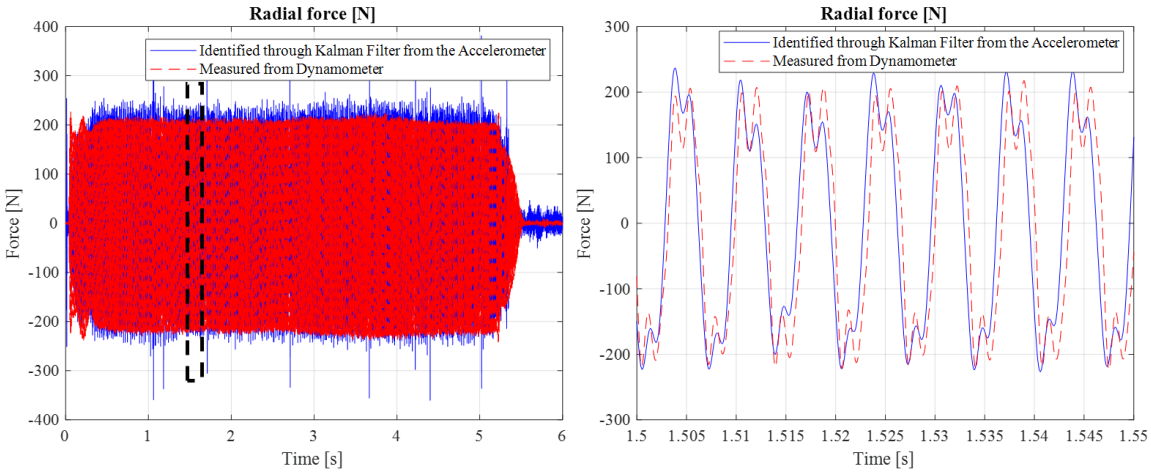

Figure 5.13. Radial force predictions from accelerometer and measured force from dynamometer for case 2. Spindle speed = 9000 rev/min, the tool had 2 flutes

5.4.3 Case 3: 20-mm diameter, 2-fluted end mill, 10500 rev/min spindle speed

In the third case, the spindle speed is increased to 10500 rev-min. The spindle and tooth passing frequencies are 175 and 350 [Hz], respectively. The same procedure as the previous two cases is repeated to estimate the radial cutting forces. The measured and compensated forces are shown in Figure 5.14 and Figure 5.15. The estimated radial forces from the sensor is still reasonably close to the compensated dynamometer measurements.

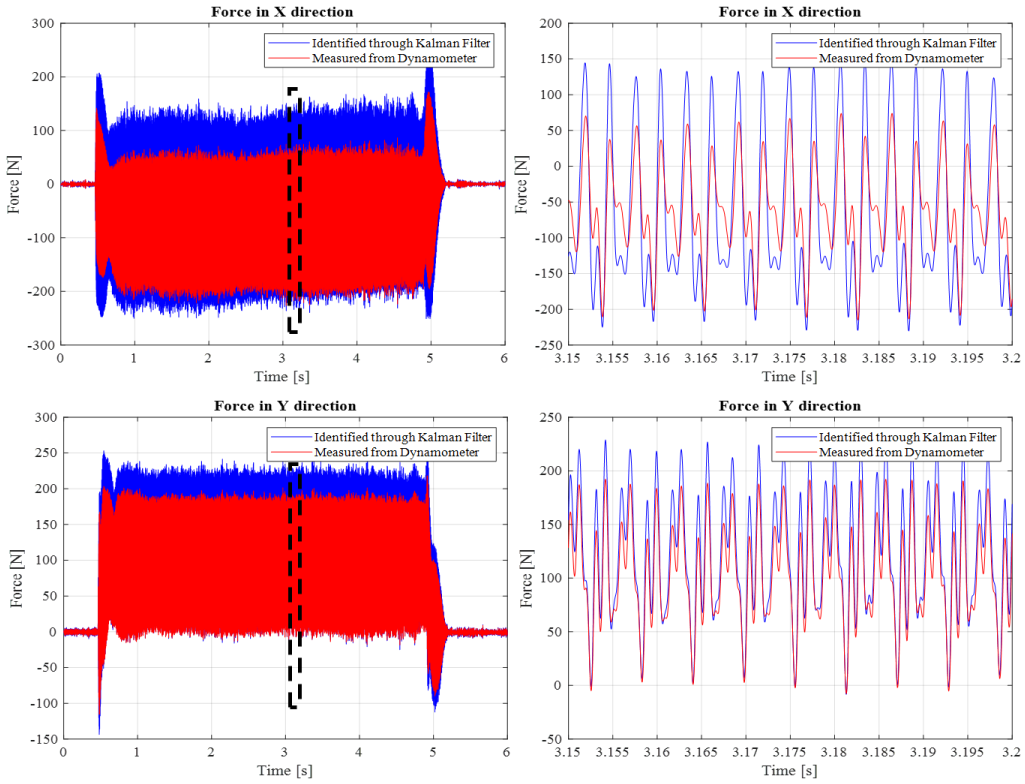

Figure 5.14. Measured and Kalman Filtered forces in X and Y direction from dynamometer for case 3. Spindle speed =10500 rev/min, the tool had 2 flutes

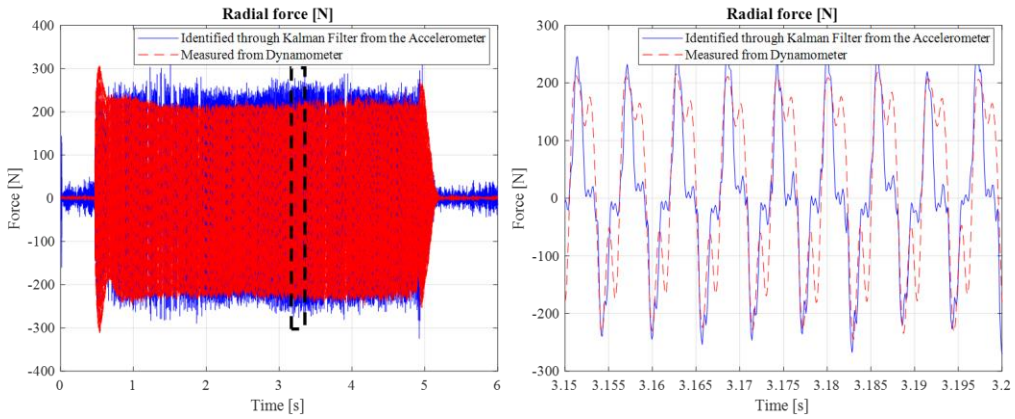

Figure 5.15. Radial force predictions from accelerometer and measured force from dynamometer for case 3. Spindle speed =10500 rev/min, the tool had 2 flutes

5.5 Summary

This chapter presents the application of Kalman filter to estimate the cutting forces from the vibration measurements collected from an accelerometer instrumented inside the tool holder. The Kinematic model of the sensory tool holder is presented to illustrate the sensibility of the vibratory mass to acceleration signal, particularly high frequency term. The transfer function between the forces at the tooltip and measured vibrations by the accelerometer is identified and used in designing the Kalman filter which compensated the disturbances caused by the structural modes of the tool holder assembly. A bandwidth of 2000 Hz was achieved, but tested only up to 350Hz due to speed limit of the tool holder. Since the accelerometers cannot measure the dc values, the proposed system cannot predict the static (i.e. dc component of milling forces which can occur at slotting and high depth of cut-wide immersion milling applications.

Chapter 6: Conclusion

A digital twin system was developed by integrating the virtual model of milling operations and online monitoring of tool wear, tool breakage and chatter. The monitoring algorithms use vibrations, sound and cutting forces. Since direct measurement of cutting forces Is not available for industrial settings, they are estimated from vibration signals measured with an accelerometer embedded in a tool holder which is commercially available.

The machining process is simulated and the predicted states such as force, torque, cumulative chip thickness, and cutter workpiece engagement area along the tool path are stored in a virtual process feedback file. The actual states during machining are collected either from the CNC or from external analog sensors during machining. The sampling frequency is limited by the CNC systems typically at 300hz to 1000 Hz, while sampling frequency can be as high as 10-20Khz from external analog sensors. The actual and simulated processes are synchronized by matching the tool path positions. When simulated and actual tool positions are matched, the simulated information from the virtual feedback can be utilized for monitoring of machining processes.

A tool wear monitoring system is developed by utilizing both online measured spindle motor current and virtually simulated cumulative chip thickness - cutter-workpiece engagement information. The measured current is normalized against cutter workpiece engagement area, which yields to cutting force coefficient sensitive states. Tool wear is correlated to the progression of current and cumulative chip thickness removed with 2 to 4 wear measurements for tool-work material pair. It is shown that tool wear can be monitored either with only virtually predicted cumulative chip thickness or online measured current normalized with the virtually predicted

cutter engagement area. When both normalized current and cumulative chip thickness are used, the monitoring algorithm can track stochastic tool wear which can occur sometimes due to material imperfections.

When the cutter enters or exits into cuts, or when the geometry changes drastically along the tool path, transient changes in the force or current resemble tool breakage effects. Previously developed tool breakage detection algorithm has been further enhanced by differentiating the transient cutting states from the virtual model of the process. With the help of a virtual machining module, the proposed method predicts the transient zones where the tool breakage algorithm can be disabled to avoid false alarms. Similarly, the robustness of the chatter detection algorithm is also improved by separating the transient changes which may excite the natural modes of the structure. The chatter detection and avoidance algorithms are activated only when the cutter is at a steady state engagement with the workpiece.

It is ideal to use only CNC inherent sensory data such as spindle motor current which is already available on the machine. However, due to data collection frequency limited by the CNC manufacturers, noise and the nonlinear relationship between the motor current and cutting force, the CNC inherent sensory data may not have the required accuracy for reconstructing the cutting forces at the tooltip. Production Laboratory at the Technical University of Vienna developed a commercial tool holder embedded with a wireless accelerometer to monitor vibrations. This thesis presents a Kalman filter-based algorithm to predict the radial cutting forces directly from the vibration signals measured by the accelerometer embedded into the tool holder. Kalman filter also

expands the bandwidth of the force sensing by compensating the disturbance effects of tool-holder-spindle structural dynamics.

The proposed algorithms have been experimentally proven with reasonable prediction errors which are within an industrially acceptable range (i.e. 15-20%). The algorithms are integrated to an Intelligent machine tool monitoring system called IntelCut which is developed at the Manufacturing Automation Laboratory at UBC in collaboration with industry partners.

6.1 Future Work

In the future, digital twin can serve as the center for more studies since it is a new and industry-needed system. The following topics can be explored further as a continuation of this thesis;

- Research carried out on digital twin systems can be applied to other applications such as adaptive control, dimensional error, and machine tool health monitoring (such as spindles and feed drives).
- Digital twin applications are tested in 3-axis milling experiments in this study. They can be further investigated in 5-axis milling experiments where there is also rotational movement of drives which lead to position-dependent dynamics of the spindle structure which affect Kalman filter design and tuning.
- The proposed tool wear monitoring algorithm can be updated using automated tool wear measurement system which are activated when the tool is not cutting. A tool life database can be constructed to be utilized for process planning of new parts to be machined.

- The sensory tool holder used in this study has only one rotatory accelerometer, so only the radial cutting force at the tooltip could be estimated. By adding another accelerometer, it is possible to estimate the tangential and radial forces.

Bibliography

[1] Manufacturing Automation Laboratory, “MACHpro Advanced Virtual Machining System.” The University of British Columbia, Canada, 2011. Accessed: Jun. 16, 2022. [Online]. Available: https://www.malinc.com/

[2] E. Ducroux, G. Fromentin, F. Viprey, D. Prat, and A. D’Acunto, “New mechanistic cutting force model for milling additive manufactured Inconel 718 considering effects of tool wear evolution and actual tool geometry,” *J Manuf Process*, vol. 64, pp. 67–80, Apr. 2021, doi: 10.1016/j.jmapro.2020.12.042.

[3] M. Nouri, B. K. Fussell, B. L. Ziniti, and E. Linder, “Real-time tool wear monitoring in milling using a cutting condition independent method,” *Int J Mach Tools Manuf*, vol. 89, pp. 1–13, 2015, doi: 10.1016/j.ijmachtools.2014.10.011.

[4] B. Denkena, M. Krüger, and J. Schmidt, “Condition-based tool management for small batch production,” *International Journal of Advanced Manufacturing Technology*, vol. 74, no. 1–4, pp. 471–480, 2014, doi: 10.1007/s00170-014-6013-2.

[5] Y. P. Liu, Z. M. Kilic, and Y. Altintas, “Monitoring of in-process force coefficients and tool wear,” *CIRP J Manuf Sci Technol*, vol. 38, pp. 105–119, Aug. 2022, doi: 10.1016/j.cirpj.2022.04.009.

[6] M. Xu, R. B. Jerard, and B. K. Fussell, “Energy Based Cutting Force Model Calibration for Milling,” 2007.

[7] K. Matsushima, P. Bertok, and T. Sata, “In-process detection of tool breakage by monitoring the spindle motor current of a machine tool,” *Measurement and control for batch manufacturing*, pp. 145–153, 1982.

[8] M.-S. Lan and Y. Naerheim, “In-process detection of tool breakage in milling,” 1986.

[9] Y. Altintas, “In-process detection of tool breakages using time series monitoring of cutting forces,” *Int J Mach Tools Manuf*, vol. 28, no. 2, pp. 157–172, 1988, doi: 10.1016/0890-6955(88)90027-2.

[10] Y. Altintas, *Manufacturing automation : metal cutting mechanics, machine tool vibrations, and CNC design*. Cambridge University Press, 2012.

[11] Y. Altintas, “Prediction of Cutting Forces and Tool Breakage in Milling from Feed Drive Current Measurements,” 1992. [Online]. Available: http://asmedigitalcollection.asme.org/manufacturingscience/article-pdf/114/4/386/6507178/386_1.pdf

[12] by B. Deniz Aslan, “Integration of Virtual and On-line Machining Process Control and Monitoring using CNC Drive Measurements,” 2011.

[13] Y. Altintas, G. Stepan, D. Merdol, and Z. Dombovari, “Chatter stability of milling in frequency and discrete time domain,” *CIRP J Manuf Sci Technol*, vol. 1, no. 1, pp. 35–44, 2008, doi: 10.1016/j.cirpj.2008.06.003.

[14] S. Smith, “Use of Audio Signals for Chatter Detection and Control,” 1992. [Online]. Available: http://asme.org/terms

[15] D. Aslan and Y. Altintas, “On-line chatter detection in milling using drive motor current commands extracted from CNC,” *Int J Mach Tools Manuf*, vol. 132, pp. 64–80, Sep. 2018, doi: 10.1016/j.ijmachtools.2018.04.007.

[16] H. Caliskan, Z. M. Kilic, and Y. Altintas, “On-line energy-based milling chatter detection,” *Journal of Manufacturing Science and Engineering, Transactions of the ASME*, vol. 140, no. 11, Nov. 2018, doi: 10.1115/1.4040617.

[17] M. H. Rahimi, H. N. Huynh, and Y. Altintas, “On-line chatter detection in milling with hybrid machine learning and physics-based model,” *CIRP J Manuf Sci Technol*, vol. 35, pp. 25–40, Nov. 2021, doi: 10.1016/j.cirpj.2021.05.006.

[18] F. J. A. M. van Houten and F. Kimura, “Virtual maintenance system: A computer-based support tool for robust design, product monitoring, fault diagnosis and maintenance planning,” *CIRP Ann Manuf Technol*, vol. 49, no. 1, pp. 91–94, 2000, doi: 10.1016/S0007-8506(07)62903-5.

[19] W. Kritzinger, M. Karner, G. Traar, J. Henjes, and W. Sihn, “Digital Twin in manufacturing: A categorical literature review and classification,” in *IFAC-PapersOnLine*, Jan. 2018, vol. 51, no. 11, pp. 1016–1022. doi: 10.1016/j.ifacol.2018.08.474.

[20] Y. Altintas and D. Aslan, “Integration of virtual and on-line machining process control and monitoring,” *CIRP Ann Manuf Technol*, vol. 66, no. 1, pp. 349–352, 2017, doi: 10.1016/j.cirp.2017.04.047.

[21] R. Teti, K. Jemielniak, G. O’Donnell, and D. Dornfeld, “Advanced monitoring of machining operations,” *CIRP Ann Manuf Technol*, vol. 59, no. 2, pp. 717–739, 2010, doi: 10.1016/j.cirp.2010.05.010.

[22] F. Klocke, S. Kratz, and D. Veselovac, “Position-oriented process monitoring in freeform milling,” *CIRP J Manuf Sci Technol*, vol. 1, no. 2, pp. 103–107, 2008, doi: 10.1016/j.cirpj.2008.09.003.

[23] H. C. Möhring, K. M. Litwinski, and O. Gümmer, “Process monitoring with sensory machine tool components,” *CIRP Ann Manuf Technol*, vol. 59, no. 1, pp. 383–386, 2010, doi: 10.1016/j.cirp.2010.03.087.

[24] Y. Altintas and S. S. Park, “Dynamic Compensation of Spindle-Integrated Force Sensors.” [Online]. Available: http://www.mech.ubc.ca/-ma1

[25] Y. Altintas, “Prediction of Cutting Forces and Tool Breakage in Milling from Feed Drive Current Measurements,” 1992. [Online]. Available: http://asmedigitalcollection.asme.org/manufacturingscience/article-pdf/114/4/386/6507178/386_1.pdf

[26] D. Aslan and Y. Altintas, “Prediction of Cutting Forces in Five-Axis Milling Using Feed Drive Current Measurements,” *IEEE/ASME Transactions on Mechatronics*, vol. 23, no. 2, pp. 833–844, Apr. 2018, doi: 10.1109/TMECH.2018.2804859.

[27] M. Postel, D. Aslan, K. Wegener, and Y. Altintas, “Monitoring of vibrations and cutting forces with spindle mounted vibration sensors,” *CIRP Annals*, vol. 68, no. 1, pp. 413–416, Jan. 2019, doi: 10.1016/j.cirp.2019.03.019.

[28] Z. Xie, Y. Lu, and J. Li, “Development and testing of an integrated smart tool holder for four-component cutting force measurement,” *Mech Syst Signal Process*, vol. 93, pp. 225–240, Sep. 2017, doi: 10.1016/j.ymssp.2017.01.038.

[29] M. Nouri, B. K. Fussell, B. L. Ziniti, and E. Linder, “Real-time tool wear monitoring in milling using a cutting condition independent method,” *Int J Mach Tools Manuf*, vol. 89, pp. 1–13, 2015, doi: 10.1016/j.ijmachtools.2014.10.011.

[30] B. Denkena, M. Krüger, and J. Schmidt, “Condition-based tool management for small batch production,” *The International Journal of Advanced Manufacturing Technology*, vol. 74, no. 1, pp. 471–480, 2014, doi: 10.1007/s00170-014-6013-2.

[31] by Yen-Po Liu BASc, “Identification of In-Process Machine Tool Dynamics,” 2021.

[32] T. MathWorks, “MATLAB (R2020b),” *The MathWorks Inc.*, 2020.

[33] Y. P. Liu, Z. M. Kilic, and Y. Altintas, “Monitoring of in-process force coefficients and tool wear,” *CIRP J Manuf Sci Technol*, vol. 38, pp. 105–119, Aug. 2022, doi: 10.1016/j.cirpj.2022.04.009.

[34] Y. Altintas and Y. J. Tlusty, “The Detection of Tool Breakage in Milling Operations,” 1988. [Online]. Available: http://asmedigitalcollection.asme.org/manufacturingscience/article-pdf/110/3/271/6506301/271_1.pdf

[35] T. U. of B. C. C. Manufacturing Automation Laboratory, “CUTPRO Advanced Machining Simulation System,” 2000.

[36] P. Schörghofer, F. Pauker, N. Leder, J. Mangler, C. Ramsauer, and F. Bleicher, “Using sensory tool holder data for optimizing production processes,” *Journal of Machine Engineering*, vol. 19, no. 3, pp. 43–55, 2019, doi: 10.5604/01.3001.0013.4079.

[37] U. di Drtechn habil Friedrich Bleicher and U. Friedrich Bleicher, “Institute of Production Engineering and Photonic Technologies ICOtronic Motivation,” 2021.

[38] F. Bleicher, C. M. Ramsauer, R. Oswald, N. Leder, and P. Schoerghofer, “Method for determining edge chipping in milling based on tool holder vibration measurements,” *CIRP Annals*, vol. 69, no. 1, pp. 101–104, Jan. 2020, doi: 10.1016/j.cirp.2020.04.100.

[39] R. G. Brown and P. Y. ~C. Hwang, *Introduction to random signals and applied Kalman filtering : with MATLAB exercises and solutions*. 1997.